NOTE TO USERS

Université d'Ottawa • University of Ottawa

Université d'Ottawa • University of Ottawa

FACULTÉ DES ÉTUDES SUPÉRIEURES ET POSTDOCTORALES

FACULTY OF GRADUATE AND POSTDOCTORAL STUDIES

Jongseok OH

AUTEUR DE LA THÈSE - AUTHOR OF THESIS

M. A. Sc. (Civil Engineering)

GRADE - DEGREE

Department of Civil Engineering

FACULTÉ, ÉCOLE, DÉPARTEMENT - FACULTY, SCHOOL, DEPARTMENT

TITRE DE LA THÈSE - TITLE OF THE THESIS

Dynamic Characteristics of Inclined Cable

H. Tanaka

DIRECTEUR DE LA THÈSE - THESIS SUPERVISOR

CO-DIRECTEUR DE LA THÈSE - THESIS CO-SUPERVISOR

EXAMINATEURS DE LA THÈSE - THESIS EXAMINERS

D. Lau

M. Mohareb

M. Saatcioglu

J.-M. De Koninck, Ph.D.

LE DOYEN DE LA FACULTÉ DES ÉTUDES SUPÉRIEURES ET POSTDOCTORALES

SIGNATURE

DEAN OF THE FACULTY OF GRADUATE AND POSTDOCTORAL STUDIES

DYNAMIC CHARACTERISTICS OF INCLINED CABLE

by
Jongseok Oh

A thesis
Presented to the University of Ottawa in partial fulfillment of the requirements for
Master of Applied Science in Civil Engineering

Department of Civil Engineering
University of Ottawa
Ottawa, Canada
K1N 6N5

The M.A.Sc. in Civil Engineering is a joint program
with Carleton University administered by the
Ottawa-Carleton Institute for Civil Engineering

Your file Votre référence
ISBN: 0-494-01567-5
Our file Notre référence
ISBN: 0-494-01567-5

ACKNOWLEDGEMENTS

This study could never have been done without the support, guidance, and dedication of people. First and foremost, my greatest gratitude goes to my supervisor, Dr. Hiroshi Tanaka for his invaluable guidance and time that he took to share ideas, discuss his own experiences, and review many drafts of this paper. Also, a warm thank you to Daniel Suk, who contributed a substantial amount of material for this study and Arum Hong, who conferred thoughtful comments on the drafts.

I owe a debt of gratitude to my family, especially my parents, for enabling me to have an opportunity to study in Canada and to realize my ambition to become a civil engineer. My deepest love and gratitude lies with my beloved mother, Gangja Lee, and special appreciation to my sister, Giwon Oh, for her support and trust.

ABSTRACT

This thesis aims to investigate dynamic characteristics, especially the natural in-plane vibrations, of a perfectly flexible elastic suspended cable. A finite element procedure using the linear elastic rod as cable elements is formulated and a program implemented in Matlab is developed to determine natural frequencies and mode shapes. Results show how the properties of inclined cables meaningfully differ from those of horizontal cables. Influence of cable inclination induces the mixture of mode shapes through the transition range and the region of non-contact crossings of frequency. These phenomena assure that the existence of crossover points is only exception for the case of horizontal cables.

TABLE OF CONTENTS

LIST OF TABLES

LIST OF FIGURES

NOTATION

A	cross sectional area of the cable
Di	diameter of the cable, *mm*
el	length of the cable element, *m*
E	Young's modulus of elasticity
{f}	cable element nodal force matrix in the local coordinate system
{F}	cable element nodal force matrix in the global coordinate system
g	gravitational acceleration
h	variation of horizontal tension due to cable vibration
H	horizontal component of cable tension, *N*
$[k]$	stiffness matrix of a cable element in the local coordinate system
$[K]$	stiffness matrix of a cable element in the global coordinate system
$[KK]$	total stiffness matrix
l	span length of the cable, *m*
L	total cable length, *m*
m	lumped mass, *kg*
$[m]$	mass matrix of a cable element
M	mass per unit length of the cable, *kg/m*
$[MM]$	total mass matrix
n	finite number of elements
R	sag-to-span ratio of the cable
RR	sag-to-total cable length of the cable
s	curvilinear coordinate along the cable profile
t	time
T	tension in the cable, *N*
ΔT	additional cable tension due to cable vibration
$[Tr]$	stiffness transformation matrix
u	horizontal displacement of the cable in the local coordinate system

u^o	horizontal displacement of the cable in the global coordinate system
$\{u\}$	vector of nodal displacements in the local coordinate system
$\{u^o\}$	vector of nodal displacements in the global coordinate system
U	strain energy in the cable
v	vertical displacement of the cable in the local coordinate system
v^o	vertical displacement of the cable in the global coordinate system
w	unit weight of the cable, *N/m*
x, y	local rectangular coordinates
X, Y	global rectangular coordinates
δ	sag of the cable, *m*
ε	strain in the cable
ϕ	slope in a cable element
η	dynamic vertical deflection of the cable
θ	inclination angle of the cable chord, degree
ω	natural frequency of the cable, *rad/sec*
Ω	non-dimensional natural frequency of the cable
ξ	dynamic longitudinal deflection of the cable

Abbreviations

C	$\cos\phi$
S	$\sin\phi$

CHAPTER 1

INTRODUCTION

1.1 General

Structural cables have been frequently used in civil engineering applications such as cable-stayed bridges, suspension bridges, guy wires, and so on. The mechanical behaviour of a suspended cable in the gravitational field presents a unique structural form, one which is exhibited by a non-linear behaviour of the cable due to change in shape or geometry. However, apart from the geometrical non-linearity, for the study of natural frequencies and corresponding mode shapes, it is generally justifiable to linearize the problem by assuming infinitesimally small amplitudes of cable vibrations. The dynamics of small-sag, horizontal cables have been studied extensively and established for both in-plane and out-of-plane motions. However, regarding the influence of large sag-to-span ratios and angle of inclination, a comprehensive presentation of the results has not yet been achieved despite the previous establishment of an analytical methodology in discrete simulation and analytical approximation method.

The purpose of the present study is to investigate into the natural in-plane vibrations of extensible cables hanging with its own weight, and attempt to define the effects of the sag of the cable and the angle of inclination on them. To accomplish this study, the Finite Element Method is applied as a numerical method for solving problems and the program based on Matlab is employed to perform the calculations and present the results.

1.2 Outline of Study

This study is carried out in four major steps as described in the following specific chapters:

- In Chapter 2, a brief review of the previous works established by others in the field is presented chronologically.

- In Chapter 3, the derivation of governing equations for both statics and dynamics of a cable and the formulation of the Finite Element Method for the determination of the natural frequencies and mode shapes of an in-plane vibration are presented. Also, the description of the calculation flows performed by the Matlab program and essential parameters used in the program are introduced.

- In Chapter 4, the results are presented for each case with discussions. To illustrate the results, two different Young's moduli of cable and the various angles of cable inclination are categorized and the natural frequencies and mode shapes of each categorized cable are expressed graphically.

- In Chapter 5, the conclusion of this study is presented.

CHAPTER 2

LITERATURE REVIEW

The investigation of the natural frequencies and modes of vibration of a cable system has been a considerably important subject for quite some time. The theory of vibration of suspended cables has been more and more refined through its development. However, in many of the previous works, the theories of cable vibration were under predefined conditions; the flexibility of the cable was assumed complete and its extensibility was null. Only in the last 30 years or so have the comprehensive treatments of cable dynamics been developed including the effects of elasticity, sag and chord inclination. A chronological review of its development is as follows (this review is based on references [5] and [11] unless specifically mentioned as other wise.):

1820	Poisson established an equation of motion for cable dynamics. He established it as a set of general Cartesian partial differential equations of motion under the action of gravitational acceleration. These equations were the dynamic analogue of the static equations given by Fuss in 1796. Poisson used these equations to improve the solutions previously obtained for vertically suspended cables and taut strings.
1868	Routh gave an exact solution for the symmetric vertical vibrations and the asymmetric vertical vibrations of a heterogeneous cable assuming that the cable was suspended in a cycloid form. Similar to conditions outlined in the previous works, he assumed that the cable was inextensible. However, under this preset condition, the taut wire case cannot be covered by his analysis.

1949 Pugsley [8] proposed a semi-empirical theory for the natural frequencies of the first three in-plane modes of a uniformly suspended chain. He demonstrated the applicability of the results by conducting experiments on cables in which the ratio of sag-to-span ranged from 1:10 up to approximately 1:4 and compared the results with his own calculation and also with those obtained by Routh for a cycloidal chain.

1953 Saxon and Cahn presented an asymptotic solution to the linearized equations of motion for a chain vibration with a small amplitude in the plane of the catenary form. They made a theory of the in-plane vibrations by assuming a uniform, inextensible cable and obtained good theoretical solutions for the large sag-to-span ratios.

1974 Irvine and Caughey [7] obtained a closed form solution for a linearized theory of elastic shallow cables. Their linear theory represented the free vibrations of a uniform, horizontally suspended cable, where the sag-to-span ratio is about 1:8 or less. They explained the symmetric and asymmetric in-plane motions of a cable and also the extensibility of a cable by formulating a parameter which involves both cable geometry and elasticity. They also predicted the existence of modal crossover points for the symmetric in-plane modes and demonstrated it through experiments.

1975 West and Suhoski [14] used a discrete model and explained the phenomena of modal crossover. They treated the cable as a linkage composed of a finite number of straight bars connected by frictionless pins with concentrated masses and included the extensional characteristics of the cable. Their results indicate modal transition ranges for small sag-to-span ratios and also explained the previously mentioned discrepancies caused by the assumption of cable inextensibility.

1977 Henghold, Russell and Morgan [3] performed a parametric analysis using a three-dimensional finite element modeling method. They applied the non-linear finite elements to a three-dimensional problem of determining the natural frequencies of a suspended elastic cable. For a horizontally suspended cable, the results for the crossover frequencies agreed with those predicted by Irvine and Caughey [7].

1979 Yamaguchi and Ito [15] obtained approximate solutions with good accuracy by applying the Galerkin method for flat and inclined cables with large sags. They built a strict formulation of a flexible and extensible cable as a continuum. They derived an eigenvalue problem from the linearized governing equations, which can be discretized into a finite degree of freedom system by the generalized coordinate method, and obtained the natural frequencies and mode shapes of a suspended cable.

1984 Triantafullou [12] tried a refined theory on inclined cables. He derived a general asymptotic solution to the problem of the linear dynamics of small-sag, inclined, elastic cables. In the case of a horizontal cable, he observed the modal crossover phenomenon, which is in agreement with the results of Irvine and Caughey [6]. However, he demonstrated that inclined cables had different characteristics from horizontal cables and the crossover did not occur.

1989 Tonis [Ph.D. thesis, U. Bundeswehr, München] attempted another non-linear analysis. (No particular reference was found)

The analysis of cable systems has been previously treated in many different ways. One of the difficulties involved with the cable analysis is its non-linear behavior due to change in geometry, even though the characteristics of cable material are perfectly linear. Once the non-linear terms are associated with the analysis of cable dynamics, each problem needs to be solved by numerical methods. Due to the enormous progresses in last decades in

computer technology and numerical methods, recent researchers can acquire those complicated calculations for some specific cases. However, there is not a complete solution in general form for this non-linear problem.

CHAPTER 3

MATHEMATICAL FORMULATION

3.1 Basic Assumptions

In order to formulate the static and dynamic equations of a suspended cable, the following assumptions are held in this paper:

1. The bending stiffness of a cable is small enough to be neglected.
   In reality, the effect of bending stiffness exists and has been discussed in references [11] and [15]. However, a general presentation of such findings for a cable has never been given, due to the difficulty in identifying precisely the actual magnitude of the bending stiffness. The cables used for calculation in this study are minutely affected by bending stiffness compared to axial stiffness. Therefore, these cables are assumed to be perfectly flexible.

2. The cable is subjected only to tensile forces.
   Along with the previous assumption, it is also assumed that cables are used to transmit large tensile forces, so there is no resistance against compression and bending. Therefore, the stress resultant in cables is only a tensile force.

3. The axial strain in a cable is so small that it can be neglected in the condition of static equilibrium.

4. The cable supporting points are fixed and the cable is composed of a material that obeys the Hooke's law.

3.2 Statics of a Suspended Cable

3.2.1 Static Equilibrium of a Suspended Cable [5] [11]

Consider the profile of a uniform cable hanging under its own weight between two fixed supports in Fig. 3.1. From the free-body diagram of an infinitesimal element of the cable shown in Fig. 3.1, the horizontal and vertical equilibrium equations can be obtained as follows:

Horizontal equilibrium equation:

$$T\frac{dx}{ds} = T\frac{dx}{ds} + d\left(T\frac{dx}{ds}\right) \qquad \therefore d\left(T\frac{dx}{ds}\right) = 0 \tag{3.1}$$

Vertical equilibrium equation:

$$T\frac{dy}{ds} + d\left(T\frac{dy}{ds}\right) = T\frac{dy}{ds} + wds \qquad \therefore d\left(T\frac{dy}{ds}\right) = wds \tag{3.2}$$

Consequently, the static equilibrium of a cable is given as follows:

$$\therefore H\frac{d^2y}{dx^2} = w\sqrt{1+\left(\frac{dy}{dx}\right)^2} \quad \text{or} \quad Hy''(x) = w\sqrt{1+(y'(x))^2} \tag{3.3}$$

where $H = T\cdot\frac{dx}{ds}$.

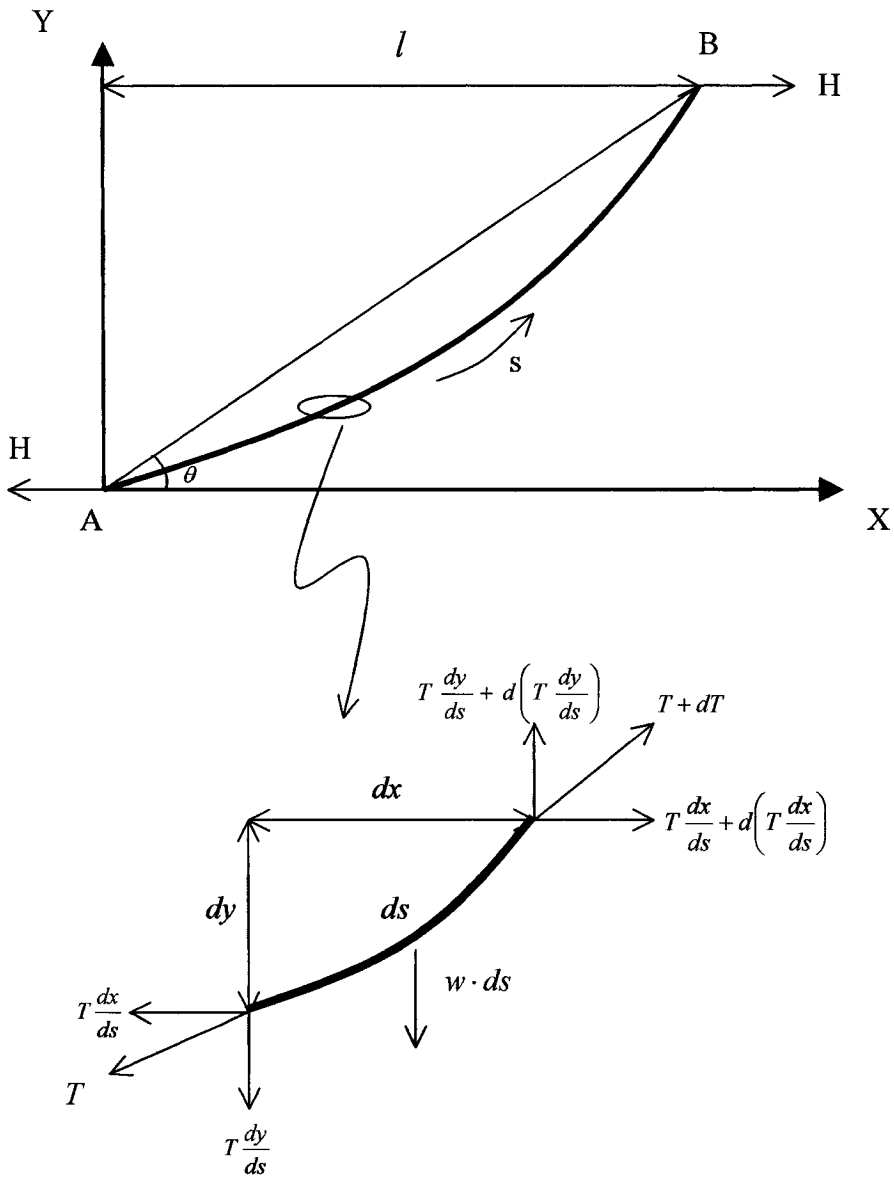

T: Tension in cable
w: Unit weight of the cable
l: Span length
H: Horizontal component of cable tension
s: Curvilinear coordinate along the cable profile
θ: Inclination angle of the cable chord

Fig. 3.1 Cable profile and infinitesimal element of the cable

The solution of the nonlinear second-order differential Eq. (3.3) is

$$y(x) = \frac{H}{w}\cosh\left(\frac{w}{H}x + C_1\right) + C_2 \tag{3.4}$$

The integral constants C_1 and C_2 can be determined by applying the boundary conditions, $y = 0$ at A and $y = l \cdot \tan\theta$ at B.

The first boundary condition gives $C_2 = -\frac{H}{w}\cosh(C_1)$

and the second boundary condition gives $C_1 = -\alpha + \sinh^{-1}\left(\frac{\alpha \cdot \tan\theta}{\sinh(\alpha)}\right)$

Therefore, the static equilibrium of the cable is

$$\therefore y(x) = \frac{H}{w}\left\{\cosh\left(\frac{w}{H}x + C_1\right) - \cosh(C_1)\right\} \tag{3.5}$$

where $C_1 = -\alpha + \sinh^{-1}\left(\frac{\alpha \cdot \tan\theta}{\sinh(\alpha)}\right)$ and $\alpha = \frac{wl}{2H}$

3.2.2 Total Cable Length (L) [11]

The total cable length is obtained by integrating the cable elements along the coordinate s as follows:

$$\mathrm{L} = \int ds = \int_0^l \sqrt{1 + (y')^2}\, dx \tag{3.6}$$

$$\mathrm{L} = \frac{l}{L} \cdot \cosh(\alpha + C_1)\sinh(\alpha), \text{ where } \alpha = \frac{wl}{2H} \tag{3.7}$$

Equation (3.7) can be rewritten as:

$$\mathrm{L} = \frac{l}{\alpha}\sqrt{\sinh^2\alpha + (\alpha \cdot \tan\theta)^2} = l\sqrt{\left(\frac{\sinh\alpha}{\alpha}\right)^2 + \tan^2\theta} \tag{3.8}$$

3.2.3 Cable Sag (δ) [11]

The sag of a cable, δ, is defined by the maximum value of $y_1(x)$. See Fig. 3.2.

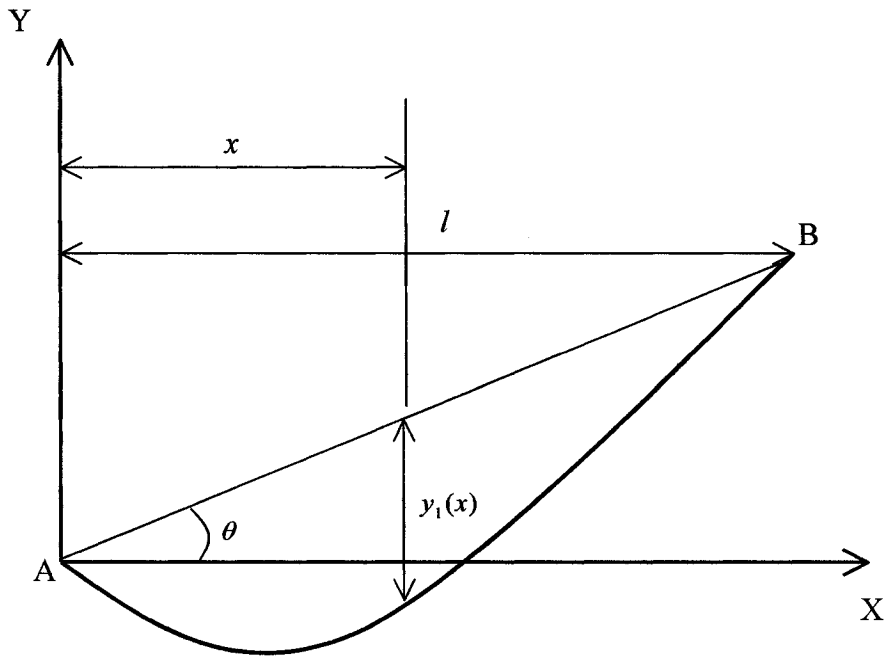

Fig. 3.2 Cable sag

$$\text{Since } y_1(x) = x \cdot \tan\theta - y(x) = x \cdot \tan\theta - \frac{H}{w}\left\{\cosh\left(\frac{w}{H}x + C_1\right) - \cosh(C_1)\right\} \tag{3.9}$$

the cable sag is derived as follows:

$$\delta = \frac{H}{w}\left[\tan\theta\left\{\sinh^{-1}(\tan\theta) - C_1\right\} - \sec\theta + \cosh(C_1)\right] \tag{3.10}$$

where $C_1 = -\alpha + \sinh^{-1}\left(\frac{\alpha \cdot \tan\theta}{\sinh(\alpha)}\right)$ and $\alpha = \frac{wl}{2H}$

3.2.4 Shallow Cables [11]

The higher the tension in a cable is, the smaller the sag of the cable is. When the sag-to-span ratio is below a certain value (say $R = \delta/l < 1/8$), the cable is termed "shallow". When a cable is assumed as a shallow one, the static equilibrium of the cable becomes much simpler.

$$Hy''(x) = w\sqrt{1+\left(y'(x)^2\right)} \longrightarrow Hy''(x) = w \quad \left(\because |y'(x)| << 1 \rightarrow \left(y'(x)\right)^2 \approx 0\right) \tag{3.11}$$

Equation (3.11) is a linear second order equation and the solution is

$$y(x) = \frac{w}{2H}x^2 + C_1 \cdot x + C_2 \tag{3.12}$$

From the boundary conditions $y = 0$ at A and $y = l \cdot \tan\theta$ at B

$$C_1 = \tan\theta - \frac{wl}{H} \text{ and } C_2 = 0$$

Therefore, the static equilibrium equation of a shallow cable is

$$\therefore y(x) = \frac{w}{2H}x(x-l) + \tan\theta \cdot x \tag{3.13}$$

3.3 Dynamics of a Horizontal, Shallow Cable

To start, a horizontal shallow cable will be used to describe the dynamic behavior of a cable. Before the consideration of geometrically nonlinear vibrations, the linear theory for free vibrations of a shallow, horizontal cable will be described and then we proceed to a deep inclined cable.

3.3.1 Dynamics of a Horizontal Shallow Cable [11]

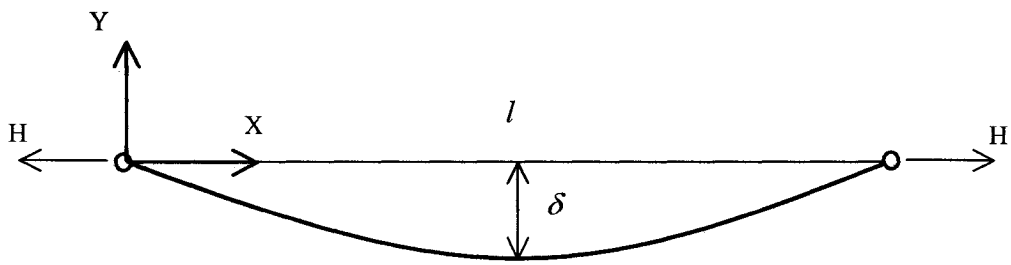

Fig. 3.3 Shallow horizontal cable ($R = \delta/l < 1/8$)

The static equilibrium of a shallow cable is described by Eq. (3.11), which is $Hy''(x) = w$. To obtain the dynamic equilibrium, the following substitution can be applied in considering the dynamic fluctuation of cable tension, vertical deflection, and vertical force acting on the cable.

$$H \rightarrow H + h(t)$$

$$y(x) \rightarrow y(x) + \eta(x,t)$$

$$w \rightarrow w - \frac{w}{g}\ddot{\eta}(x,t)$$

$h(t)$: Change of H due to vibration

$\eta(x,t)$: Dynamic vertical deflection

g : Acceleration due to gravity

t : Time

$h(t)$ is a function of time alone and $\eta(x,t)$ is a function of both position and time. By substituting new variables into Eq. (3.11),

$$\left(H + h(t)\right)\cdot\left(y''(x) + \eta''(x,t)\right) = \left(w - \frac{w}{g}\ddot{\eta}(x,t)\right) \tag{3.14}$$

Consequently, the equation of motion is given by

$$\frac{w}{g}\ddot{\eta}(x,t) + \left(H + h(t)\right)\cdot\eta''(x,t) + h(t)\cdot y''(x) = 0 \tag{3.15}$$

Equation (3.15) is a nonlinear second order differential equation, because of the existence of $h(t)\cdot\eta''(x,t)$. To linearize Eq. (3.15), another assumption can be introduced; the vibration amplitude of a cable is small. The second order term $h(t)\cdot\eta''(x,t)$, because of this assumption, can then be neglected and Eq. (3.15) becomes a linear differential equation as follows:

$$M\cdot\ddot{\eta}(x,t) + H\cdot\eta''(x,t) + h(t)\cdot y''(x) = 0 \tag{3.16}$$

where $M = w/g$: mass per unit length of the cable.

3.3.2 Cable Equation [11]

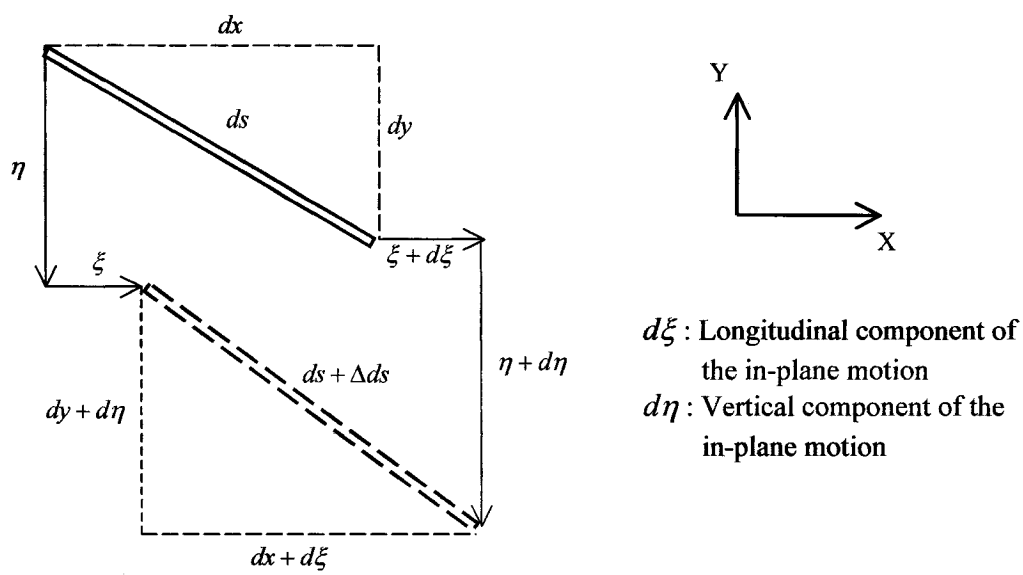

Fig. 3.4 Infinitesimal element of cable in motion

From Fig. 3.4, the dynamic displacement of an infinitesimal cable element due to vibration is expressed as

$$(ds+\Delta ds)^2=(dx+d\xi)^2+(dy+d\eta)^2 \tag{3.17}$$

where $ds^2=dx^2+dy^2$ (3.18)

$d\xi$ is relatively small when compared with $d\eta$, since the assumption is that the cable used is a shallow one. Hence,

$$\Delta ds=\sqrt{ds^2\cdot\left\{1+2\cdot\left(\frac{dx}{ds}\cdot\frac{d\xi}{ds}+\frac{dy}{ds}\cdot\frac{d\eta}{ds}\right)+\left(\frac{d\eta}{ds}\right)^2\right\}}-ds \tag{3.19}$$

and Eq. (3.19) can be rewritten as

$$\frac{\Delta ds}{ds}=\left(\frac{dx}{ds}\right)^2\cdot\left\{\frac{d\xi}{dx}+\frac{dy}{dx}\cdot\frac{d\eta}{dx}+\frac{1}{2}\cdot\left(\frac{d\eta}{dx}\right)^2\right\} \tag{3.20}$$

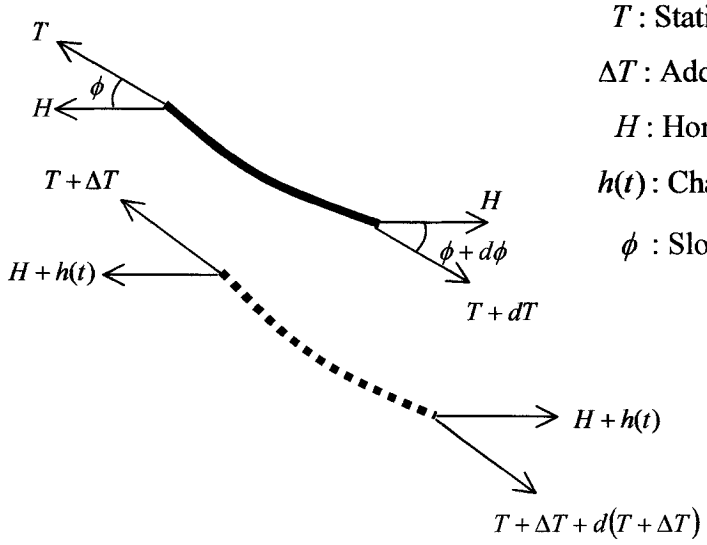

T : Static cable tension

ΔT : Additional cable tension due to vibration

H : Horizontal component of cable tension

$h(t)$: Change of H due to vibration

ϕ : Slope in a cable element

Fig. 3.5 Infinitesimal element of the cable in motion

Figure 3.5 represents the change in cable tension when a cable is vibrating. As long as the material stays in the linearly elastic range,

$$\therefore \frac{\Delta ds}{ds} = \frac{\Delta T}{EA} \quad \text{where } E\text{: Young's modulus}$$

A: Cross sectional area of the cable

By applying the Hooke's law and substituting $\Delta T = h(t) \cdot \sec\phi$ and $\frac{dx}{ds} = \cos\phi$ into Eq. (3.20).

$$\frac{h(t)}{EA}\sec^3\phi = \frac{d\xi}{dx} + \frac{dy}{dx}\cdot\frac{d\eta}{dx} + \frac{1}{2}\cdot\left(\frac{d\eta}{dx}\right)^2 \tag{3.21}$$

Integration of both sides of Eq. (3.21) along the whole length of the cable gives

$$\therefore \frac{h(t)}{EA}\cdot\int_0^l \sec^3\phi = -y''(x)\cdot\int_0^l \eta(x,t)dx + \frac{1}{2}\cdot\int_0^l\left(\frac{d\eta}{dx}\right)^2 dx \tag{3.22}$$

For the case of the linear theory, assuming that the vibration amplitude is small, the second term of the right side of Eq. (3.22) is negligible. By eliminating this term, finally the linearized cable equation is obtained.

$$h(t) = -\frac{EA}{L_E}\cdot y''(x)\cdot\int_0^l \eta(x,t)dx \quad \text{where } L_E = \int_0^l \sec^3\phi\, dx \tag{3.23}$$

A full description of the in-plane motion in the linear theory can be given by concentrating on two equations. These are the equation of motion for vertical component and the cable equation, as follows:

Equation of motion: $M\cdot\ddot{\eta}(x,t) + H\cdot\eta''(x,t) + h(t)\cdot y''(x) = 0$

Cable equation: $h(t) = -\frac{EA}{L_E}\cdot y''(x)\cdot\int_0^l \eta(x,t)dx$

3.3.3 Asymmetric In-plane Modes [11]

When a cable vibrates in an asymmetric mode, no additional cable tension ($h(t)$) is induced by the motion since $\int_0^l \eta\,(x,t)dx = 0$. Therefore, the equation of motion is much simpler.

$$M \cdot \ddot{\eta}(x,t) + H \cdot \eta''(x,t) = 0 \tag{3.24}$$

The solution of this linear homogeneous second order equation is readily given by $\eta(x,t) = \eta(x) \cdot \sin(\omega \cdot t)$, where ω is the circular frequency. By substituting this into Eq. (3.24), the linear second order differential equation for asymmetric modes takes the following form:

$$\eta''(x) - \alpha^2 \cdot \eta(x) = 0 \quad \text{where } \alpha^2 = \frac{M \cdot \omega^2}{H} \tag{3.25}$$

The solution of Eq. (3.25) is given by

$$\eta(x) = C \cdot \cos(\alpha \cdot x) + D \cdot \sin(\alpha \cdot x) \tag{3.26}$$

C and D in Eq. (3.26) are decided by applying boundary conditions $\eta(0) = \eta(l) = 0$.

$\eta(0) = 0 \rightarrow C = 0$ $\qquad$ $\eta(x) = D \cdot \sin\alpha \cdot x$

$\eta(l) = 0 \rightarrow D \cdot \sin(\alpha \cdot l) = 0$ $\qquad$ $\alpha \cdot l = k \cdot \pi \quad [k = 2,4,6,8,\cdots]$

Since $\alpha = \sqrt{\frac{M \cdot \omega^2}{H}}$, the circular frequencies for asymmetric modes are given by

$$\therefore \omega_k = \frac{k \cdot \pi}{l} \cdot \sqrt{\frac{H}{M}} \qquad [k = 2,4,6,8,\cdots] \tag{3.27}$$

Equation (3.27) can be also expressed in a dimensionless form as

$\Omega_k = k \cdot \pi$ $\qquad$ where Ω : Non-dimensional natural frequency, which is

$$\Omega_k = \alpha \cdot l = \omega_k \cdot l \sqrt{\frac{M}{H}} \tag{3.28}$$

The corresponding mode shape is

$$\eta_k(x) = D \cdot \sin\left(\frac{k \cdot \pi}{H} \cdot x\right) \tag{3.29}$$

where $k = 2,4,6,8,\cdots$ and D is the maximum amplitude.

3.3.4 Symmetric In-plane Modes [11]

Unlike the asymmetric in-plane mode, the additional cable tension ($h(t)$) is non-zero when a cable vibration is in symmetric modes. Therefore, the equation of motion has to remain as

$$M \cdot \ddot{\eta}(x,t) + H \cdot \eta''(x,t) + h(t) \cdot y''(x) = 0 \tag{3.30}$$

From Eq. (3.23)

$$h(t) = -\frac{EA}{L_E} \cdot y''(x) \cdot \int_0^l \eta(x)dx \cdot \sin(\omega \cdot t) = -\mathrm{h} \cdot \sin(\omega \cdot t)$$

where $\mathrm{h} = \frac{EA}{L_E} \cdot y''(x) \cdot \int_0^l \eta(x)dx$

The solution of Eq. (3.30) is given by $\eta(x,t) = \eta(x) \cdot \sin(\omega \cdot t)$, where ω is the circular frequency.

$$\therefore \eta''(x) - \alpha^2 \cdot \eta(x) = \frac{\mathrm{h} \cdot w}{H^2} \quad \text{where } \alpha^2 = \frac{M}{H} \cdot \omega^2 \tag{3.31}$$

The general solution of Eq. (3.31) is

$$\eta(x) = A \cdot \sin(\alpha \cdot x) + B \cdot \cos(\alpha \cdot x) + \frac{g \cdot \mathrm{h}}{\omega^2 \cdot H} \tag{3.32}$$

A and B are determined by applying the boundary conditions $\eta(0) = \eta(l) = 0$.

$$\therefore A = \frac{1}{\sin(\alpha \cdot l)} \cdot \left(\frac{g \cdot \mathrm{h}}{\omega^2 \cdot H} \cdot \cos(\alpha \cdot l) - \frac{g \cdot \mathrm{h}}{\omega^2 \cdot H}\right) \text{ and } B = -\frac{g \cdot \mathrm{h}}{\omega^2 \cdot H}$$

Consequently, the frequency equation is given by

$$\tan\left(\frac{\alpha \cdot l}{2}\right) = \frac{\alpha \cdot l}{2} - \frac{(\alpha \cdot l)^3}{2\lambda^2} \text{ where } \lambda^2 = \frac{EA}{H} \cdot \left(\frac{w \cdot l}{H}\right)^2 \cdot \frac{l}{L_E} \tag{3.33}$$

Again, Eq. (3.33) can be rewritten with the non-dimensional frequency (Ω).

$$\tan\frac{\Omega}{2} = \frac{\Omega}{2} - \frac{(\Omega)^3}{2\lambda^2} \tag{3.34}$$

Irvine[5] called λ^2 as the most fundamental parameter for the dynamics of an extensible cable, since it accounts for both geometric and elastic effects.

3.3.5 Modal Crossover [6]

In the previous mathematical formulation, the linearized in-plane modes of a horizontal cable are considered in two classes: the asymmetric mode and the symmetric mode. Two sets of frequency equations are derived as follows:

Asymmetric modes: $\Omega = k \cdot \pi \ \ (k = 2, 3, 4, \cdots)$

Symmetric modes: $\tan\frac{\Omega}{2} = \frac{\Omega}{2} - \frac{(\Omega)^3}{2\lambda^2}$

In the case of the asymmetric mode equation, the natural frequency is independent of the geometric and elastic effects. However, in the case of the symmetric mode, the natural frequency depends on these effects. To obtain the natural frequency in the symmetric modes, a numerical method can be applied. Figure 3.6 represents a graphical solution of Eq. (3.34) with several values of λ^2 $\left(\infty, \pi^2, 4\pi^2, 16\pi^2\right)$. It is seen that as the value of λ^2 changes, the first non-zero roots $(1.3413\pi, 2\pi, \ 2.7375\pi, 2.8566\pi)$, which are the natural frequencies corresponding to the first symmetric mode, are obtained. With this numerical solution, the natural frequencies are plotted in the first, second, and third symmetric modes along λ^2 in Fig. 3.7.

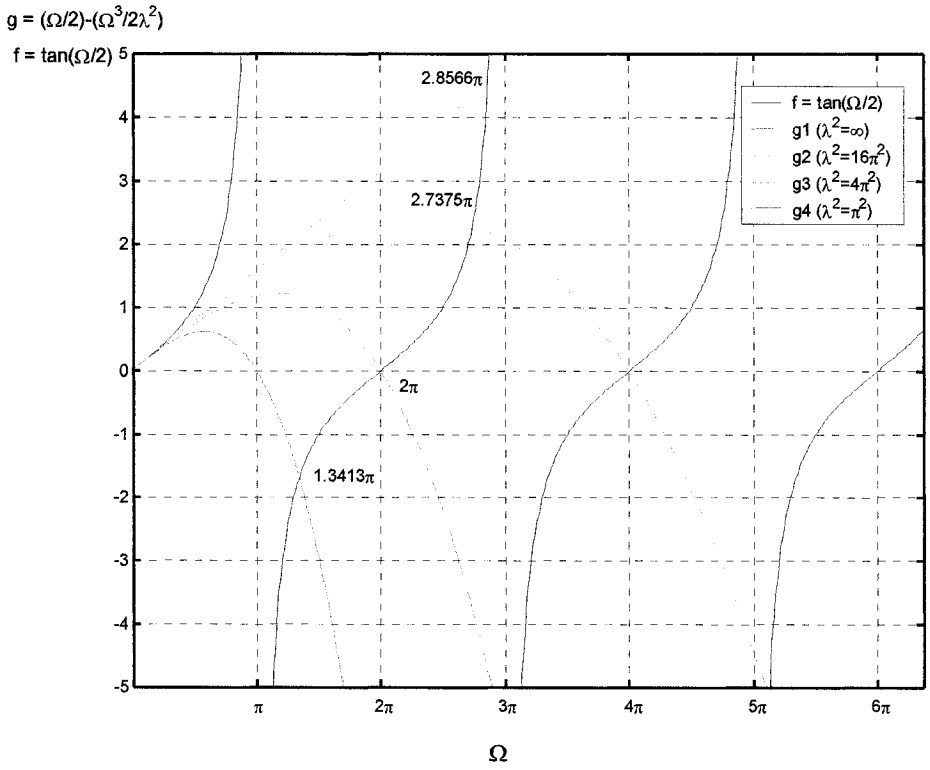

Fig. 3.6 Graphical solution for non-zero root of the symmetric mode equation

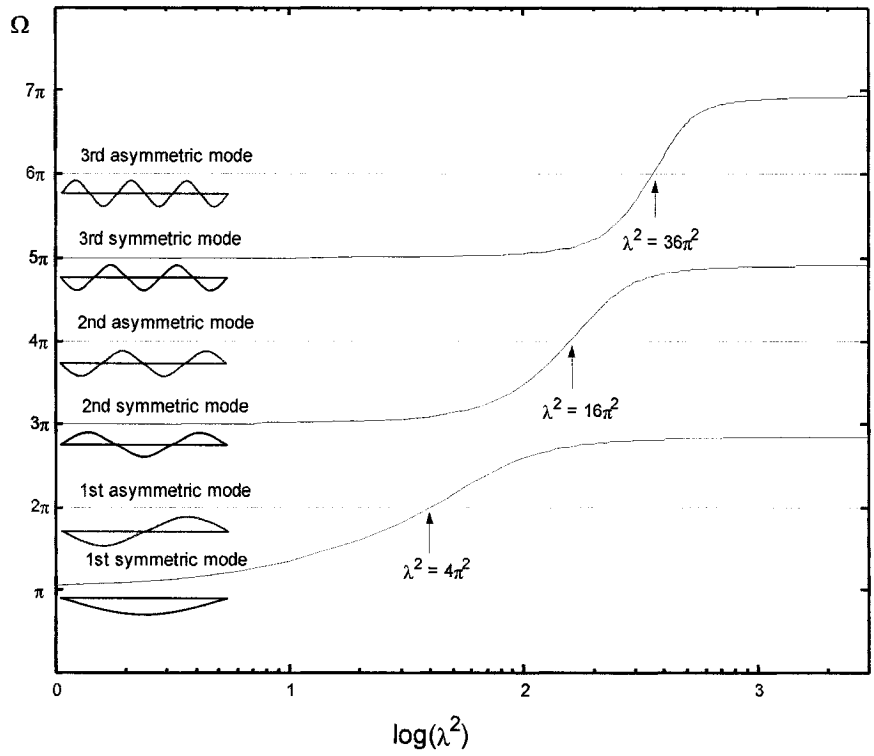

Fig. 3.7 Natural frequencies of shallow horizontal cable

Figure 3.7 shows the natural frequencies plotted as functions of λ^2, in the case of the first three asymmetric and three symmetric modes. In the first symmetric and asymmetric lines, there are three noticeable ranges. At a small λ^2 $\left(\lambda^2 < 4\pi^2\right)$, the symmetric mode frequencies are smaller than those of the asymmetric but they increase toward the first asymmetric line as λ^2 increases. The first symmetric frequency line coincides with the first asymmetric line at $\lambda^2 = 4\pi^2$, and thereafter $\left(\lambda^2 > 4\pi^2\right)$ the first symmetric mode frequencies are greater than the first asymmetric mode frequencies. This phenomenon is called the 'modal crossover' [6]. $\lambda^2 = 4\pi^2$, $\lambda^2 = 16\pi^2$, and $\lambda^2 = 36\pi^2$ are the first, second and third modal crossover points respectively because the symmetric and asymmetric modes have the same natural frequencies at these points.

3.4 Dynamics of a Deep Inclined Cable

Yamaguchi [15] obtained the characteristics of deep inclined cables with good accuracy. He strictly formulated a flexible and extensible cable as a continuum and derived the non-linear governing equations represented in terms of the dynamic displacement. From those governing equations, Yamaguchi proved that the three components of cable motion are coupled in the non-linear terms of the equations but that the out-of-plane and in-plane motions become decoupled in the linear theory, assuming infinitesimally small amplitudes. Therefore, in the linear theory of cable dynamics, the in-plane motion of cable is totally independent of the out-of-plane motion. Also, the eigenvalue problem can be derived from the linearized governing equations of motion. By solving the eigenvalue problem using the Galerkin method, he obtained the natural frequencies and mode shapes of a suspended cable. In Yamaguchi's calculations, he put the material parameter ($k = \sqrt{\frac{EA}{H}}$) as a constant and plotted the non-dimensional frequencies ($\omega^* = \omega / \left(\frac{\pi}{l} \cdot \sqrt{\frac{H}{\rho_o}} \right)$, where ρ_o is the mass per unit length of cable) by varying the sag-to-span ratio (R).

Figure 3.8 shows a plot of numerically analyzed non-dimensional natural frequencies, ω^*, versus the sag-to-span ratios, R, for the six lowest natural frequencies for horizontal cable with k=30, and Fig. 3.9 shows the same information for the inclined cable with $\theta = 30^\circ$ and k=30. Regarding these figures, Yamaguchi concluded that: (1) there exist modal crossovers for in-plane motion of the horizontal cables; and (2) for a very large sag, some natural frequencies for in-plane motion converge to the natural frequencies of a vertically suspended cable which is supported at only one end. In Yamaguchi's results, modal crossover takes place in the case of the horizontal cable. From Fig. 3.8, the first modal crossover occurs at the point where $\log(R) = 0.026$, the second where $\log(R) = 0.052$, and the third where $\log(R) = 0.080$. However, there is no modal crossover when the inclination of cable is 30° (see Fig. 3.9). Triantafyllou [12] also suggested in his studies that the modal crossover never occurs for a taut inclined cable.

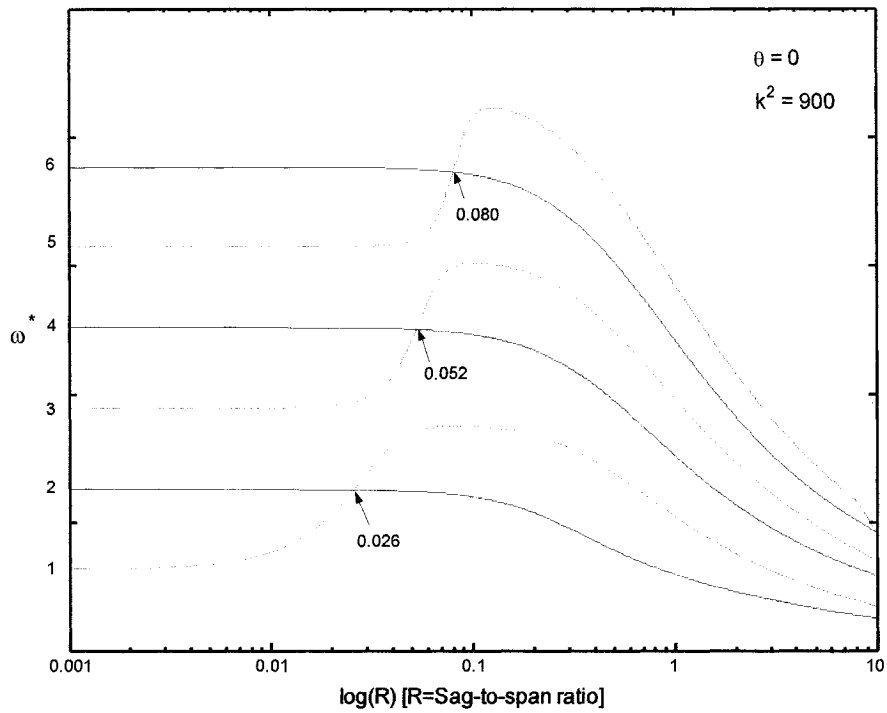

Fig. 3.8 Non-dimensional natural frequency (ω^*) vs. sag-to-span ratio (R)

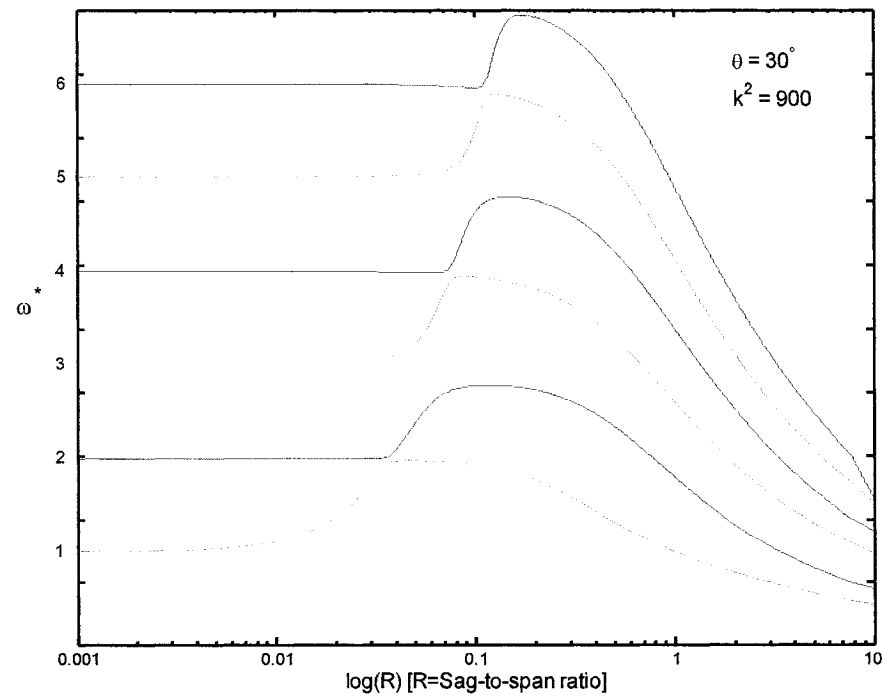

Fig. 3.9 Non-dimensional natural frequency (ω^*) vs. sag-to-span ratio (R)

In order to formulate the dynamics of a deep inclined cable, the general static equilibrium of cable must remain as follows:

$$Hy''(x) = w\sqrt{1+(y'(x))^2}$$

To obtain the dynamic equilibrium, the following substitutions are considered:

$$H \rightarrow H + h(t)$$

$$y(x) \rightarrow y(x) + \eta(x,t)$$

$$w \rightarrow w - \frac{w}{g} \cdot \ddot{\eta}(x,t)$$

Hence

$$\left(H + h(t)\right) \cdot \left(y''(x) + \eta''(x,t)\right) = \left(w - \frac{w}{g} \cdot \ddot{\eta}(x,t)\right) \cdot \sqrt{1+\left(y'(x) + \eta'(x,t)\right)^2} \tag{3.35}$$

It is not possible to solve this nonlinear equation analytically. However, since the principal purpose is to find the natural frequencies of the cable, the linearized eigenvalue problem can be derived by discretizing the cable system into the finite degree-of-freedom system under the finite element method, and the natural frequencies and mode shapes of the inclined deep cable can be numerically obtained by solving this eigenvalue problem.

3.5 Finite Element Method Formulation

There are two general approaches associated with the finite element method. One approach, called the force or flexibility method, uses internal forces as the unknowns of the problem. The second approach, called the displacement or stiffness method, assumes the displacements of the nodes as the unknowns of the problem. For computational purposes of the present project, the stiffness (or displacement) method is more desirable because its formulation is much simpler for the cable problem. The formulation of the stiffness method for the cable dynamics adopted for the project is briefly explained in the following sections.

3.5.1 Discretization and Selection of the Elements

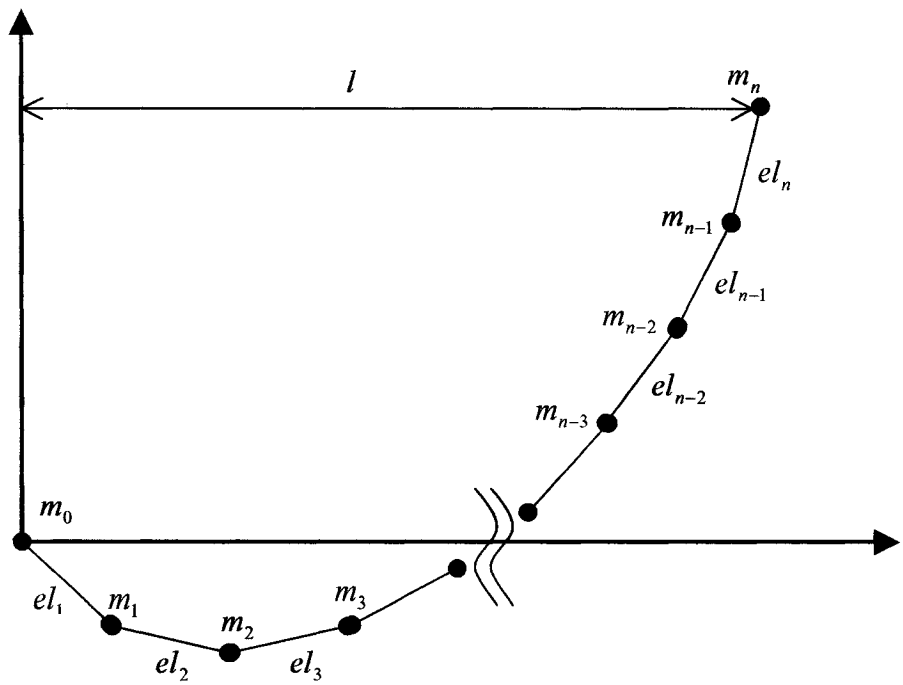

el : Length of the cable element *m* : Lumped mass *n* : Number of the element

Fig. 3.10 A suspended cable system

Figure 3.10 shows the structural model system employed in this project. The following specific points describe the general feature of the model:

1. The cable system is composed of a finite number (n) of discrete structural rod elements (el) joined by frictionless pins. Each element is assumed to be loaded uniaxially and thus the cable has no moment resisting capacity.
2. The cable mass is lumped at the points where the cable elements are connected (m).
3. The joints (nodes) of the elements are free to have displacement both vertically and horizontally within the plane of the catenary, which is the dead load equilibrium configuration.
4. The cable supporting points are fixed; that is to say that there is no displacement at both ends of the cable. Therefore, the mass of the lumped mass at both fixed ends (m_0 & m_n) can be ignored.

3.5.2 Derivation of the Mass Matrix

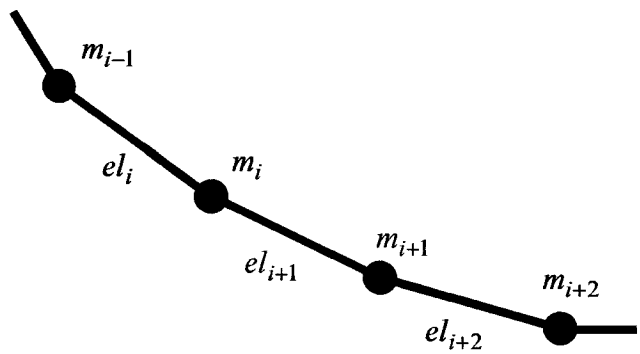

Fig. 3.11 Typical elements and joints

To obtain the masses m_i, lump the total mass of the rod element equally at the two nodes; that is,

$$m_i = \frac{el_i}{2} \times M + \frac{el_{i+1}}{2} \times M = \left(\frac{el_i + el_{i+1}}{2} \right) \times M \tag{3.36}$$

where M is the cable mass per unit length.

When a cable is equally divided by a finite number of elements (n), the length of each element is equal and is given by

$$el = \frac{L}{n} \quad \text{where } L \text{ is the total cable length.} \tag{3.37}$$

Accordingly, the lumped mass is also the same at every joint.

$$m = \frac{L}{n} \cdot M \tag{3.38}$$

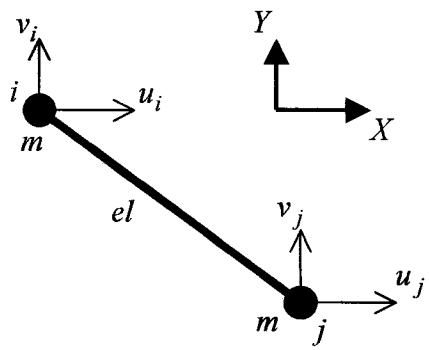

u : Horizontal displacement
v : Vertical displacement

Fig. 3.12 A cable element with lumped masses

In Fig. 3.12, a cable element is shown as two nodes, which are free to move both horizontally and vertically in the plane. Consequently, the mass matrix of a cable element takes the form of a 4×4 matrix.

$$[\mathrm{m}] = \begin{matrix} \\ u_i \\ v_i \\ u_j \\ v_j \end{matrix} \begin{matrix} \begin{matrix} u_i & v_i & u_j & v_j \end{matrix} \\ \begin{bmatrix} m & 0 & 0 & 0 \\ 0 & m & 0 & 0 \\ 0 & 0 & m & 0 \\ 0 & 0 & 0 & m \end{bmatrix} \end{matrix} \tag{3.39}$$

When a cable has n elements, it has $n-1$ nodes, not including both ends of the cable. Therefore, the total mass matrix $[MM]$ becomes $2\cdot(n-1)\times 2\cdot(n-1)$ matrix.

$$
[\mathrm{MM}] = \begin{array}{c} \begin{matrix} u_1 & v_1 & u_2 & v_2 & & & u_{n-2} & v_{n-2} & u_{n-1} & v_{n-1} \end{matrix} \\ \begin{bmatrix} m & 0 & 0 & 0 & \cdots & \cdots & 0 & 0 & 0 & 0 \\ 0 & m & 0 & 0 & \cdots & 0 & 0 & 0 & 0 & 0 \\ 0 & 0 & m & 0 & \cdots & \cdots & 0 & 0 & 0 & 0 \\ 0 & 0 & 0 & m & \cdots & \cdots & 0 & 0 & 0 & 0 \\ \vdots & \vdots & \vdots & \vdots & \ddots & \vdots & \vdots & \vdots & \vdots & \vdots \\ \vdots & \vdots & \vdots & \vdots & \vdots & \ddots & \vdots & \vdots & \vdots & \vdots \\ 0 & 0 & 0 & 0 & \cdots & \cdots & m & 0 & 0 & 0 \\ 0 & 0 & 0 & 0 & \cdots & \cdots & 0 & m & 0 & 0 \\ 0 & 0 & 0 & 0 & \cdots & \cdots & 0 & 0 & m & 0 \\ 0 & 0 & 0 & 0 & \cdots & \cdots & 0 & 0 & 0 & m \end{bmatrix} \end{array} \begin{matrix} u_1 \\ v_1 \\ u_2 \\ v_2 \\ \vdots \\ \vdots \\ u_{n-2} \\ v_{n-2} \\ u_{n-1} \\ v_{n-1} \end{matrix}
\tag{3.40}
$$

3.5.3 Derivation of the Stiffness Matrix

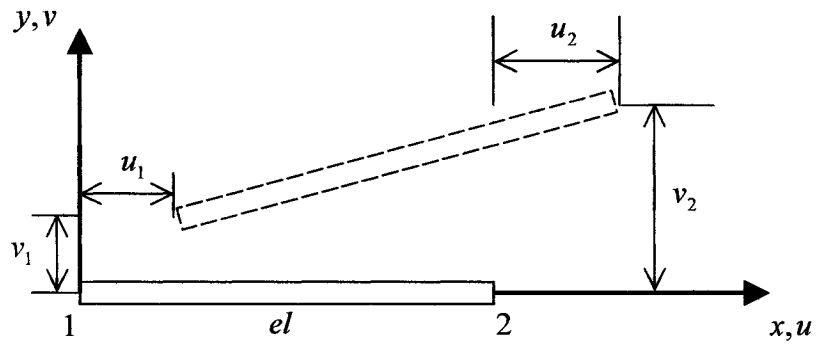

Fig. 3.13 A rod element with the local coordinate system (x, y)

In Fig. 3.13, a rod element lies in a local coordinate system and the nodal dynamic displacement functions u and v are defined. The stiffness matrices for the rod elements are obtained by assuming the displacement functions u and v as follows:

$$
\begin{aligned} u &= a_1 + a_2 \cdot x \\ v &= b_1 + b_2 \cdot x \end{aligned}
\tag{3.41}
$$

where a_1, a_2, b_1, and b_2 are constant.

From the boundary conditions

$$\text{at } x = 0 \rightarrow u_1 = a_1 \text{ and } v_1 = b_1$$
$$\text{at } x = el \rightarrow u_2 = a_1 + a_2 \cdot el \text{ and } v_2 = b_1 + b_2 \cdot el \tag{3.42}$$

By substituting Eq. (3.42) into Eq. (3.41)

$$u = u_1 + (u_2 - u_1) \cdot \frac{x}{el} \qquad v = v_1 + (v_2 - v_1) \cdot \frac{x}{el} \tag{3.43}$$

The strain energy stored in the rod is

$$dU = \sigma_x \cdot dx \cdot dy \cdot dz \cdot d\varepsilon_x$$

$$U = \int_V \left(\int_0^{\varepsilon_x} \sigma_x d\varepsilon_x \right) dV$$

where U : Strain energy
σ_x : Stress in x direction
ε_x : Strain in x direction
V: Volume

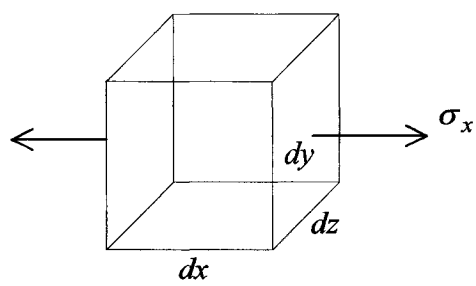

Fig. 3.14 Infinitesimal element

The characteristics of the cable material are assumed to be linear and elastic. Therefore, applying Hooke's law and integrating with respect to ε_x,

$$U = \int_V \frac{1}{2} \cdot E \cdot \varepsilon_x{}^2 dV = \frac{EA}{2} \cdot \int_0^{el} \varepsilon_x{}^2 dx \tag{3.44}$$

The axial strain of a rod element (ε_x) is expressed in terms of the static strain (ε_s), the static equilibrium configuration (x, y), and the dynamic displacement (u, v) by using the definition of strain in reference to the rod element configuration in Fig. 3.13. However, because of the assumption of the small static strain (see assumption 3 in section 3.1), the static strain (ε_s) is overlooked. In Fig. 3.15, an infinitesimal rod element displays only a y-direction displacement. Considering the infinitesimal element of length ds, which is strained by a displacement dv,

$$ds^2 = dx^2 + dv^2$$

$$ds = \sqrt{1+\left(\frac{dv}{dx}\right)^2}\cdot dx \qquad (3.45)$$

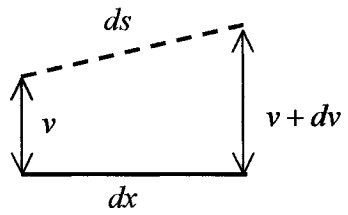

Fig. 3.15 Infinitesimal rod element

Expanding the right-hand-side term in Eq. (3.45) into a power series

$$\frac{ds}{dx} = \left\{1+\frac{1}{2}\cdot\left(\frac{dv}{dx}\right)^2 - \frac{1}{8}\cdot\left(\frac{dv}{dx}\right)^4 + \cdots\right\}$$

and by neglecting the term $\left(dv/dx\right)^4$ and other higher order terms

$$\frac{ds}{dx} = 1+\frac{1}{2}\cdot\left(\frac{dv}{dx}\right)^2 \qquad (3.46)$$

The second term in the right side of Eq. (3.46) is the additional strain in the x direction due to the displacement dv. Therefore, the total strain in the x direction consists of the axial strain due to the displacement u, namely, du/dx and the axial strain due to the displacement v, which is $\frac{1}{2}\cdot\left(\frac{dv}{dx}\right)^2$.

$$\varepsilon_x = \frac{du}{dx}+\frac{1}{2}\cdot\left(\frac{dv}{dx}\right)^2 \qquad (3.47)$$

These combined effects will result in the derivation of the stiffness matrix, by substituting this strain-displacement relation Eq. (3.47) into Eq. (3.44) and expanding it.

$$U = \frac{EA}{2}\cdot\int_0^{el}\left(\frac{du}{dx}\right)^2 + \left(\frac{du}{dx}\right)\cdot\left(\frac{dv}{dx}\right)^2 + \frac{1}{4}\cdot\left(\frac{dv}{dx}\right)^4 dx \qquad (3.48)$$

By eliminating the higher order term $\frac{1}{4}\cdot\left(\frac{dv}{dx}\right)^4$ and substituting Eq. (3.43) into Eq. (3.48).

$$U = \frac{EA}{2}\cdot\int_0^{el}\left(\frac{u_2-u_1}{el}\right)^2+\left(\frac{u_2-u_1}{el}\right)\cdot\left(\frac{v_2-v_1}{el}\right)^2 dx$$

Solving the integration and rearranging it, the strain energy stored in the rod is found as:

$$U=\frac{EA}{2\cdot el}\cdot\left(u_1{}^2-2\cdot u_1\cdot u_2+u_2{}^2\right)+\frac{T}{2\cdot el}\cdot\left(v_1{}^2-2\cdot v_1\cdot v_2+v_2{}^2\right) \tag{3.49}$$

where T: Tension in the rod $\left(T=\frac{EA}{el}\cdot(u_2-u_1)\right)$

By Hamilton's principle,

$$\begin{aligned}
\frac{\partial U}{\partial u_1} &= \frac{EA}{el}\cdot(u_1-u_2)\\
\frac{\partial U}{\partial v_1} &= \frac{T}{el}\cdot(v_1-v_2)\\
\frac{\partial U}{\partial u_2} &= \frac{EA}{el}\cdot(-u_1+u_2)\\
\frac{\partial U}{\partial v_2} &= \frac{T}{el}\cdot(-v_1+v_2)
\end{aligned} \tag{3.50}$$

By rewriting Eq. (3.50) in the form of matrix.

$$[k]\{u\}=\left(\frac{EA}{el}\cdot\begin{bmatrix}1&0&-1&0\\0&0&0&0\\-1&0&1&0\\0&0&0&0\end{bmatrix}+\frac{T}{el}\cdot\begin{bmatrix}0&0&0&0\\0&1&0&-1\\0&0&0&0\\0&-1&0&1\end{bmatrix}\right)\begin{Bmatrix}u_1\\v_1\\u_2\\v_2\end{Bmatrix} \tag{3.51}$$

where $[k]$: Element stiffness matrix in the local coordinate

$\{u\}$: Vector of nodal displacements in the local coordinate

Equation (3.51) represents the relationship between stiffness and displacement of a rod element in the local coordinate system. Since elements of a cable are free to displace in the plane, these rod elements are inclined at various angles to the horizontal. Therefore, the element stiffness matrix in the global coordinate ($[K]$) should be obtained.

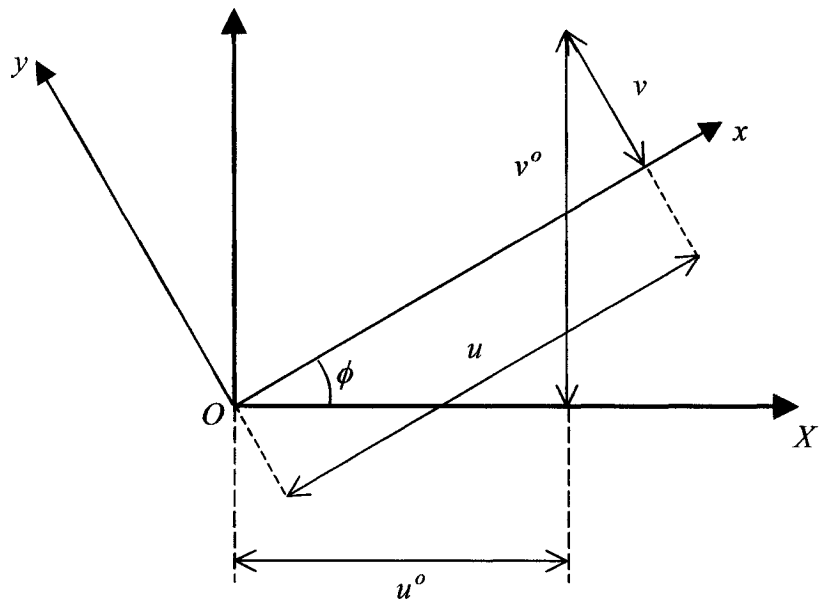

Fig. 3.16 Global (X,Y) and local (x,y) coordinate systems

Figure 3.16 represents the relation between the global coordinate and the local coordinate. From Fig. 3.16, the relationship between the local displacement functions u and v, and the global displacements functions u^o and v^o can be define as follows:

$$\begin{aligned} u &= u^o \cdot \cos\phi + v^o \cdot \sin\phi \\ v &= v^o \cdot \cos\phi - u^o \cdot \sin\phi \end{aligned} \tag{3.52}$$

Equation (3.52) can be rewritten in the form of a matrix.

$$\begin{Bmatrix} u \\ v \end{Bmatrix} = \begin{bmatrix} \cos\phi & \sin\phi \\ -\sin\phi & \cos\phi \end{bmatrix} \begin{Bmatrix} u^o \\ v^o \end{Bmatrix}$$

Since an element has two nodal points

$$\begin{Bmatrix} u_1 \\ v_1 \\ u_2 \\ v_2 \end{Bmatrix} = \begin{bmatrix} \cos\phi & \sin\phi & 0 & 0 \\ -\sin\phi & \cos\phi & 0 & 0 \\ 0 & 0 & \cos\phi & \sin\phi \\ 0 & 0 & -\sin\phi & \cos\phi \end{bmatrix} \begin{Bmatrix} u_1^o \\ v_1^o \\ u_2^o \\ v_2^0 \end{Bmatrix} \text{ or } \{u\} = [\mathrm{Tr}]\{u^o\} \tag{3.53}$$

$$\text{where } [\mathrm{Tr}] = \begin{bmatrix} \cos\phi & \sin\phi & 0 & 0 \\ -\sin\phi & \cos\phi & 0 & 0 \\ 0 & 0 & \cos\phi & \sin\phi \\ 0 & 0 & -\sin\phi & \cos\phi \end{bmatrix} \text{ and } \begin{matrix} \{u\}: \text{Local vector} \\ \{u^o\}: \text{Global vector} \end{matrix}$$

The relationship between the global force and the local force is similar to that of displacement. Therefore, it can be written as

$$\{f\} = [\mathrm{Tr}]\{F\} \tag{3.54}$$

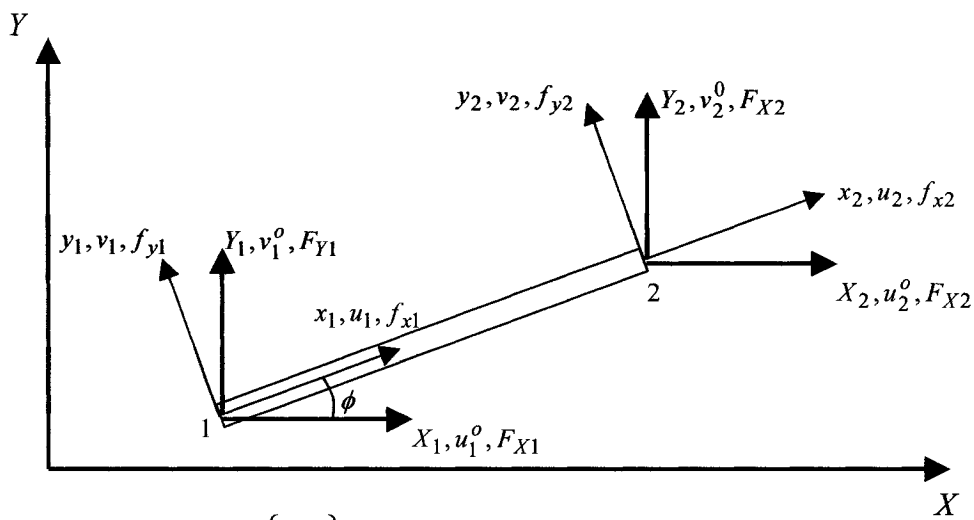

$$\{f\} = \begin{Bmatrix} f_{x1} \\ f_{y1} \\ f_{x2} \\ f_{y2} \end{Bmatrix} : \text{Local force} \qquad \{F\} = \begin{Bmatrix} F_{X1} \\ F_{Y1} \\ F_{X2} \\ F_{Y2} \end{Bmatrix} : \text{Global force}$$

Fig. 3.17 A rod element in local and global coordinate systems

The force-displacement relationships are

$$\{f\}=[k]\{u\} \text{ and } \{F\}=[K]\{u^o\} \tag{3.55}$$

By substituting Eq. (3.55) and Eq. (3.53) into Eq. (3.54).

$$[\mathrm{Tr}][K]\{u^o\}=[k][\mathrm{Tr}]\{u^o\}\rightarrow[K]\{u^o\}=[\mathrm{Tr}]^{-1}[k][\mathrm{Tr}]\{u^o\} \tag{3.56}$$

Therefore, the global element stiffness matrix is

$$[K]=[\mathrm{Tr}]^{-1}[k][\mathrm{Tr}] \tag{3.57}$$

By substituting $[\mathrm{Tr}]^{-1}$, $[Tr]$, and $[k]$ into Eq. (3.57).

$$[\mathrm{Tr}]^{-1}=\begin{bmatrix}\cos\phi & -\sin\phi & 0 & 0\\ \sin\phi & \cos\phi & 0 & 0\\ 0 & 0 & \cos\phi & -\sin\phi\\ 0 & 0 & \sin\phi & \cos\phi\end{bmatrix} \qquad [\mathrm{Tr}]=\begin{bmatrix}\cos\phi & \sin\phi & 0 & 0\\ -\sin\phi & \cos\phi & 0 & 0\\ 0 & 0 & \cos\phi & \sin\phi\\ 0 & 0 & -\sin\phi & \cos\phi\end{bmatrix}$$

$$[k]=\left(\frac{EA}{el}\cdot\begin{bmatrix}1 & 0 & -1 & 0\\ 0 & 0 & 0 & 0\\ -1 & 0 & 1 & 0\\ 0 & 0 & 0 & 0\end{bmatrix}+\frac{T}{el}\cdot\begin{bmatrix}0 & 0 & 0 & 0\\ 0 & 1 & 0 & -1\\ 0 & 0 & 0 & 0\\ 0 & -1 & 0 & 1\end{bmatrix}\right)$$

$$\therefore[K]=\frac{EA}{el}\begin{bmatrix}C^2 & S\cdot C & -C^2 & -S\cdot C\\ S\cdot C & S^2 & -S\cdot C & -S^2\\ -C^2 & -S\cdot C & C^2 & S\cdot C\\ -S\cdot C & -S^2 & S\cdot C & S^2\end{bmatrix}+\frac{T}{el}\begin{bmatrix}S^2 & -S\cdot C & -S^2 & S\cdot C\\ -S\cdot C & C^2 & S\cdot C & -S^2\\ -C^2 & S\cdot C & S^2 & -S\cdot C\\ S\cdot C & -C^2 & -S\cdot C & C^2\end{bmatrix} \tag{3.58}$$

C: Abbreviation of $\cos\phi$

S: Abbreviation of $\sin\phi$

Up to the present, the stiffness matrix for a single cable element has been dealt with. The stiffness matrix $[K]$, which is obtained in the previous formulation, represents the global stiffness matrix for an individual cable element by forming a 4×4 matrix. To obtain the overall structural stiffness matrix for a complete cable structure, combine these individual elements in an ordered and sequential manner through a direct stiffness method. Referring

to a two-cable element assemblage in Fig. 3.18, the stiffness matrix for each cable element is as follows:

$$[K]^{i-j} = \begin{array}{c} \begin{matrix} u_i & v_i & u_j & v_j \end{matrix} \\ \begin{bmatrix} k_{11}^{i-j} & k_{12}^{i-j} & k_{13}^{i-j} & k_{14}^{i-j} \\ k_{21}^{i-j} & k_{22}^{i-j} & k_{23}^{i-j} & k_{24}^{i-j} \\ k_{31}^{i-j} & k_{32}^{i-j} & k_{33}^{i-j} & k_{34}^{i-j} \\ k_{41}^{i-j} & k_{42}^{i-j} & k_{43}^{i-j} & k_{44}^{i-j} \end{bmatrix} \end{array} \begin{matrix} u_i \\ v_i \\ u_j \\ v_j \end{matrix}$$

$$[K]^{j-r} = \begin{array}{c} \begin{matrix} u_j & v_j & u_r & v_r \end{matrix} \\ \begin{bmatrix} k_{11}^{j-r} & k_{12}^{j-r} & k_{13}^{j-r} & k_{14}^{j-r} \\ k_{21}^{j-r} & k_{22}^{j-r} & k_{23}^{j-r} & k_{24}^{j-r} \\ k_{31}^{j-r} & k_{32}^{j-r} & k_{33}^{j-r} & k_{34}^{j-r} \\ k_{41}^{j-r} & k_{42}^{j-r} & k_{43}^{j-r} & k_{44}^{j-r} \end{bmatrix} \end{array} \begin{matrix} u_j \\ v_j \\ u_r \\ v_r \end{matrix}$$

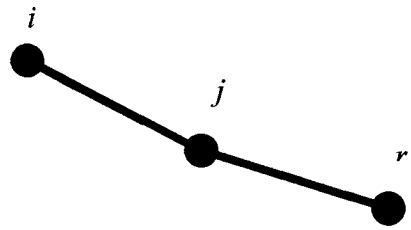

Fig. 3.18 Two-cable element

The combined matrix of this two-cable element assemblage by direct stiffness method takes the form of a 6×6 matrix.

$$[K]^{i-j-k} = \begin{array}{c} \begin{matrix} u_i & v_i & u_j & v_j & u_r & v_r \end{matrix} \\ \begin{bmatrix} k_{11}^{i-j} & k_{12}^{i-j} & k_{13}^{i-j} & k_{14}^{i-j} & 0 & 0 \\ k_{21}^{i-j} & k_{22}^{i-j} & k_{23}^{i-j} & k_{24}^{i-j} & 0 & 0 \\ k_{31}^{i-j} & k_{23}^{i-j} & k_{33}^{i-j}+k_{11}^{j-r} & k_{34}^{i-j}+k_{12}^{j-r} & k_{13}^{j-r} & k_{14}^{j-r} \\ k_{41}^{i-j} & k_{24}^{i-j} & k_{34}^{i-j}+k_{21}^{j-r} & k_{44}^{i-j}+k_{22}^{j-r} & k_{23}^{j-r} & k_{24}^{j-r} \\ 0 & 0 & k_{31}^{j-r} & k_{32}^{j-r} & k_{33}^{j-r} & k_{34}^{j-r} \\ 0 & 0 & k_{41}^{j-r} & k_{42}^{j-r} & k_{34}^{j-r} & k_{44}^{j-r} \end{bmatrix} \end{array} \begin{matrix} u_i \\ v_i \\ u_j \\ v_j \\ u_r \\ v_r \end{matrix} \tag{3.59}$$

When a cable has n elements, the combined total stiffness matrix $[KK]$ forms a $2\cdot(n+1)\times2\cdot(n+1)$ matrix. However, the both ends of the cable are assumed to be fixed. Therefore, the total stiffness matrix is forming a $2\cdot(n-1)\times2\cdot(n-1)$ matrix.

3.6 Description of the Flow of Calculation

The description of the flows of calculation used in this study is given in this section. The program is based on Matlab, which provides M-file to write the program. The program, which is used to calculate the natural frequency of a suspended cable, is composed of four M-files. The flowchart of the program designed is as follows:

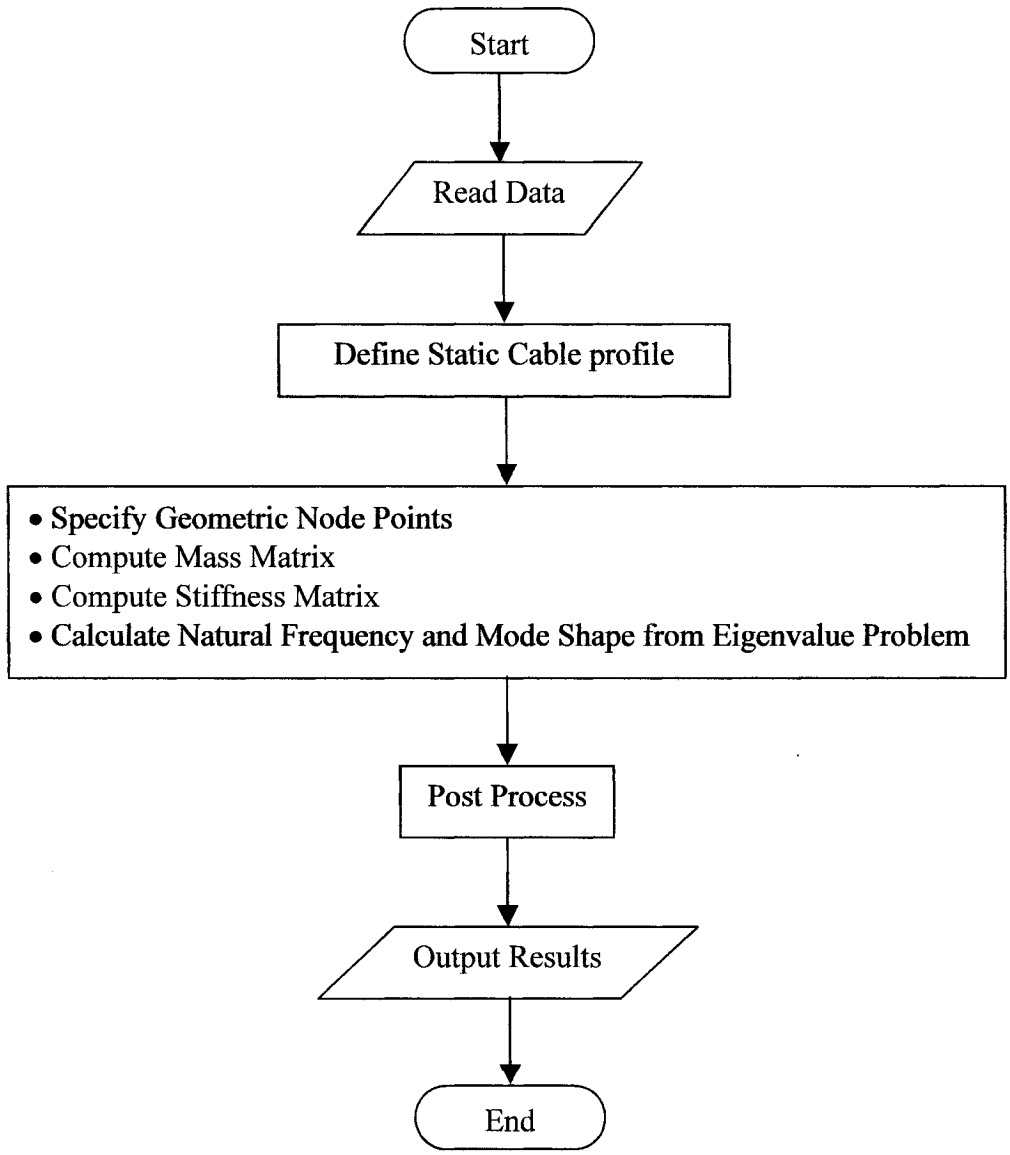

Fig. 3.19 Flowchart of cable program

3.6.1 Read Data

Before defining the geometric shape of the static cable and further calculating the natural frequency, there are seven essential parameters required as input data.

- Diameter of cable (Di)
- Young's modulus of elasticity (E)
- Total cable length (L)
- Mass per unit length of cable (M)
- Inclination of cable (θ)
- Sag to span ratio of cable (R)
- Number of element (n)

Therefore, the first M-file will be used to input these essential data and these data will remain constant throughout the whole process in the program.

3.6.2 Defining Cable Profile

From Eq. (3.5), the static equilibrium of cable is

$$y(x) = \frac{H}{w}\left\{\cosh\left(\frac{w}{H}x + C_1\right) - \cosh(C_1)\right\}$$

$$\text{where } C_1 = -\alpha + \sinh^{-1}\left(\frac{\alpha \cdot \tan\theta}{\sinh(\alpha)}\right) \text{ and } \alpha = \frac{wl}{2H}$$

In this equation, unknown parameters from the input data are span length (l), horizontal cable tension (H), and α. To obtain these parameters, Eq. (3.10) can be used.

$$\delta = \frac{H}{w}\left[\tan\theta\left\{\sinh^{-1}(\tan\theta) - C_1\right\} - \sec\theta + \cosh(C_1)\right]$$

By substituting $H = \frac{wl}{2\alpha}$ into Eq. (3.10) and arranging this, the newly obtained equation becomes:

$$\frac{\delta}{l} = R = \frac{1}{2\alpha} \cdot \left[\tan\theta \cdot \left\{ \sinh^{-1}(\tan\theta) - C_1 \right\} - \sec\theta + \cosh(C_1) \right] \tag{3.60}$$

By solving this first-degree equation, parameter α can be obtained. Since α is known, the span length (l) is given from Eq. (3.8).

$$l = \frac{L \cdot \alpha}{\sqrt{\sinh^2 \alpha + (\alpha \cdot \tan\theta)^2}} \tag{3.61}$$

Consequently, the horizontal tension is $H = \frac{wl}{2\alpha}$ (3.62)

3.6.3 Specifying Geometric Node Points

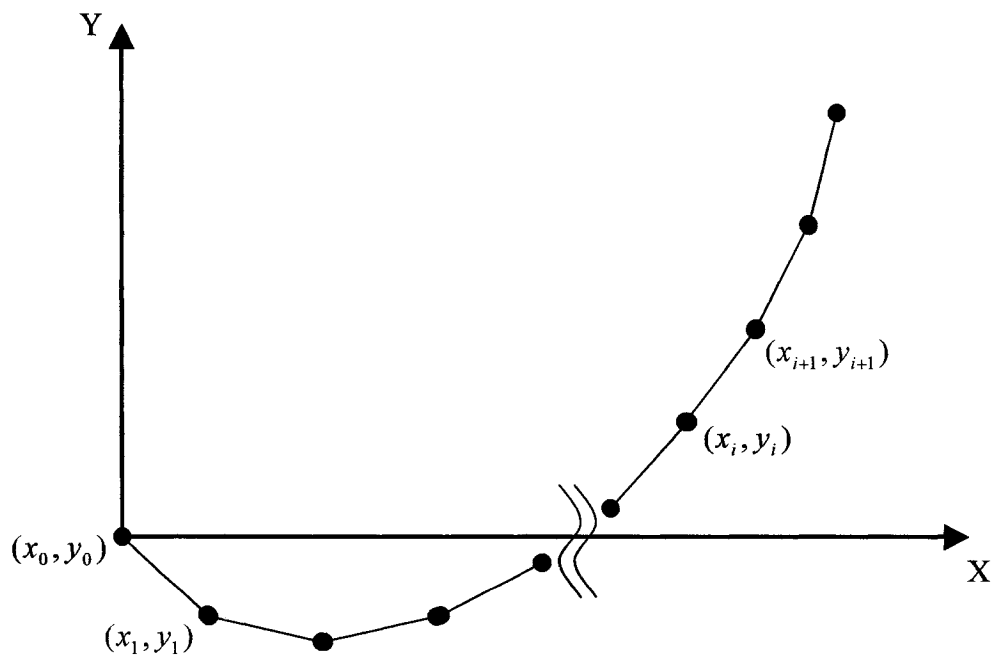

Fig. 3.20 Cable in the global coordinate

In Fig. 3.20, a cable is divided by n elements in the global coordinate system and each element has equal length $\left(el = L/n\right)$. From Eq. (3.6)

$$el = \int_{x_i}^{x_{i+1}} ds = \int_{x_i}^{x_{i+1}} \sqrt{1 + (y')^2}\, d = \int_{x_i}^{x_{i+1}} \cosh\left(\frac{w}{H}x + C_1\right)dx$$

$$= \frac{H}{w} \cdot \sinh\left(\frac{w}{H} \cdot x_{i+1} + C_1\right) - \frac{H}{w} \cdot \sinh\left(\frac{w}{H}x_i + C_1\right) \tag{3.63}$$

Rearranging Eq. (3.63) for x_{i+1}.

$$x_{i+1} = \frac{H}{w} \cdot \sinh^{-1}\left(\frac{w}{H} \cdot \frac{L}{k} + \sinh\left(\frac{w}{H} \cdot x_i + C_1\right)\right) - \frac{H}{w} \cdot C_1 \tag{3.64}$$

From Fig. 3.20, $x_0 = 0$.

$$x_1 = \frac{H}{w} \cdot \sinh^{-1}\left(\frac{w}{H} \cdot \frac{L}{k} + \sinh\left(\frac{w}{H} \cdot 0 + C_1\right)\right) - \frac{H}{w} \cdot C_1 \tag{3.65}$$

Therefore, all x coordinates can be obtained when coordinates $x_1, x_2, x_3 \cdots$ are substituted into Eq. (3.64) sequentially and y coordinates are

$$y_i = \frac{H}{w}\left\{\cosh\left(\frac{w}{H}x_i + C_1\right) - \cosh(C_1)\right\} \tag{3.66}$$

3.6.4 Mass and Stiffness Matrix

The next step in specifying geometric mode points is generating the total mass matrix $[MM]$ and total stiffness matrix $[KK]$ based on the finite element method formulation obtained earlier. When a cable has n elements, the total mass and stiffness matrices will take on the form of a $2 \cdot (n-1) \times 2 \cdot (n-1)$ matrix respectively.

3.6.5 Eigenvalue Problem

The equation for the undamped free vibration is

$$M \cdot \ddot{u} + K \cdot u = 0 \tag{3.67}$$

where M : Mass K : Stiffness

This equation has a solution in the form $u = q \cdot \sin(\omega \cdot t + \phi)$, where q is an arbitrary vector, ω is the circular frequency of vibration, and ϕ is a phase angle. When this solution is substituted into the Eq. (3.67), it gives

$$\left(K - \omega^2 M\right) \cdot q \cdot \sin(\omega \cdot t + \phi) = 0 \tag{3.68}$$

Since Eq. (3.68) must be true for all values of t, $\sin(\omega \cdot t + \theta)$ is omitted.

$$\left(K - \omega^2 M\right) \cdot q = 0 \tag{3.69}$$

Therefore, substituting the total mass and stiffness matrices into Eq. (3.69) and solving this equation will allow us to determine q and ω.

CHAPTER 4

RESULTS AND DISCUSSION

4.1 Parameters as Input Data

As described in the previous chapter, to perform the present computer program, 7 parameters are needed as input data. Once these parameters are determined, the program performs the calculation and produces the natural frequencies and corresponding mode shapes as output.

4.1.1 Mechanical Properties of Cables

To investigate the natural frequencies and corresponding mode shapes, a typical cable is chosen. In order to examine the characteristics of inclined cables, the cable inclination angle is varied throughout the calculation. Also, to examine the role of axial stiffness, two different Young's moduli are chosen. Table 4.1 shows the physical properties of a cable used for the calculations.

Table 4.1 Mechanical properties of cable model

	Material Properties	Physical dimensions
Case #1	$E = 2\times10^{11} N/m^2$ $M = 5.55kg/m$	$L = 100m$ $Di = 0.03m$
Case #2	$E = 2\times10^{10} N/m^2$ $M = 5.55kg/m$	$L = 100m$ $Di = 0.03m$

* L: Total cable length Di: Diameter of cable M: Mass per unit length of cable

Case #1 is equivalent to actual steel cable with diameter of $30\,mm$. Case #2 is not a simulation of actual materials. However, for the purpose of investigating the effect of axial stiffness, an E divided by a factor of 10 on Case #1 is given.

4.1.2 Convergence of Finite Element Calculation

The accuracy of calculation results depends upon the number of cable elements (n) in the finite element modeling. In order to check the accuracy of the finite element calculation, comparison can be made with the analytical solution from the linear theory. For the application of the linear theory in Chapter 3, the sag-to-span ratio should be smaller than 1/8. The mechanical properties of the cable assumed for this calculation are as follows:

- Young's modulus of elasticity (E) = $2\times10^{11}\,N/m^2$
- Mass per unit length of the cable (M)= $5.55\,kg/m$
- Sag-to-span ratio ($R=\delta/l$) = 1/10
- Total cable length (L)= $100\,m$
- Diameter of cable (D)= $0.03\,m$
- Inclination angle of cable (θ)= 0°

From the linear theory in Chapter 3, the horizontal cable tension is $6711.8\,N$ and the span length is $97.448\,m$. Therefore, the first, second, and third asymmetric natural frequencies are derived from Eq (3.27), which is $\omega_k = \frac{k\cdot\pi}{l}\cdot\sqrt{\frac{H}{M}}$

$$\omega_2 = \frac{2\times\pi}{97.448}\cdot\sqrt{\frac{6711.8}{5.55}} = 2.2422\ rad/s \qquad (1^{st}\text{ asymmetric natural frequency})$$

$$\omega_4 = \frac{4\times\pi}{97.448}\cdot\sqrt{\frac{6711.8}{5.55}} = 4.4845\ rad/s \qquad (2^{nd}\text{ asymmetric natural frequency})$$

$$\omega_6 = \frac{6\times\pi}{97.448}\cdot\sqrt{\frac{6711.8}{5.55}} = 6.7267\ rad/s \qquad (3^{rd}\text{ asymmetric natural frequency})$$

In Fig. 4.1, the first, second, and third asymmetric natural frequencies calculated from the finite element method are plotted against the number of cable elements assumed for simulation. The figure shows the convergence of the natural frequency as the number of cable elements increases. In actuality, each natural frequency is seen converging to 2.1387, 4.3880, and 6.6081, and these values are realized when the number of elements (n) is between 90 and 100. Therefore, discretizing the cable by 100 elements will prove sufficient to obtain stable results from the finite element calculation for this case.

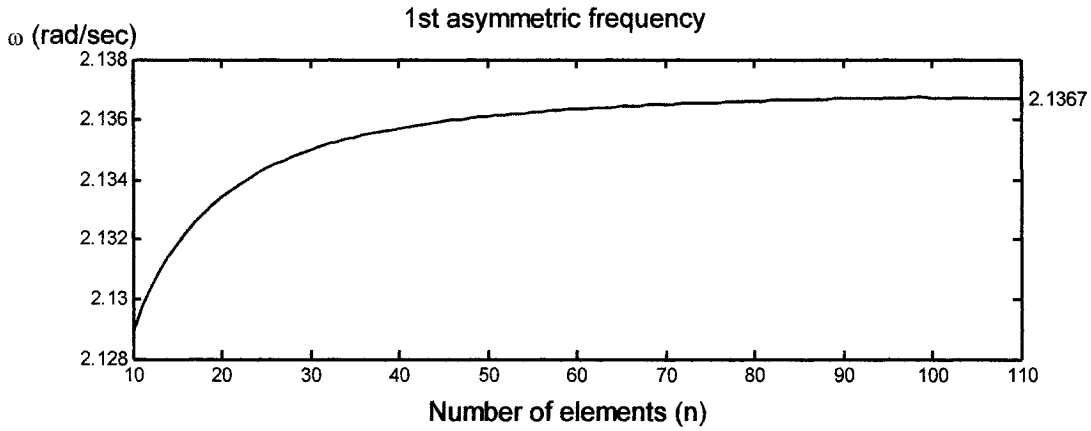

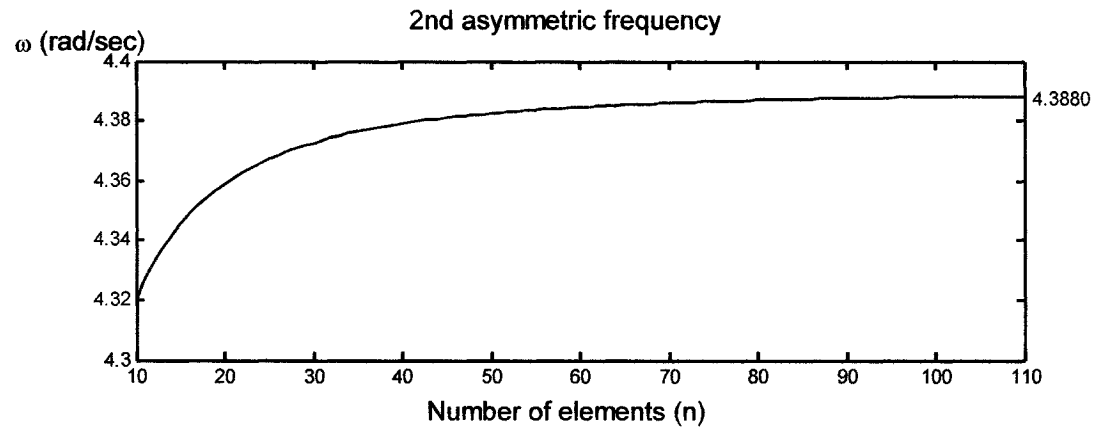

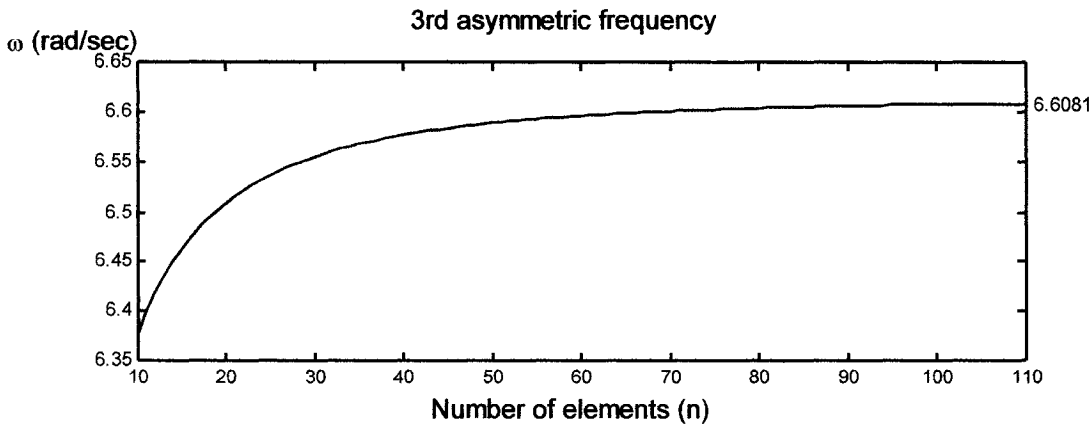

Fig.4.1 1st, 2nd, and 3rd natural frequencies as number of elements increases

4.1.3 Sag-to-Span Ratio (R) and Sag-to-Total Cable Length Ratio (RR)

When the calculation is initiated, the sag-to-span ratio (R) is required as an input data. However, once results are obtained, the sag-to-total cable length ratio (RR) can be used as a convenient parameter to describe the results. Both R and RR are the functions of the horizontal cable tension (H), but the difference between these two parameters becomes distinct as H decreases. R becomes infinite when H is equal to zero, whereas, RR becomes 0.5 under the same condition ($H = 0$). Therefore, using RR as a parameter is more convenient in illustrating the results on figures and interpreting them. The results of the finite element calculation are composed of two cases of the Young's moduli, $2 \times 10^{11} N/m^2$ and $2 \times 10^{10} N/m^2$. In each case, the inclination and the cable span are changed.

4.2 Case #1

4.2.1 Input Parameters

The following properties are assumed for this case:

•Young's modulus (E): $2\times10^{11} N/m^2$	•Cable length (L): $100m$
•Mass per unit length of cable (M): $5.55kg/m$	•Cable diameter (Di): $0.03m$
•Inclination angle of cable (θ): 0, 1°, 10°, 30°, 60°, 80°	

This case is equivalent to an actual steel cable of given dimensions. The natural frequency is expressed in a dimensionless form as $\Omega = \omega \cdot l \cdot \sqrt{\frac{M}{H}}$ (see Eq. (3.28)) and the sag-to-span ratio is in the log scale ($\log(RR^3)$) for explicit presentation. Some values of the sag-to-total cable length ratio corresponding to the log scale are given in Table 4.2.

Table 4.2 Sag-to-total cable length (RR) with corresponding log scale ($\log(RR^3)$)

$\log(RR^3)$	RR	$\log(RR^3)$	RR	$\log(RR^3)$	RR
-9	0.00100	-6	0.01000	-3	0.09942
-8.5	0.00147	-5.5	0.01468	-2.5	0.14655
-8	0.00215	-5	0.02154	-2	0.21547
-7.5	0.00316	-4.5	0.03163	-1.5	0.31653
-7	0.00464	-4	0.04641	-1	0.46414
-6.5	0.00689	-3.5	0.06814	-0.90309	0.5

4.2.2 Horizontal Cable $[\theta = 0^\circ]$

In Fig. 4.4 (a), the six non-dimensional natural frequencies are plotted against the sag-to-total cable length ratio in log scale ($\log(RR^3)$) when the cable is horizontal and the level between $\log(RR^3) = -6$ and $\log(RR^3) = -4$ is enlarged in Fig. 4.4 (b) to clarify the behaviour around the modal crossovers. Fig. 4.4 (b) shows that the first and second frequencies coincide at the point where $\log(RR^3) = -5.5292$ (First frequency and mode crossover), the third and fourth frequencies do the same at $\log(RR^3) = -4.9268$ (Second frequency and mode crossover), and the fifth and sixth frequencies cross at $\log(RR^3) = -4.5749$ (Third frequency and mode crossover). The exact values of $\log(RR^3)$ and RR at the first three modal (or frequency) crossover points are listed in Table 4.3.

Table 4.3 Exact modal crossover points

	$\log(RR^3)$	Sag-to-total cable length (RR)
1st modal crossover point	$-5.529171945\cdots$	$0.014353\cdots$
2nd modal crossover point	$-4.926824195\cdots$	$0.022789\cdots$
3rd modal crossover point	$-4.574948773\cdots$	$0.029855\cdots$

Before the first modal crossover point at $\log(RR^3) = -5.5292$, the frequency of the first symmetric mode is less than the frequency of the first asymmetric mode and after the point, the first symmetric mode frequency becomes greater than the first asymmetric mode frequency. Similar phenomena are observed between the third and fourth frequency lines and also between the fifth and sixth frequencies. Figure 4.5 to Fig. 4.10 depict the mode shapes being clearly different immediately before and after each modal crossover point. Figure 4.11 to Fig. 4.14 illustrate the first six mode shapes for different levels of $\log(RR^3)$, at points A, B, C, and D in Fig. 4.4 (b). The point A is before the first modal crossover, B between the first and second modal crossover, C between the second and third modal crossover, and D is after the third modal crossover. These four figures (from Fig. 4.11 to Fig 4.14) demonstrate that the mode shapes change at each modal crossover point. In Fig. 4.4 (a), it is also shown that all first six natural frequencies converge to the

natural frequencies of a vertically suspended cable when the sag-to-total cable length ratio increases (for a large sag). Figure 4.15 describes the first six mode shapes at level E with a large sag.

Forghani-Arani [2] also suggested the existence of frequency and modal crossover points for the horizontal cables. He investigated natural frequencies and mode shapes of vibration of the horizontal and inclined cables by using the Finite Element Method. By doing that, he presented frequency and modal crossover points and corresponding mode shapes for the horizontal cable in his paper. Figure 4.2 represents the Forghani-Arani's results of his research with horizontal cables.

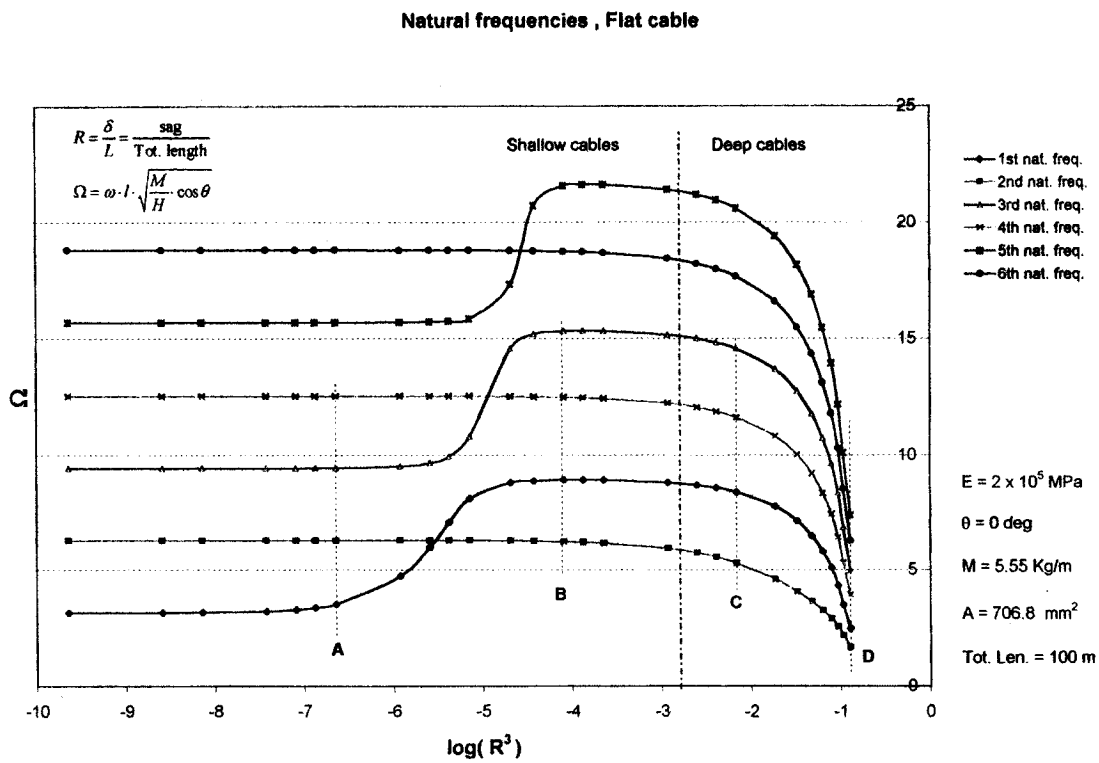

Fig. 4.2 Natural frequencies of the horizontal cable from Forghani-Arani's paper

In Fig. 4.2, six natural frequencies are plotted along the sag-to-total cable length ratio. He differed these lines of frequencies with corresponding mode shapes; that is, the first, third, and fifth lines are sorted into the frequencies of symmetric mode and the second, fourth, and sixth lines the frequencies of asymmetric mode. In the case of horizontal cables, the

result presented in the Forghani-Arani's report is in agreement with the results of this study: (1) the existence of frequency and modal crossover points; (2) the change of mode shapes around the crossover points; and (3) the convergence of frequencies and mode shapes for the large sag-to-total cable length ratio to the frequencies and mode shapes of the vertically suspended cable. Figure 4.3 depicts the first four mode shapes at level A, B, C, and D shown in Fig. 4.2, which is also from Forghani-Arani's works.

(a) Level A

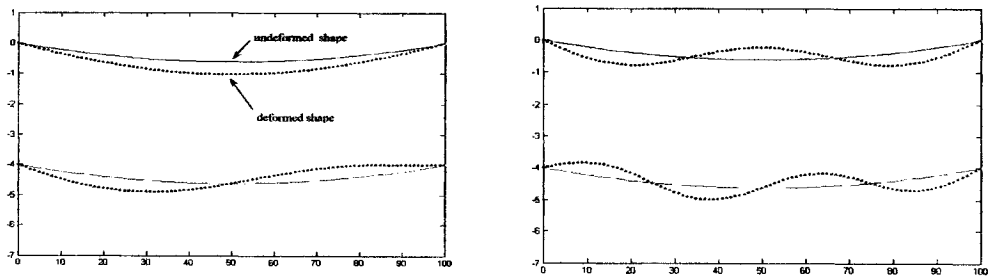

(b) Level B

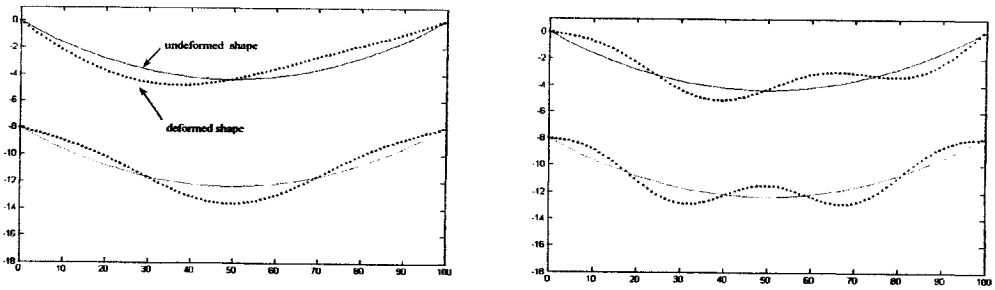

(c) Level C

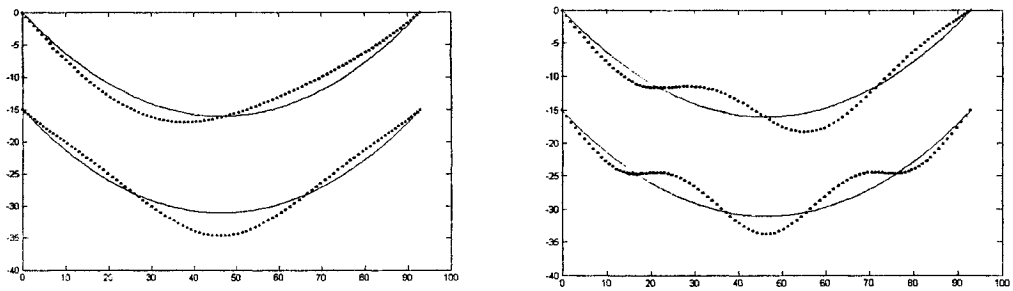

(d) Level D

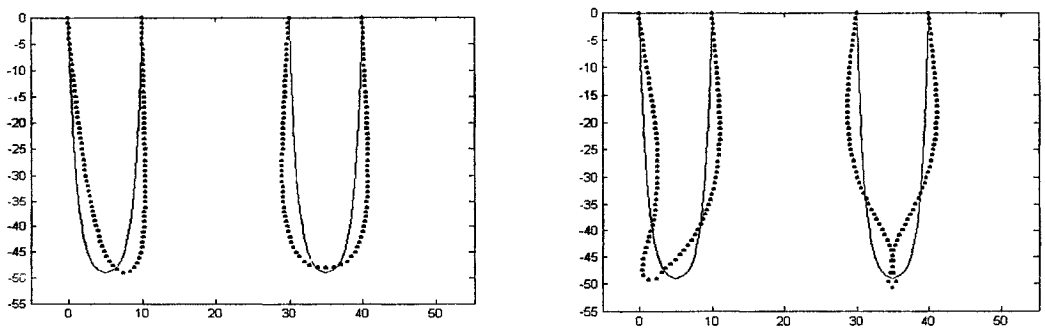

Fig. 4.3 Mode shapes at each level in Fig. 4.2

(a)

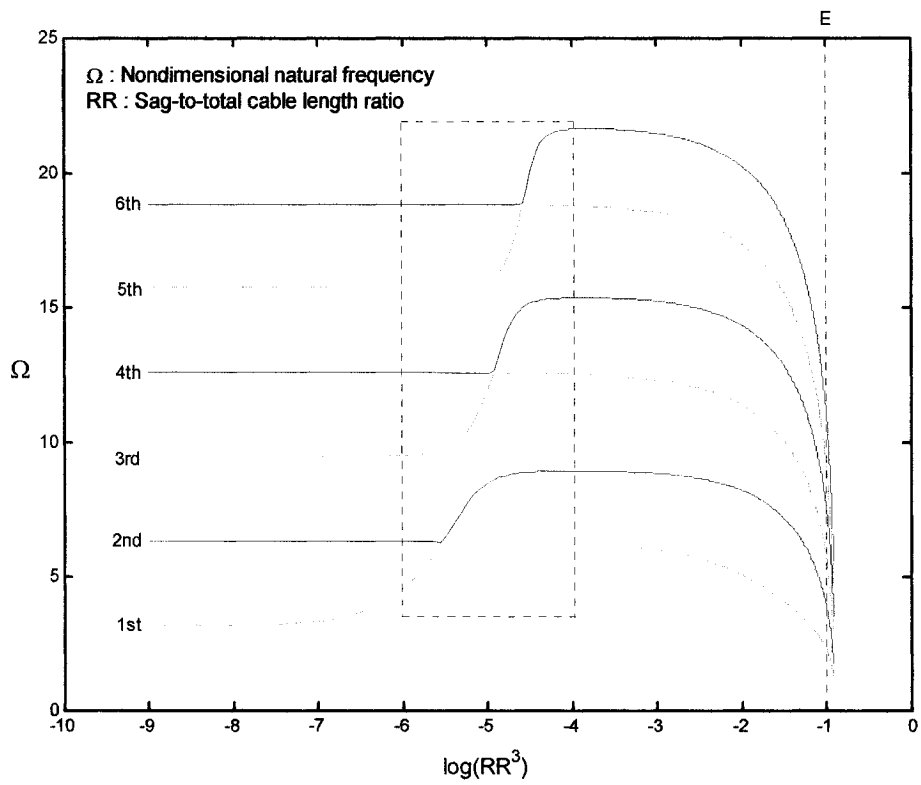

(b)

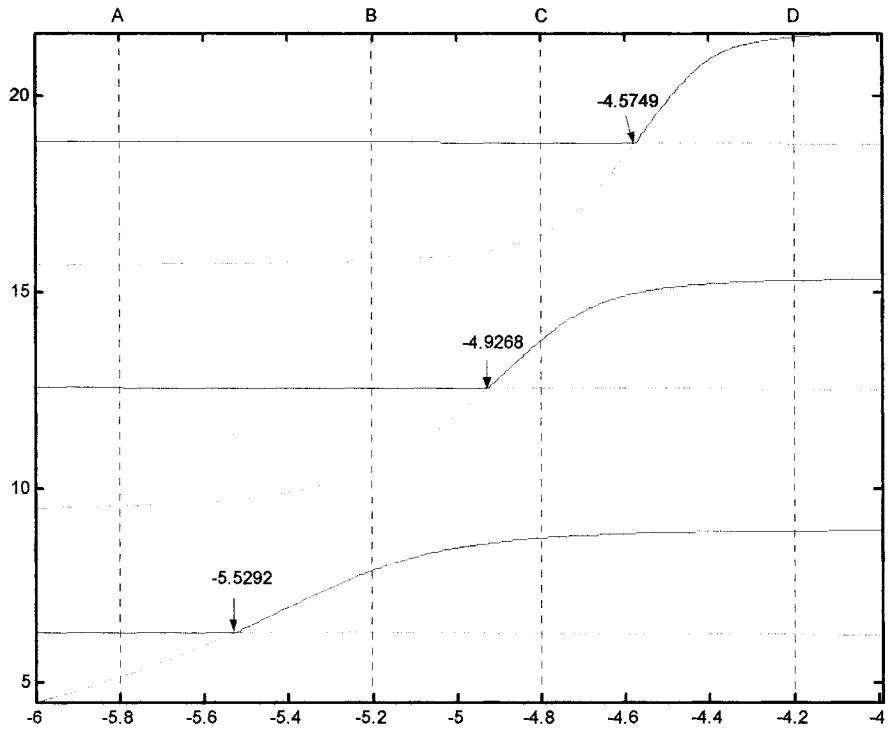

Fig. 4.4 Non-dimensional natural frequency vs. sag-to-total cable length ratio (θ = 0)

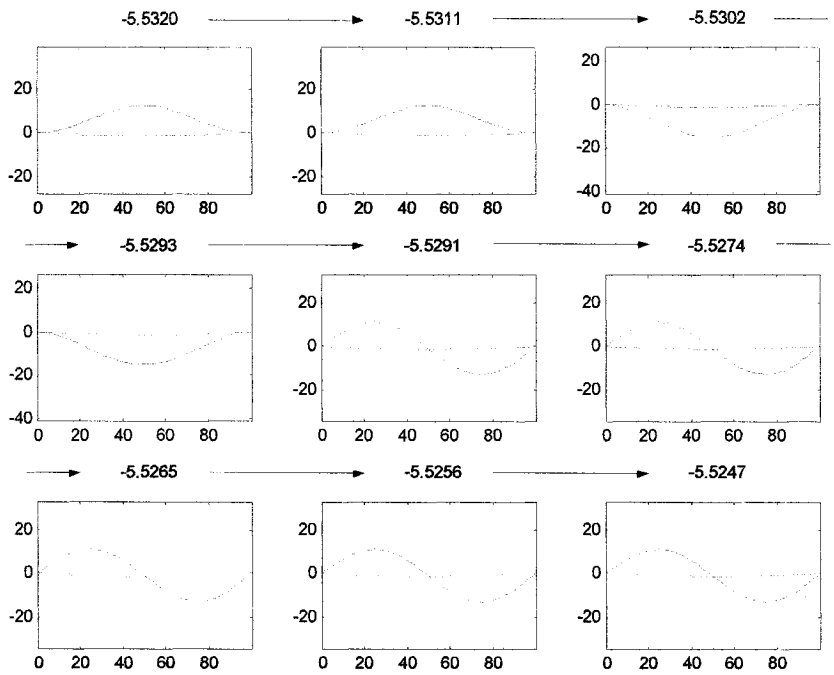

Fig. 4.5 Mode shapes right before and after at the point -5.5292 in the 1st frequency line ($\theta = 0$)

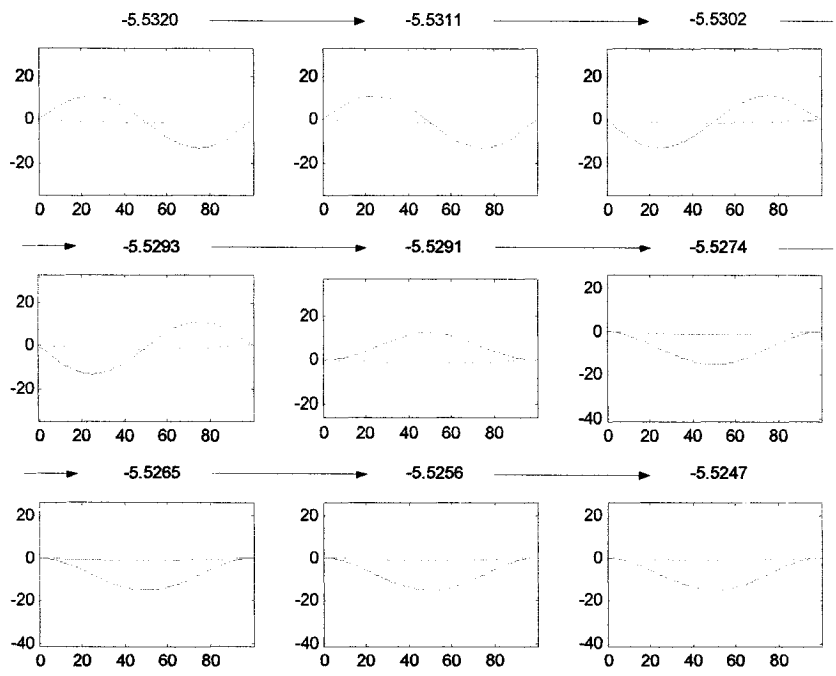

Fig. 4.6 Mode shapes right before and after at the point -5.5292 in the 2nd frequency line ($\theta = 0$)

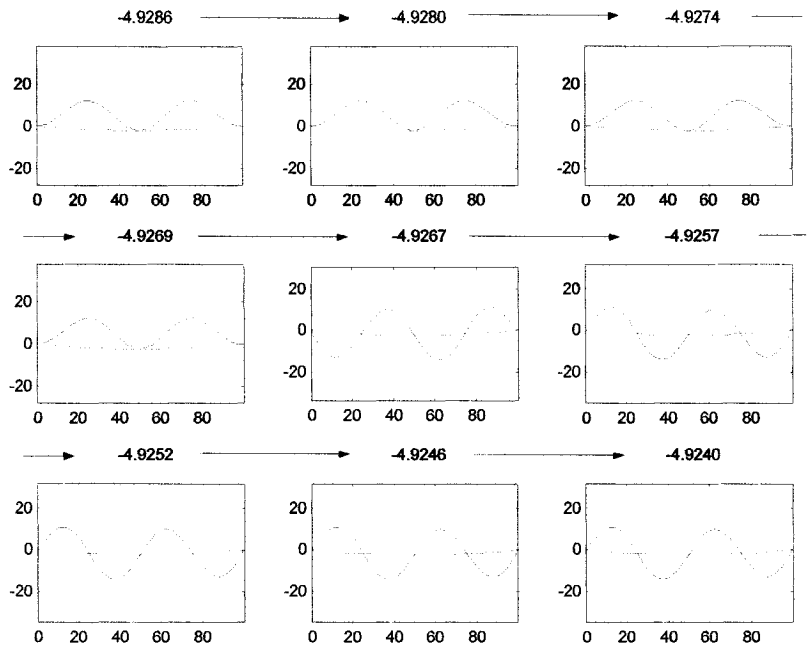

Fig. 4.7 Mode shapes right before and after at the point –4.9268 in the 3rd frequency line ($\theta = 0$)

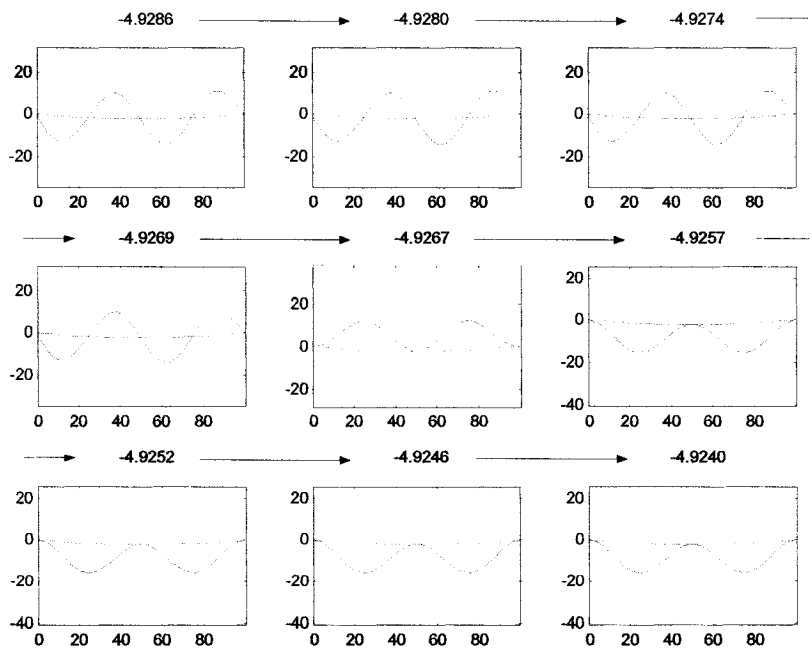

Fig. 4.8 Mode shapes right before and after at the point –4.9268 in the 4th frequency line ($\theta = 0$)

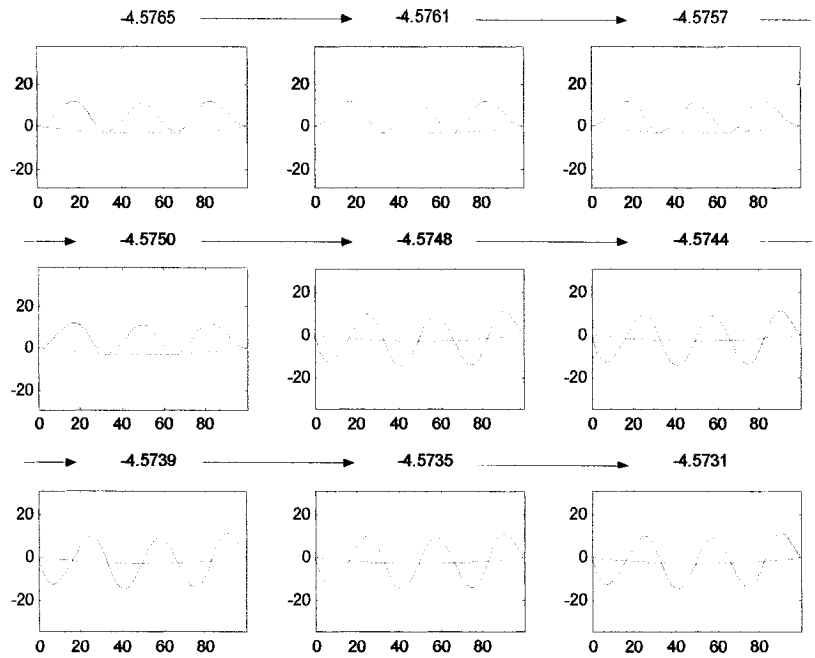

Fig. 4.9 Mode shapes right before and after at the point –4.5749 in the 5th frequency line ($\theta = 0$)

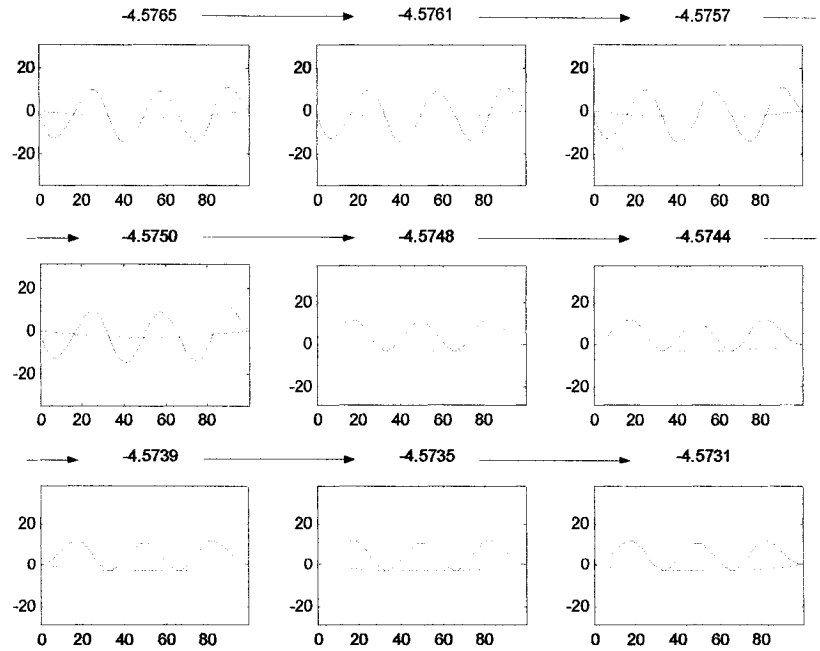

Fig. 4.10 Mode shapes right before and after at the point –4.5749 in the 6th frequency line ($\theta = 0$)

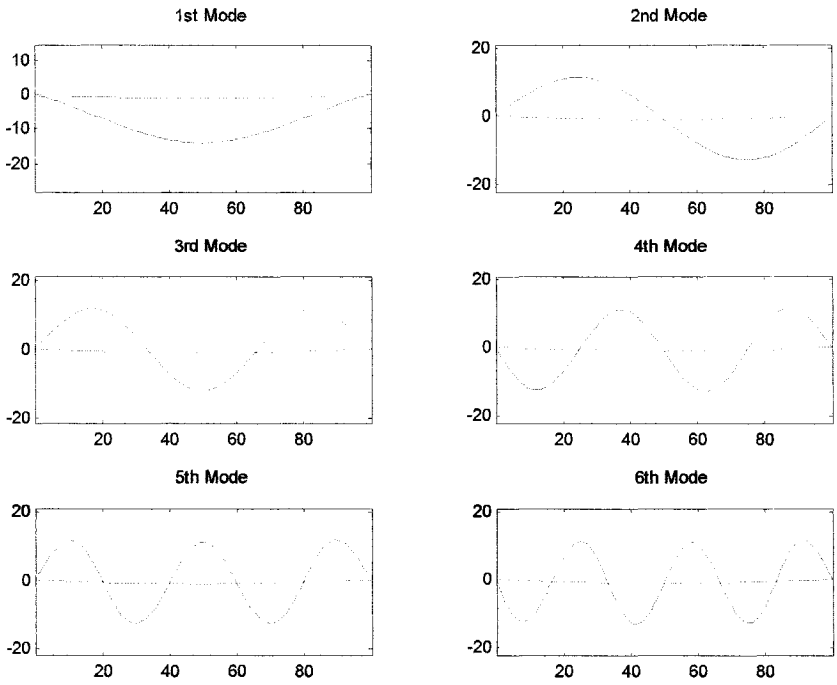

Fig. 4.11 Mode shapes at A ($\theta = 0$)

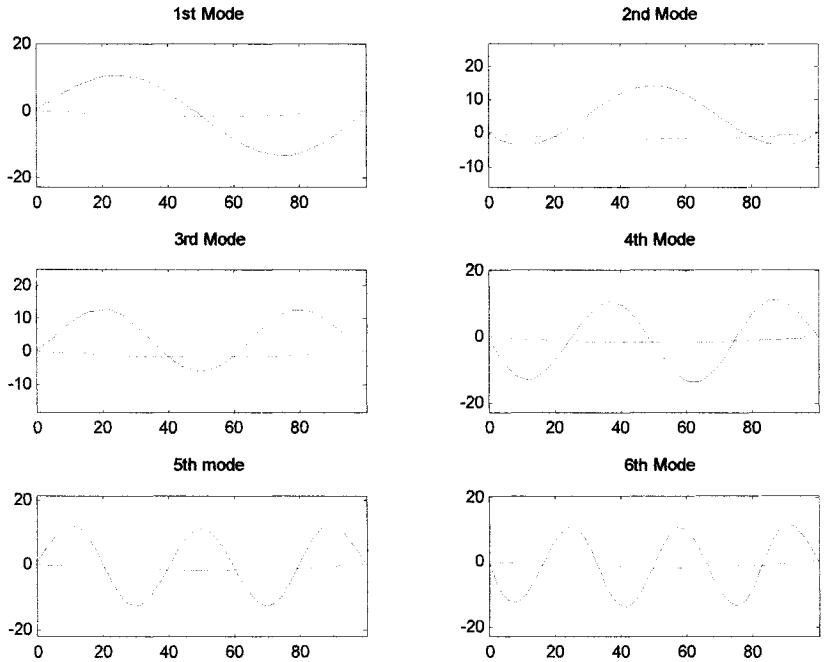

Fig. 4.12 Mode shapes at B ($\theta = 0$)

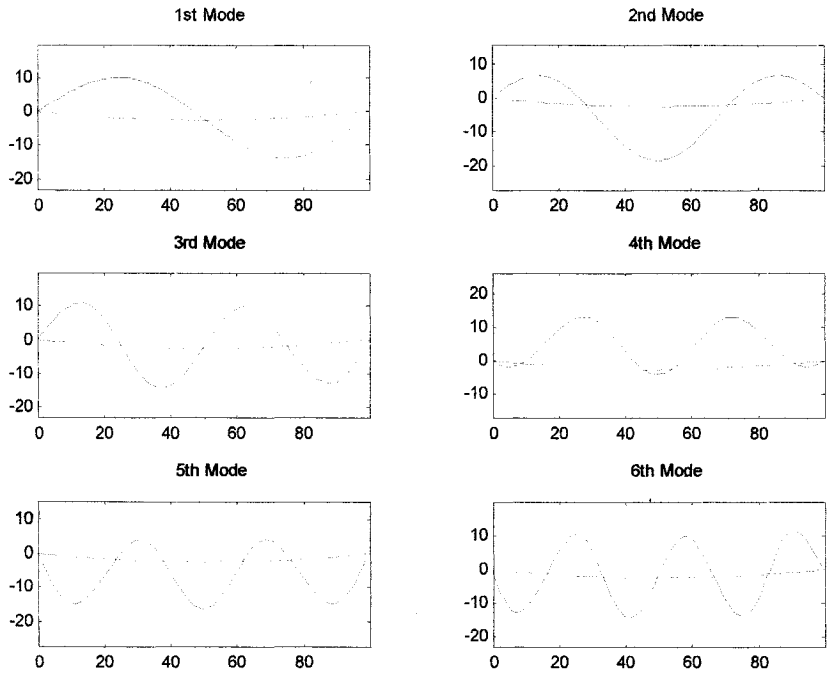

Fig. 4.13 Mode shapes at C ($\theta = 0$)

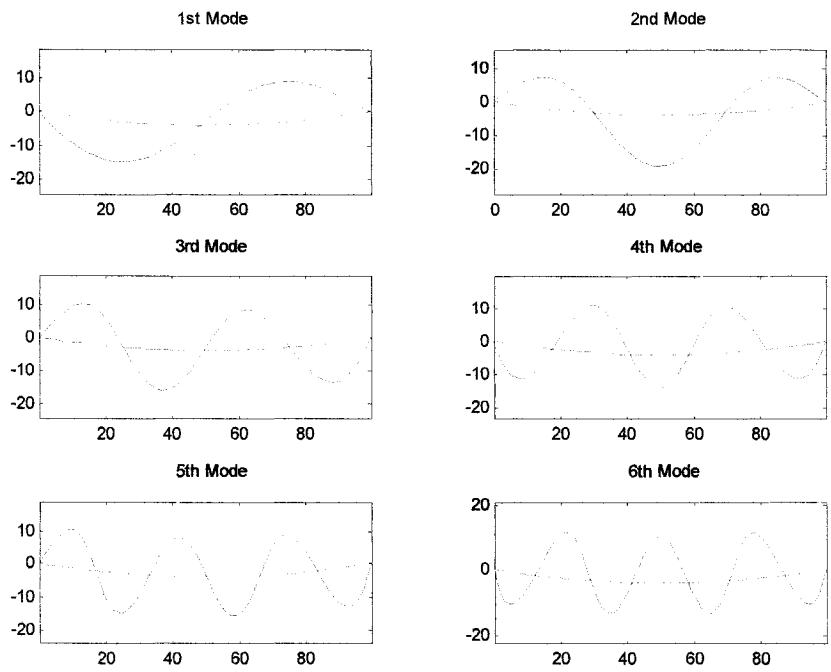

Fig. 4.14 Mode shapes at D ($\theta = 0$)

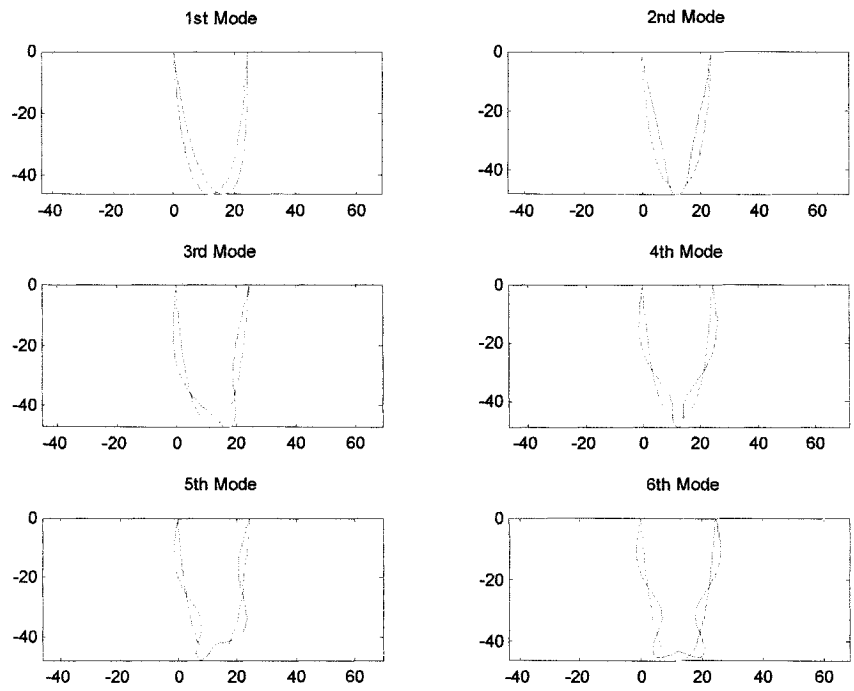

Fig. 4.15 Mode shapes at E ($\theta = 0$)

4.2.3 Inclined Cable $[\theta = 1°]$

To study the dynamic characteristics of inclined cables, the inclined angle of cables is initiated from 1° in the Finite Element calculation. In Fig. 4.17, the first six non-dimensional natural frequencies are plotted for the case $\theta = 1°$, and Fig. 4.18 shows the enlarged results at around the first modal crossover area, amplified a hundredfold for $\theta = 0°$ and $\theta = 1°$. In the case that a cable is at a 1° inclination, the first natural frequency line (first symmetric line) comes acutely closer to the second natural frequency line (first asymmetric line) as the $\log(RR^3)$ increases but the frequencies never coincide with each other. However, the modal crossover takes place in a different way from the case of a horizontal cable. When the first symmetric and asymmetric lines approach one another, both the mode shapes are no longer symmetric or asymmetric. Both of these mode shapes are a mixture of symmetric and asymmetric if they are examined at the range between $\log(RR^3)$= -5.5322 and $\log(RR^3)$= -5.5249. It is a transition range (TR), so to speak. Figure 4.19 and Fig. 4.20 represent the change of mode shapes at the transition area of the first and second frequencies when $\theta = 1°$. After going through this transition range, the first symmetric mode line becomes discontinuously a continuation of the first asymmetric mode line and the first asymmetric mode line becomes a continuation of the first symmetric mode line, again discontinuously. In reality, this phenomenon is hardly observed when the inclination angle of the cable is small. For instance, when the inclination of cable is 1°, the span length (l) changes only 0.001% while the corresponding $\log(RR^3)$ is changing between the transition areas; that is, the cable span changes only from 99.930 m to 99.929 m between the transition ranges (from $\log(RR^3)$= -5.5232 to $\log(RR^3)$ = -5.5249). However, this phenomenon becomes noticeably distinct as the inclined angle increases. The transition range becomes much wider as the inclination of the cable increases. Figure 4.23 shows the difference of transition width for $\theta = 1°$ and $\theta = 10°$.

Forghani-Arani [2] also presented the dynamic characteristics of inclined cables in his paper. However, according to his conclusion, the modal crossover and frequency

crossover of inclined cables are fairly similar to that of horizontal cables, regardless of the inclination angle and the only difference between horizontal cables and inclined cables is the sag ratios corresponding to modal crossover. Figure 4.16 shows one of his results of numerical calculations for inclined cables with the inclination of 30°.

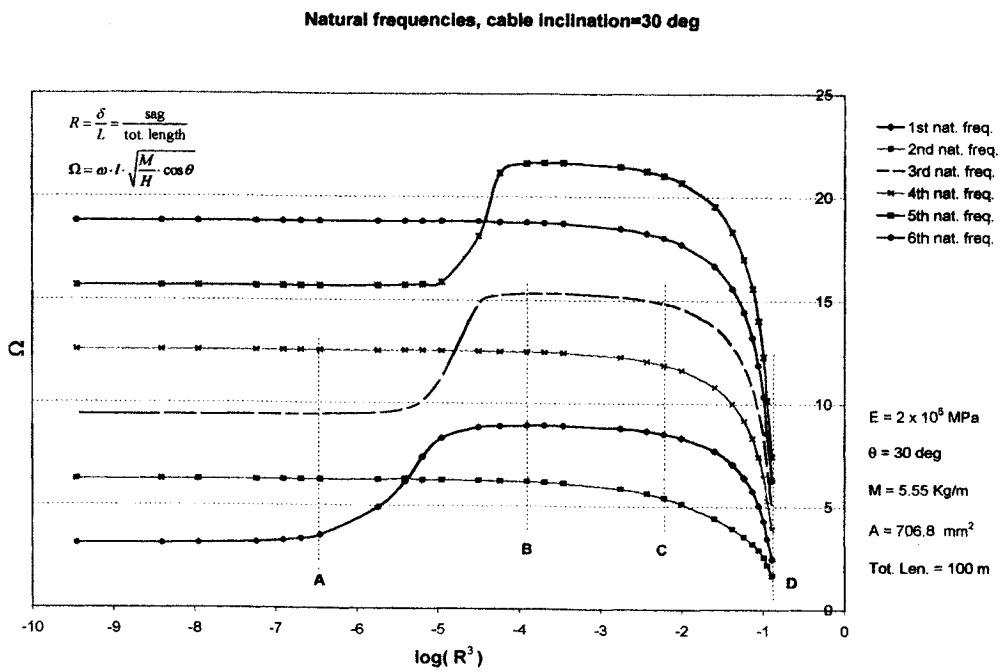

Fig. 4.16 Natural frequencies of an inclined cable ($\theta = 30°$) from Forgahni-arani's paper

Unlike the results presented in this study, Fig. 4.16 shows the frequency crossover; that is, the first and second frequencies coincide at a certain level of the sag-to-total cable length ratio, the third and fourth frequencies do the same, and the fifth and sixth frequencies also cross each other. Throughout the investigation of the dynamic characteristics of inclined cables besides this case, Forghani-Arani suggested that the characteristics of inclined cables are quite similar to what had been found by the analytical approach and Finite Element calculations for horizontal cables. However, in this study, the frequency crossover occurs only for the horizontal cables and the way of the modal crossover for inclined cables is classified from that of horizontal cables. Figure 4.21 to Fig 4.46 represent the results of calculations when the inclination angle of the cable is10°, 30°, and 60°.

(a)

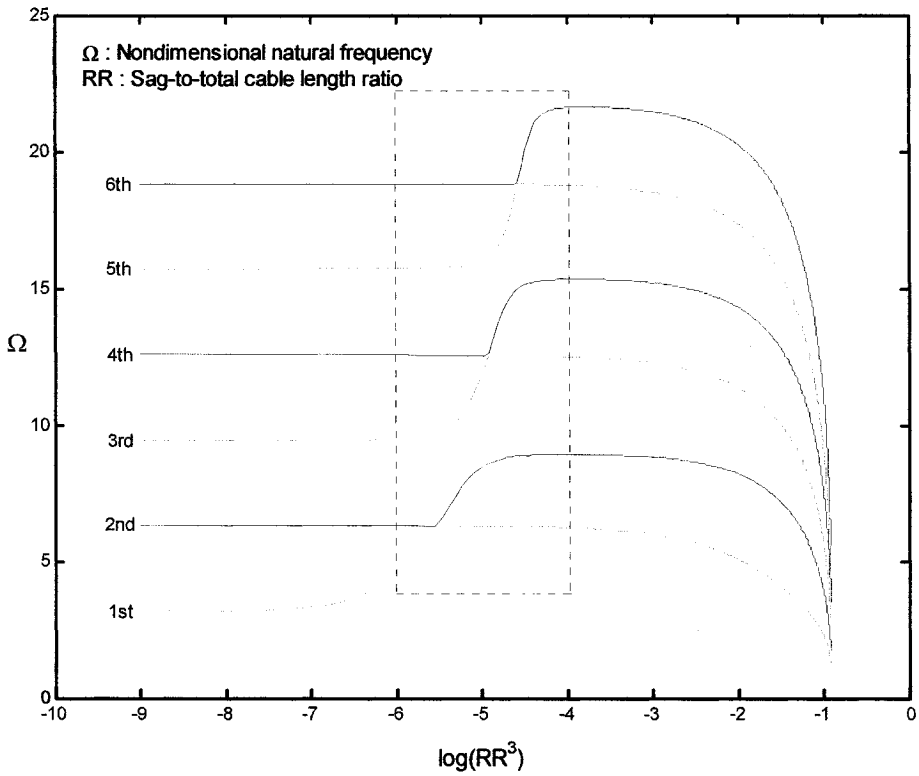

(b)

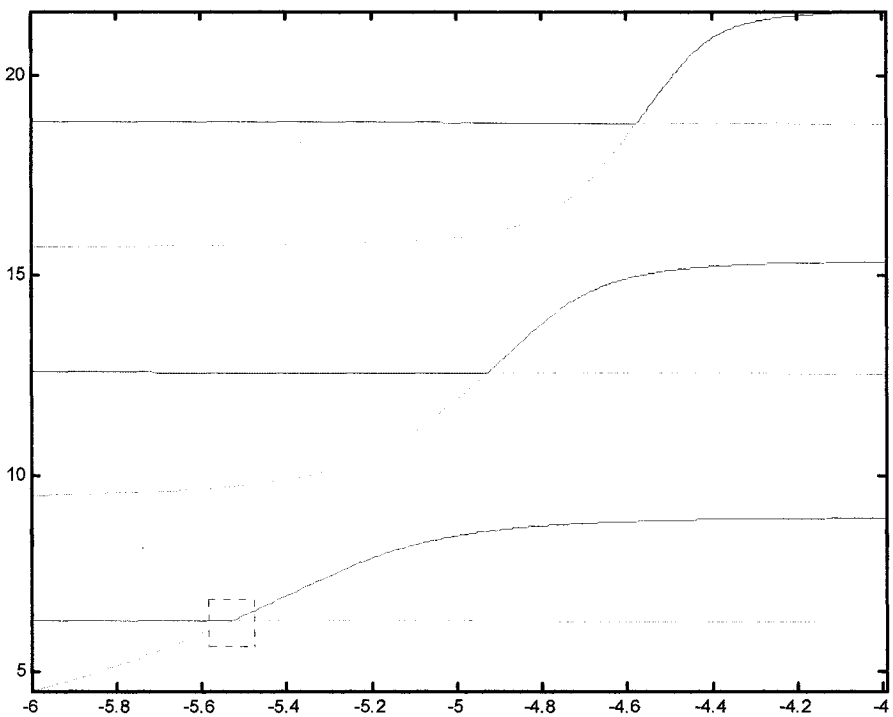

Fig. 4.17 Non-dimensional natural frequency vs. sag-to-total cable length ratio ($\theta = 1°$)

(a)

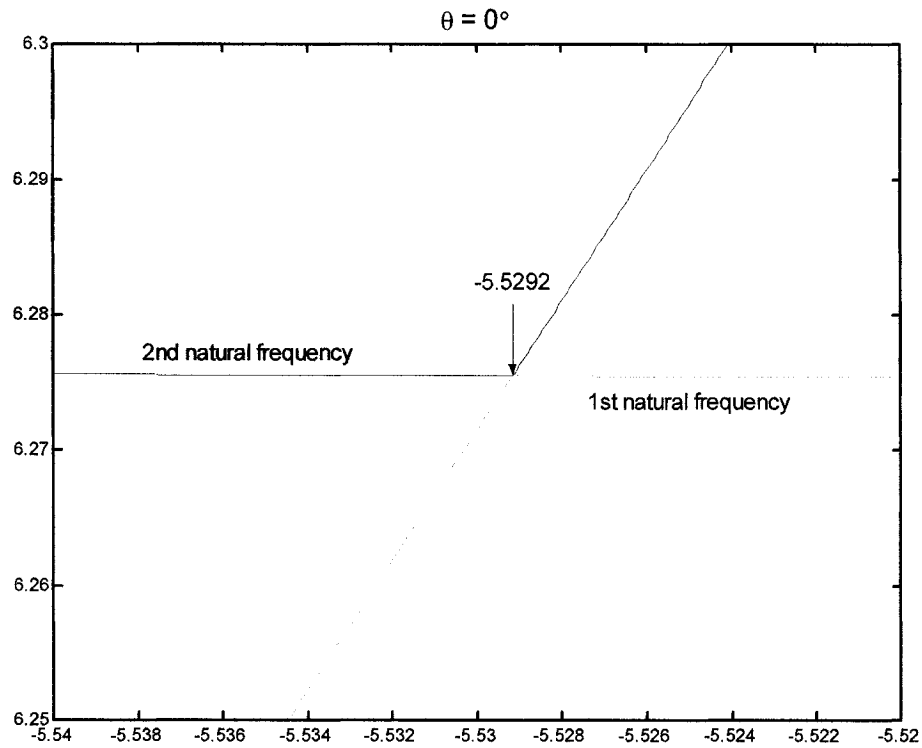

(b)

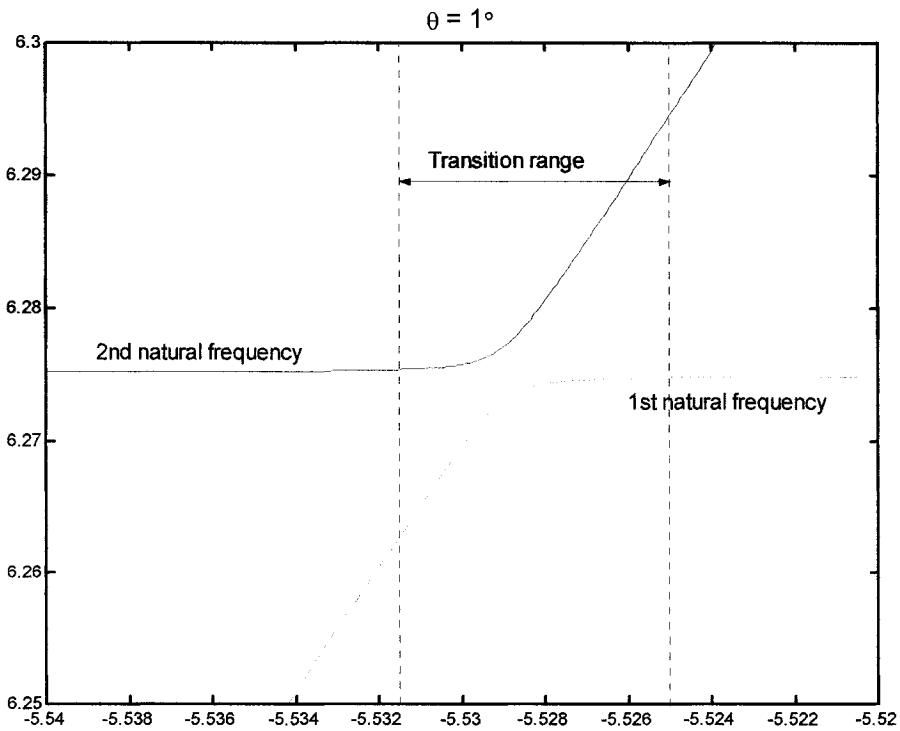

Fig. 4.18 1st and 2nd natural frequency when $\theta = 0°$ and $\theta = 1°$

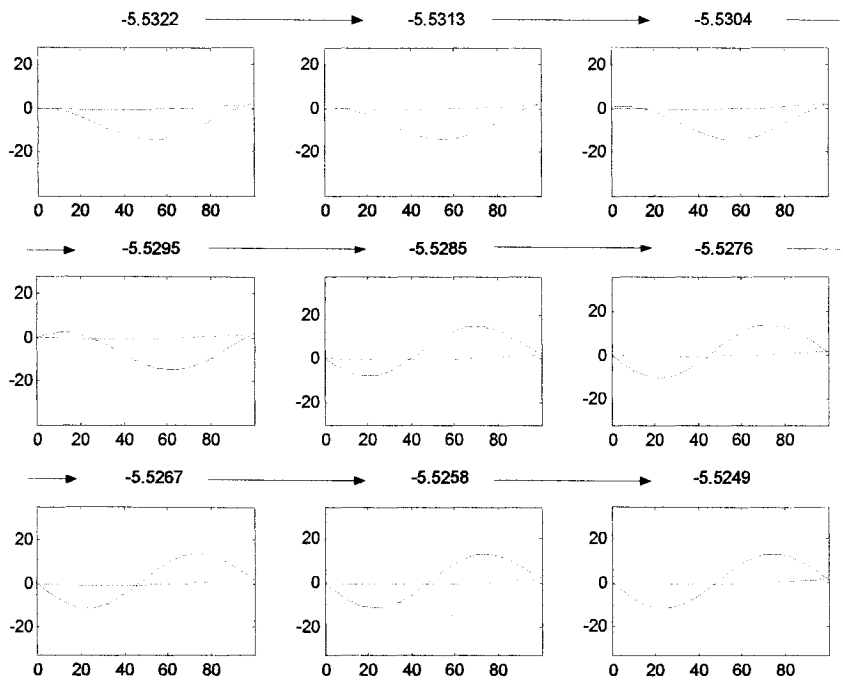

Fig. 4.19 Mode shapes between the transition range in the 1st frequency line ($\theta = 1°$)

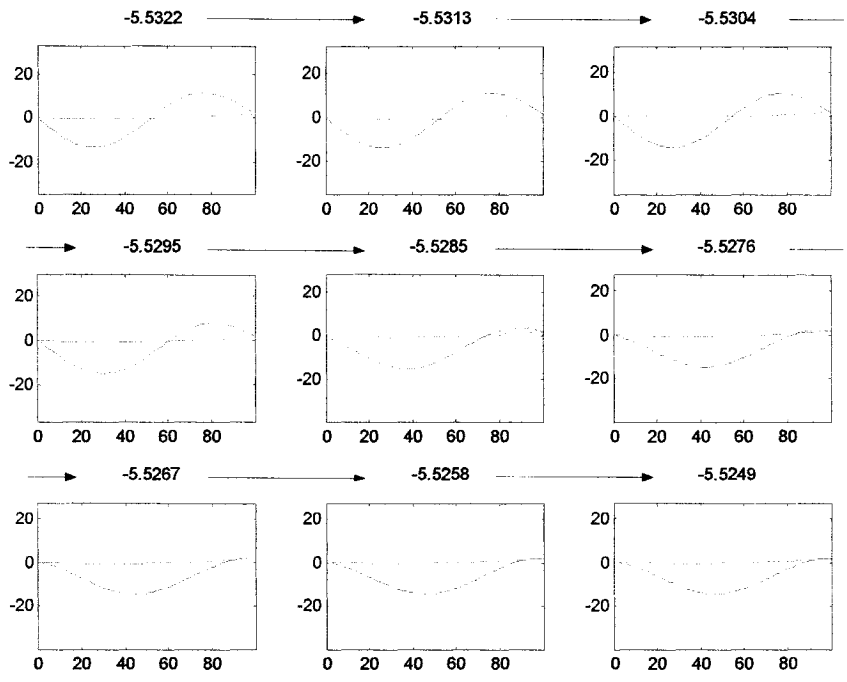

Fig. 4.20 Mode shapes between the transition range in the 2nd frequency line ($\theta = 1°$)

4.2.4 Inclined Cable [$\theta = 10°$]

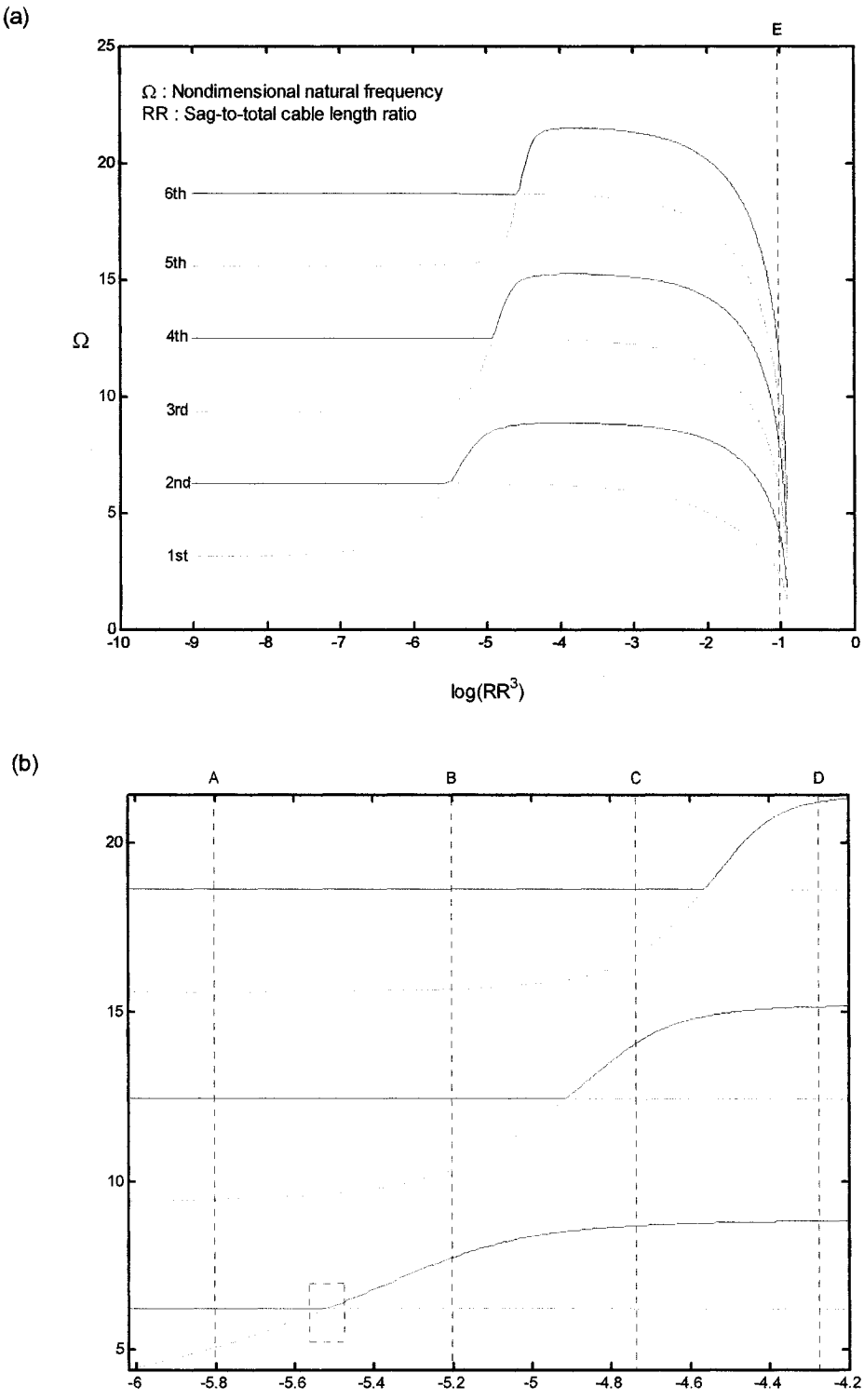

Fig. 4.21 Non-dimensional natural frequency vs. sag-to-total cable length ratio ($\theta = 10°$)

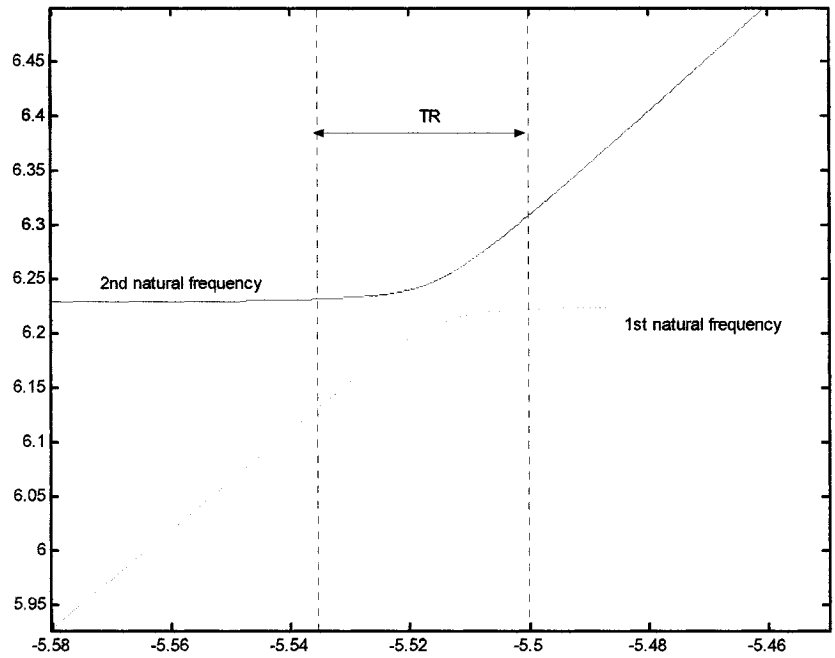

Fig. 4.22 1st and 2nd natural frequency line when $\theta = 10°$

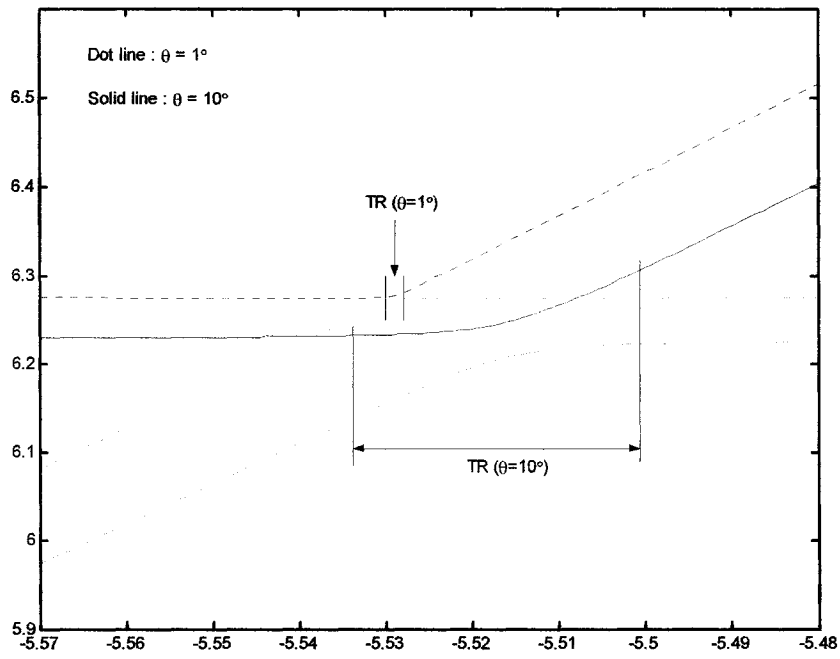

Fig. 4.23 1st and 2nd natural frequency when $\theta = 1°$ and $\theta = 10°$

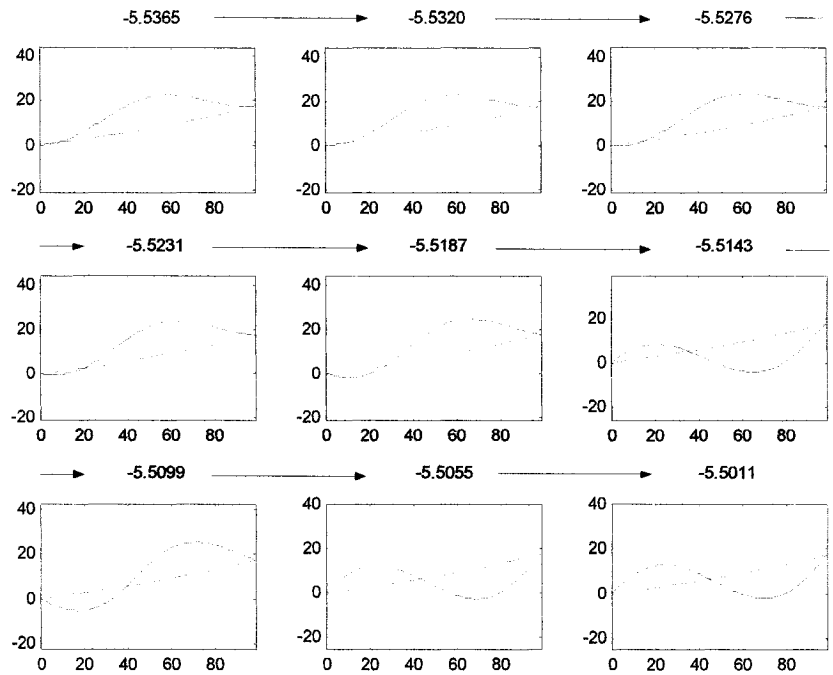

Fig. 4.24 Mode shapes between the transition range in the 1st frequency line ($\theta = 10°$)

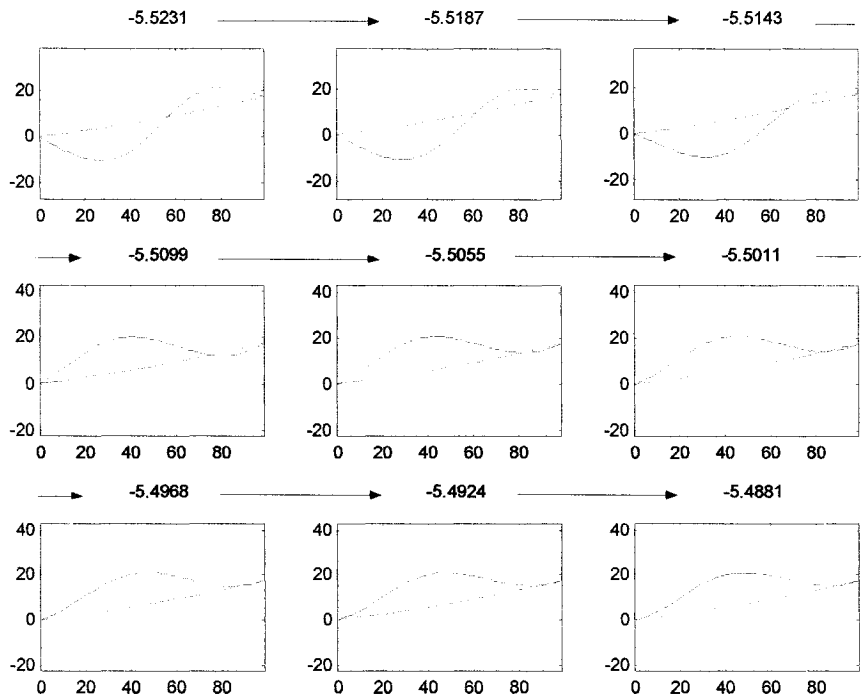

Fig. 4.25 Mode shapes between the transition range in the 2nd frequency line ($\theta = 10°$)

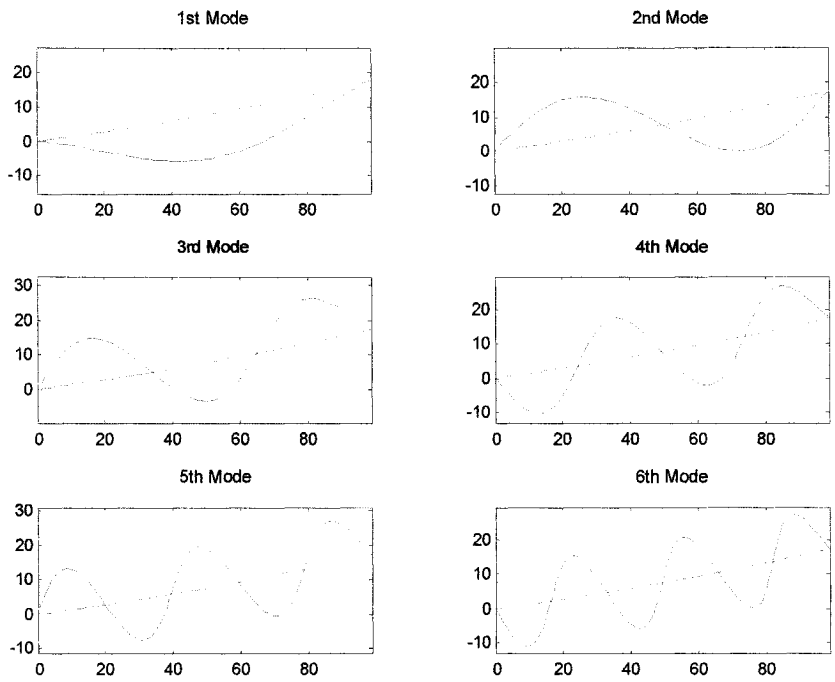

Fig. 4.26 Mode shapes at A ($\theta = 10°$)

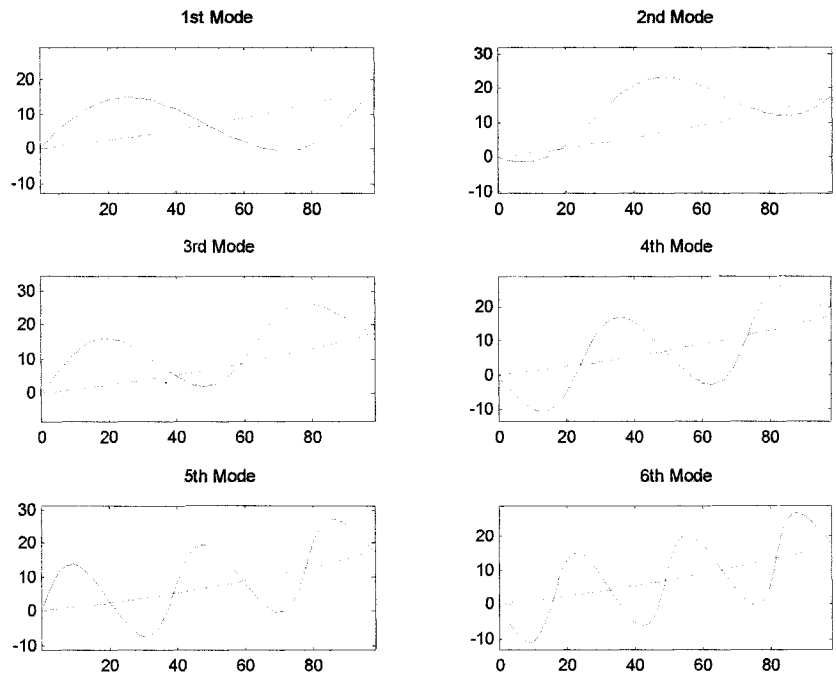

Fig. 4.27 Mode shapes at B ($\theta = 10°$)

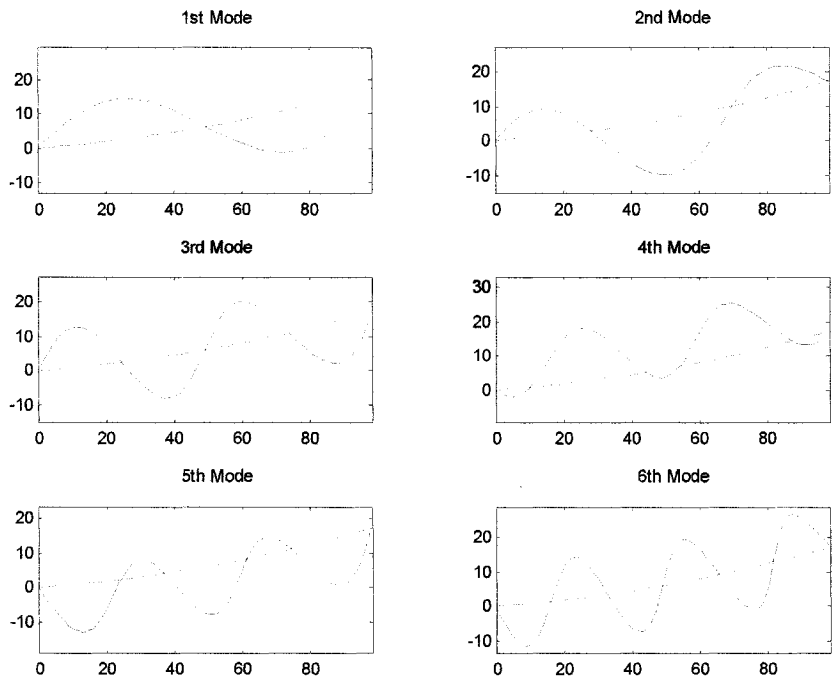

Fig. 4.28 Mode shapes at C ($\theta = 10°$)

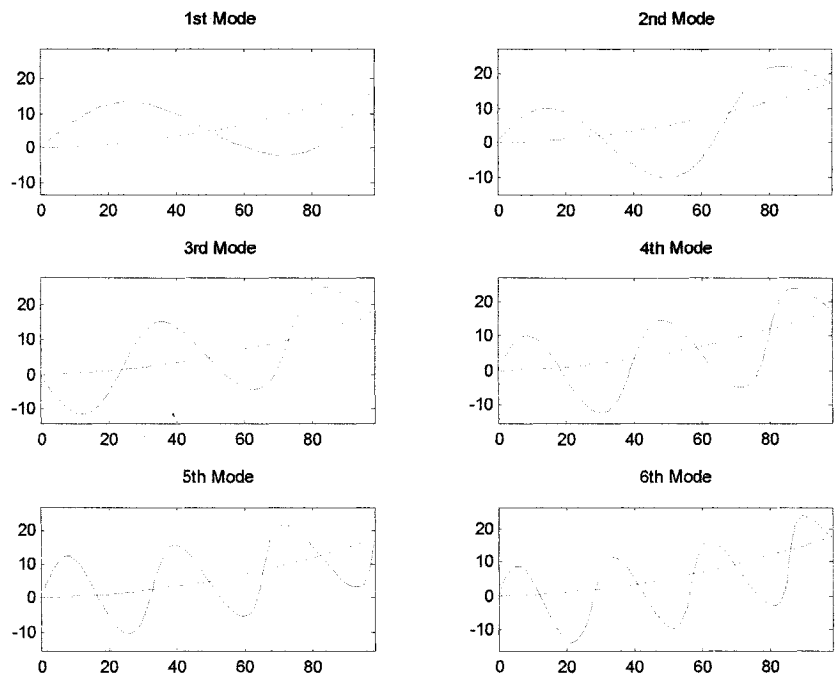

Fig. 4.29 Mode shapes at D ($\theta = 10°$)

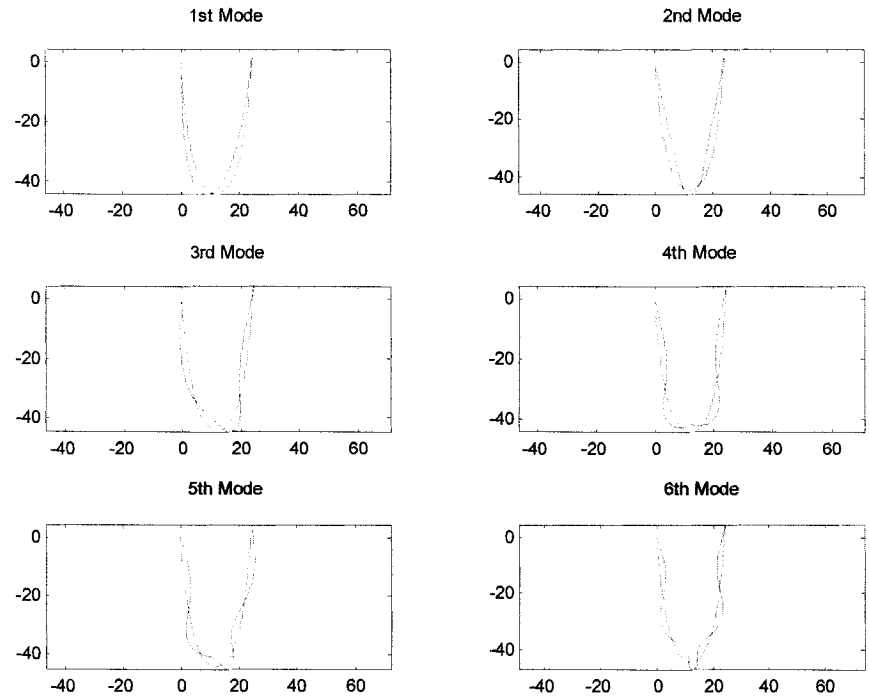

Fig. 4.30 Mode shapes at E ($\theta = 10°$)

4.2.5 Inclined Cable [$\theta = 30°$]

(a)

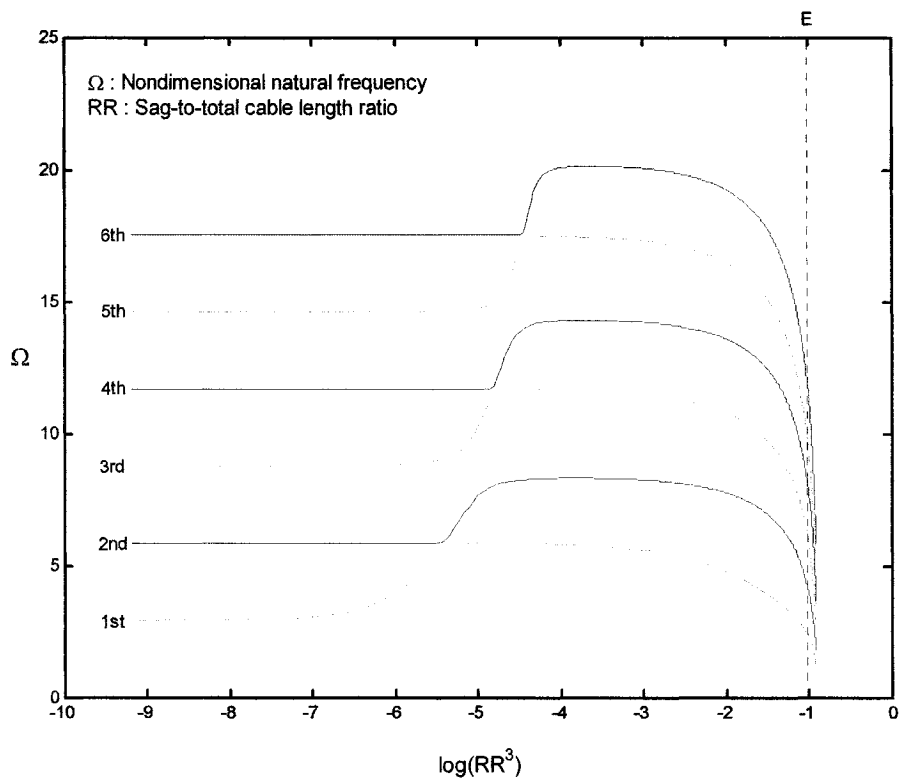

(b)

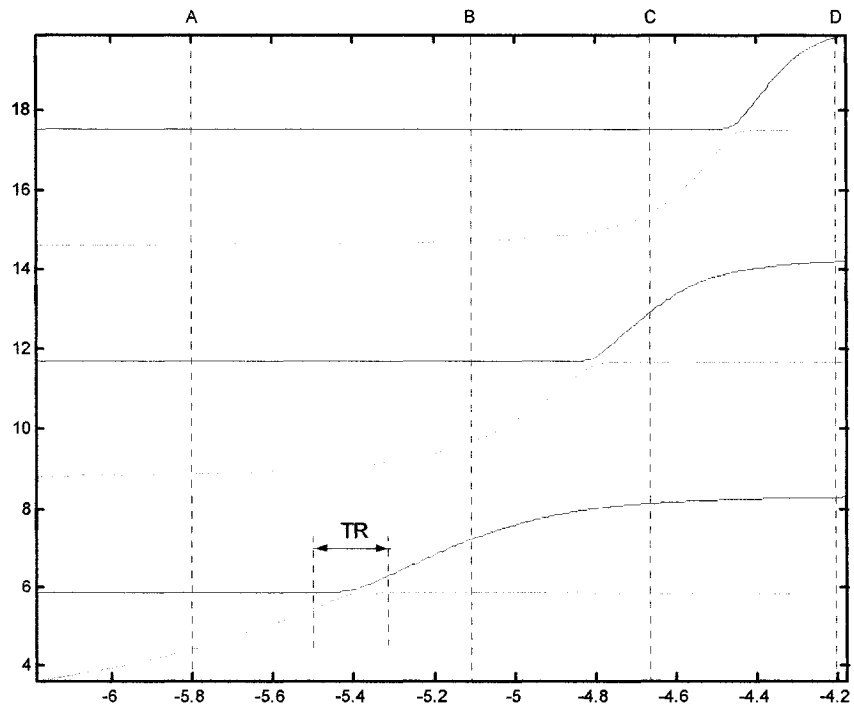

Fig. 4.31 Non-dimensional natural frequency vs. sag-to-total cable length ratio ($\theta = 30°$)

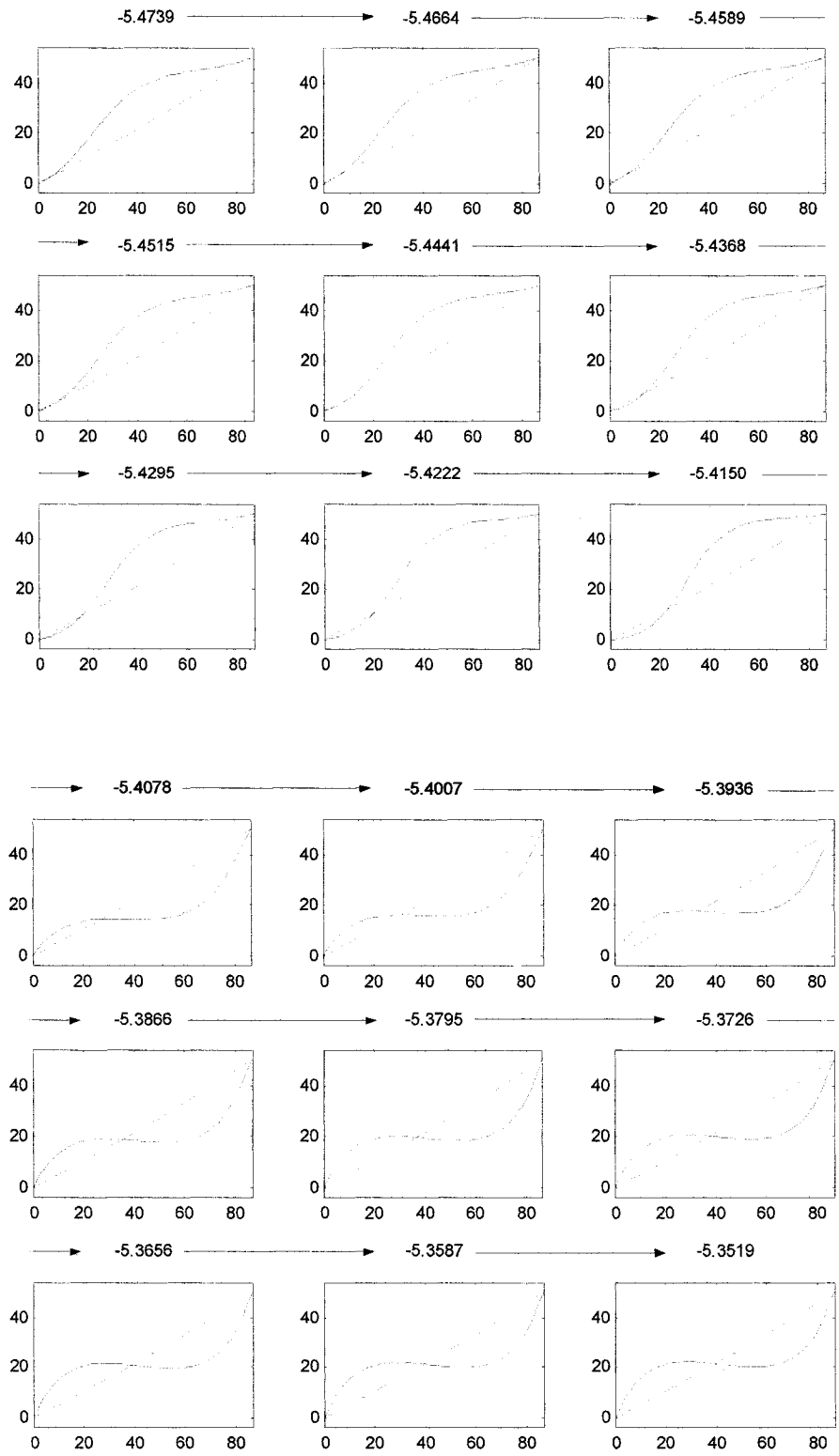

Fig. 4.32 Mode shapes between the transition range in the 1st frequency line ($\theta = 30°$)

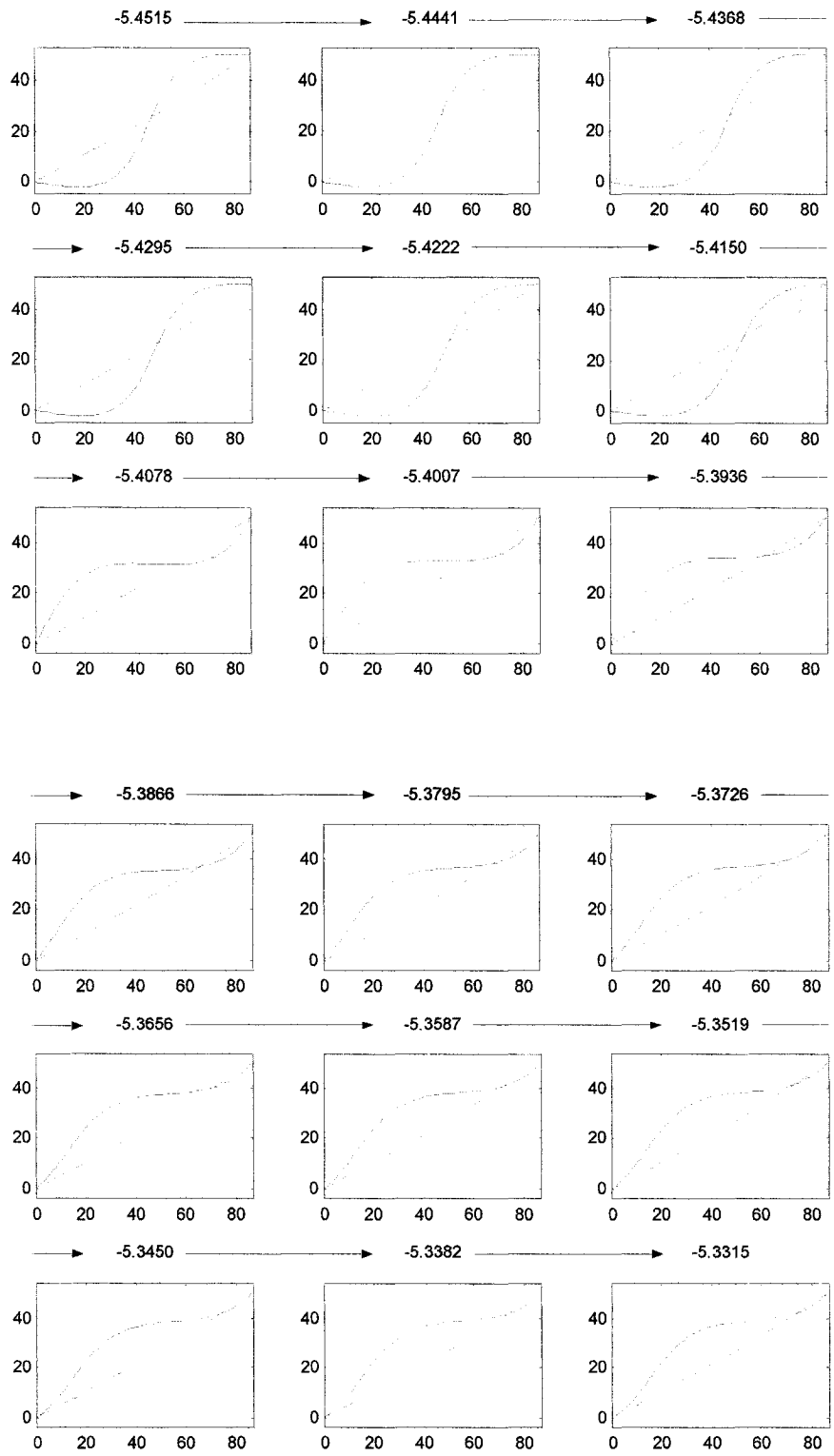

Fig. 4.33 Mode shapes between the transition range in the 2nd frequency line ($\theta = 30°$)

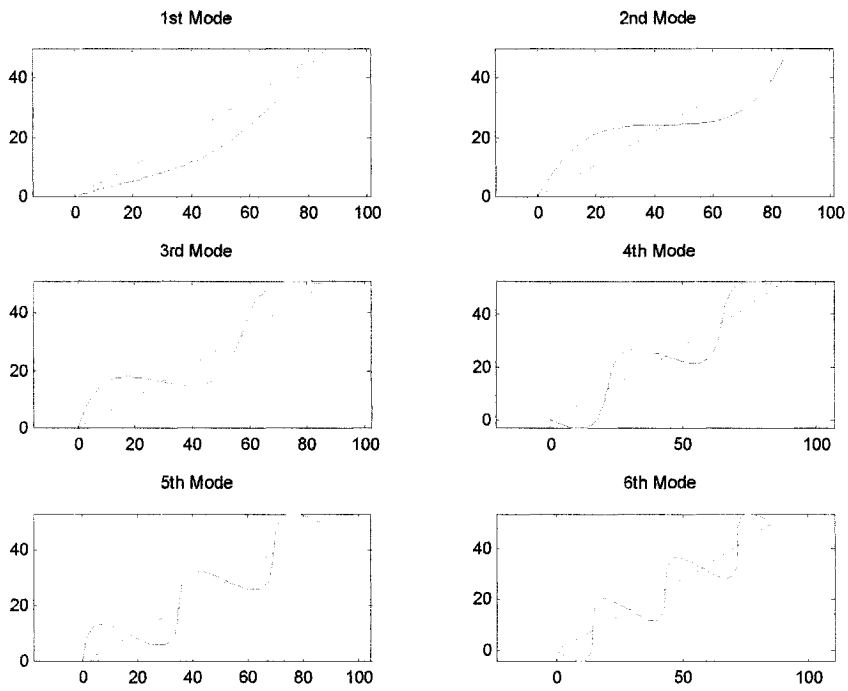

Fig. 4.34 Mode shapes at A ($\theta = 30°$)

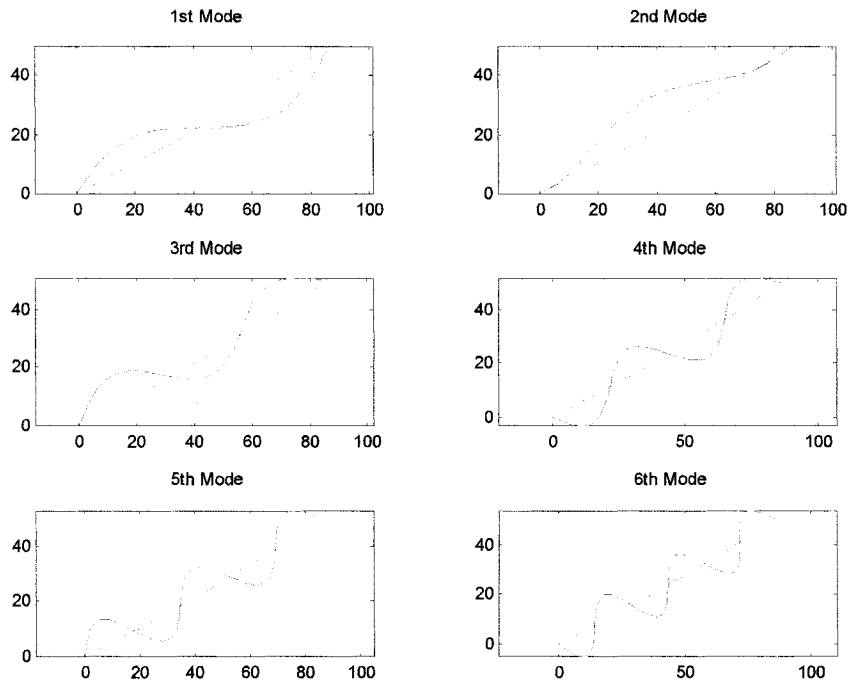

Fig. 4.35 Mode shapes at B ($\theta = 30°$)

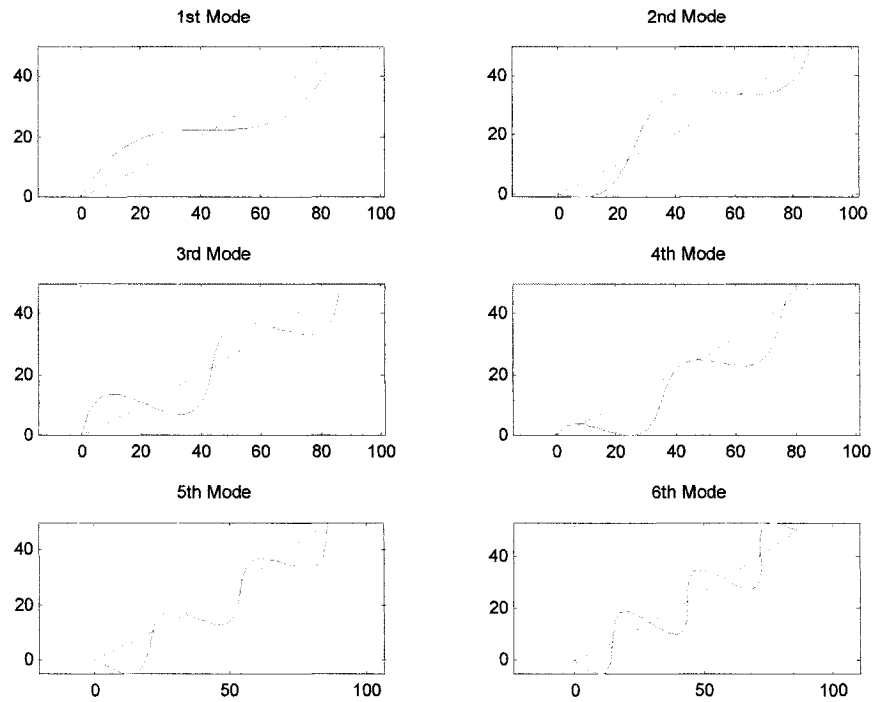

Fig. 4.36 Mode shapes at C ($\theta = 30°$)

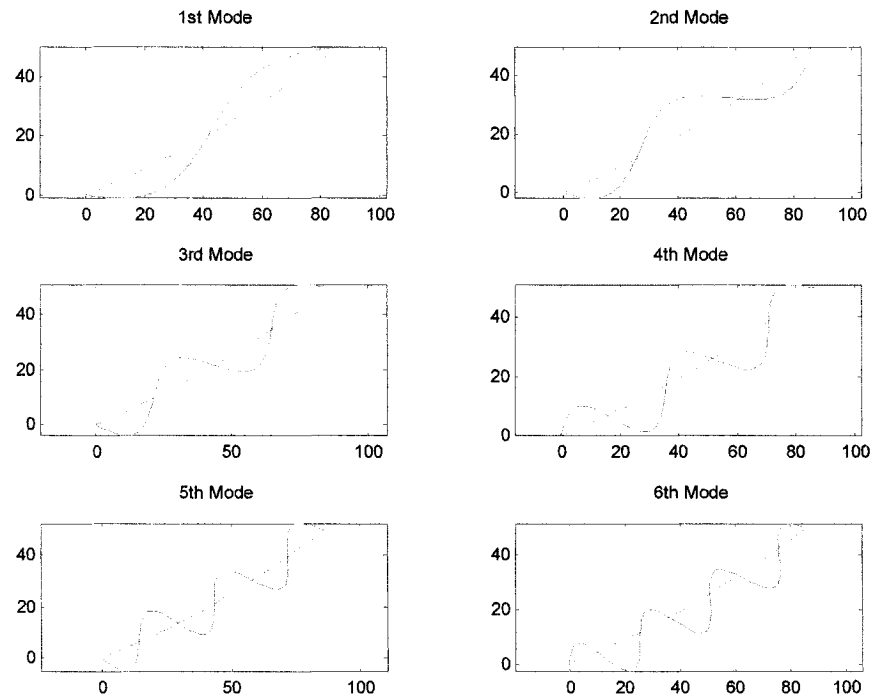

Fig. 4.37 Mode shapes at D ($\theta = 30°$)

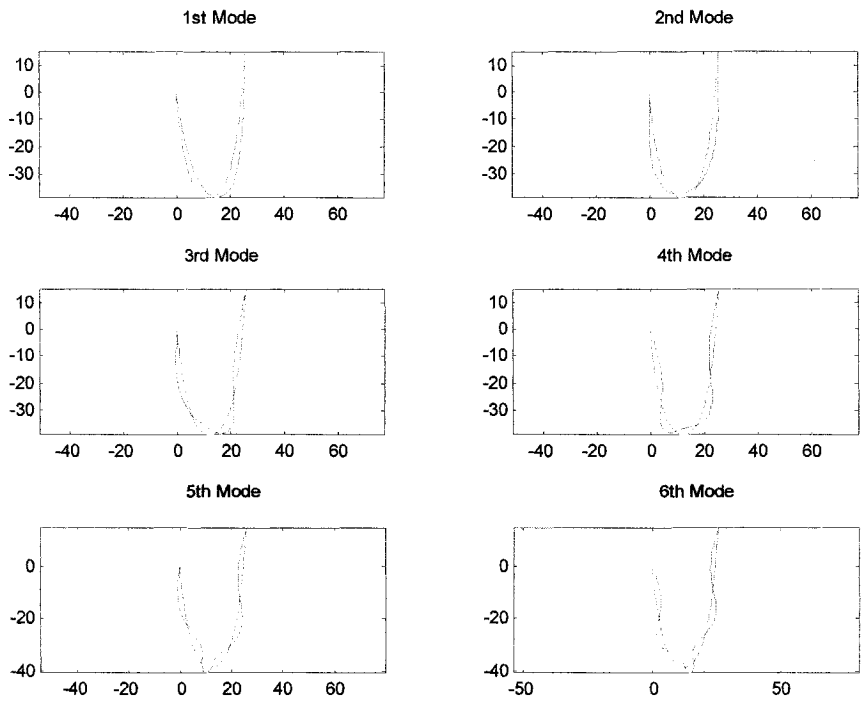

Fig. 4.38 Mode shapes at E ($\theta = 30°$)

4.2.6 Inclined Cable ($\theta = 60°$)

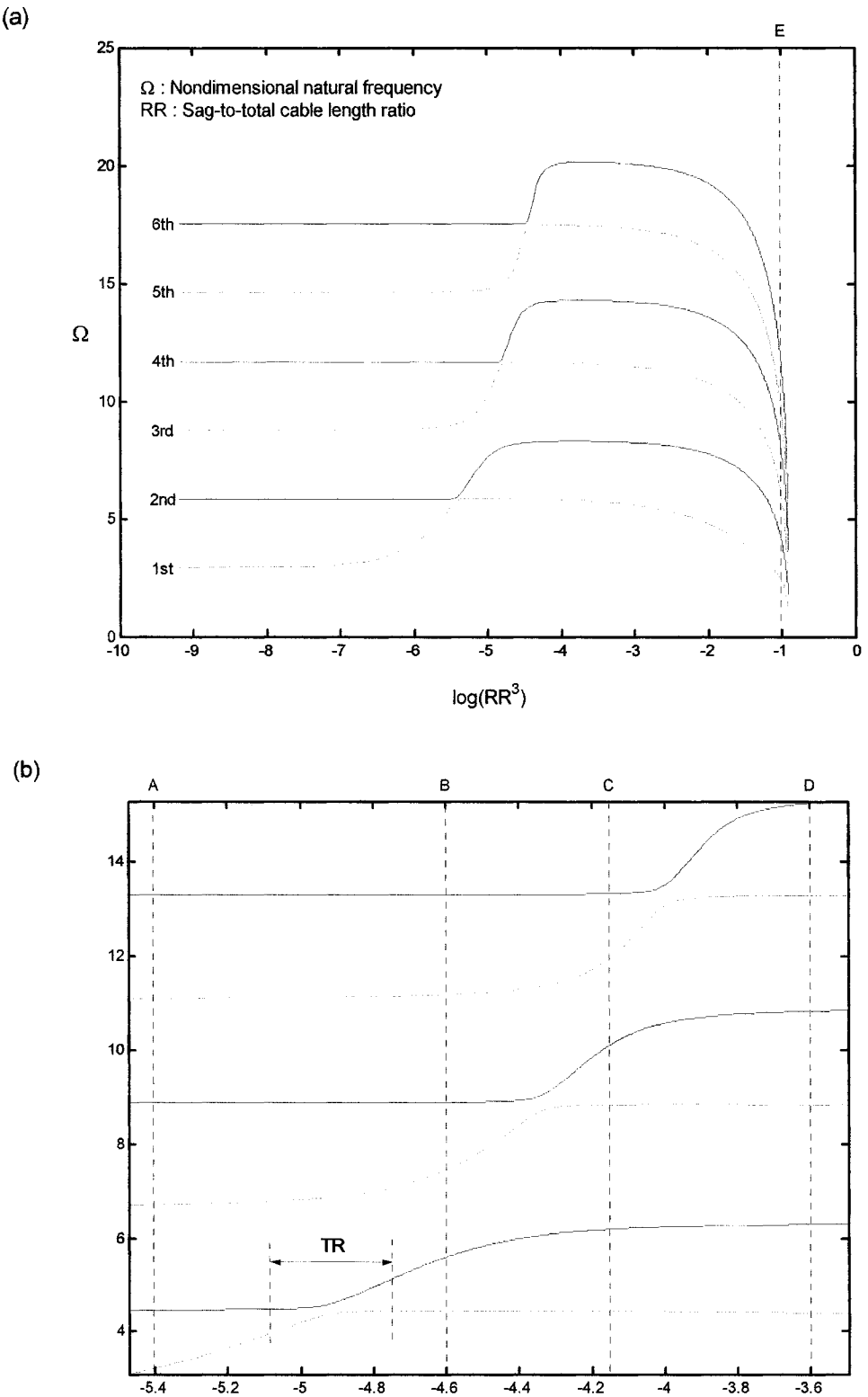

Fig. 4.39 Non-dimensional natural frequency vs. sag-to-total cable length ratio ($\theta = 60°$)

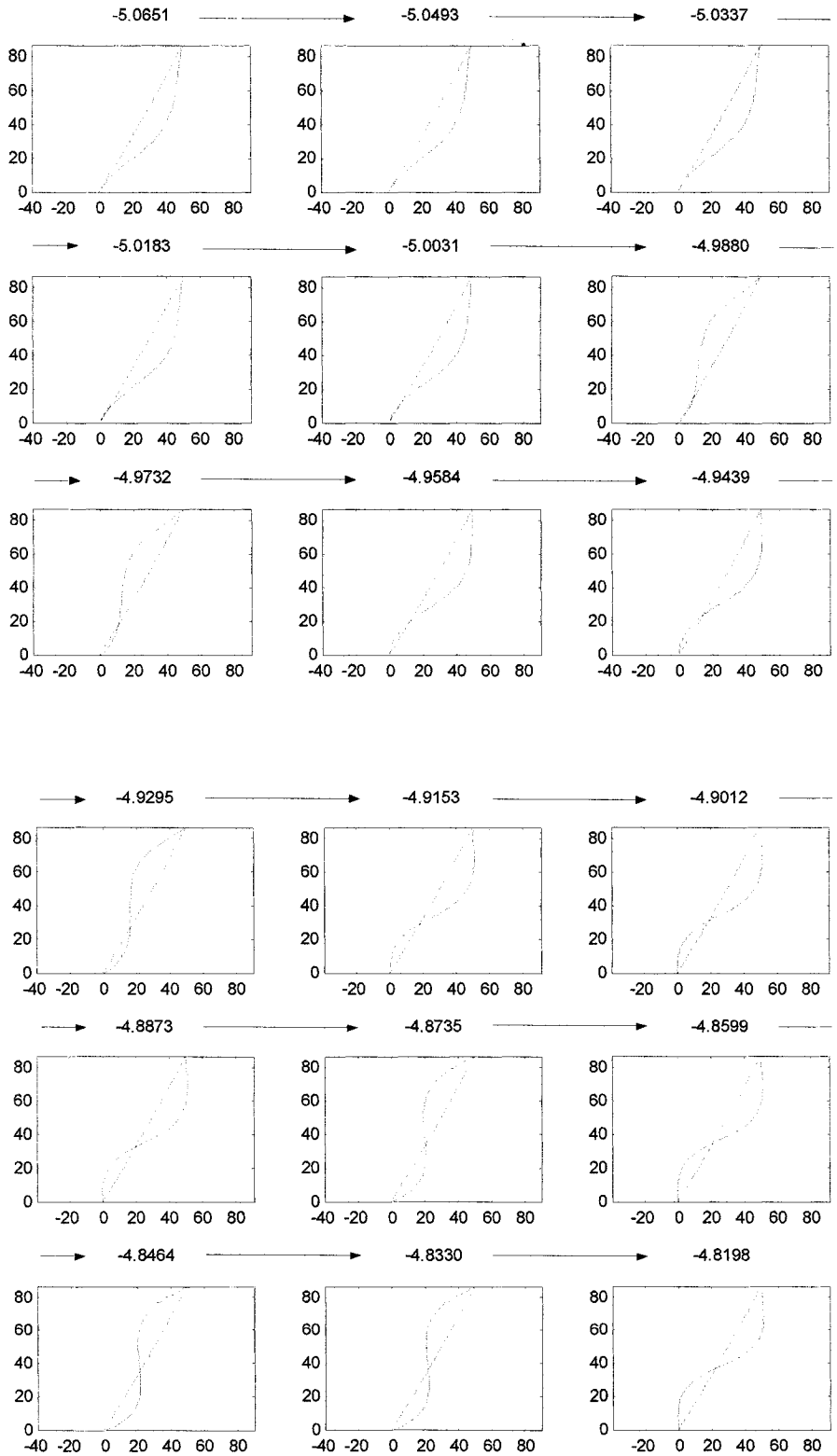

Fig. 4.40 Mode shapes between the transition range in the 1st frequency line ($\theta = 60°$)

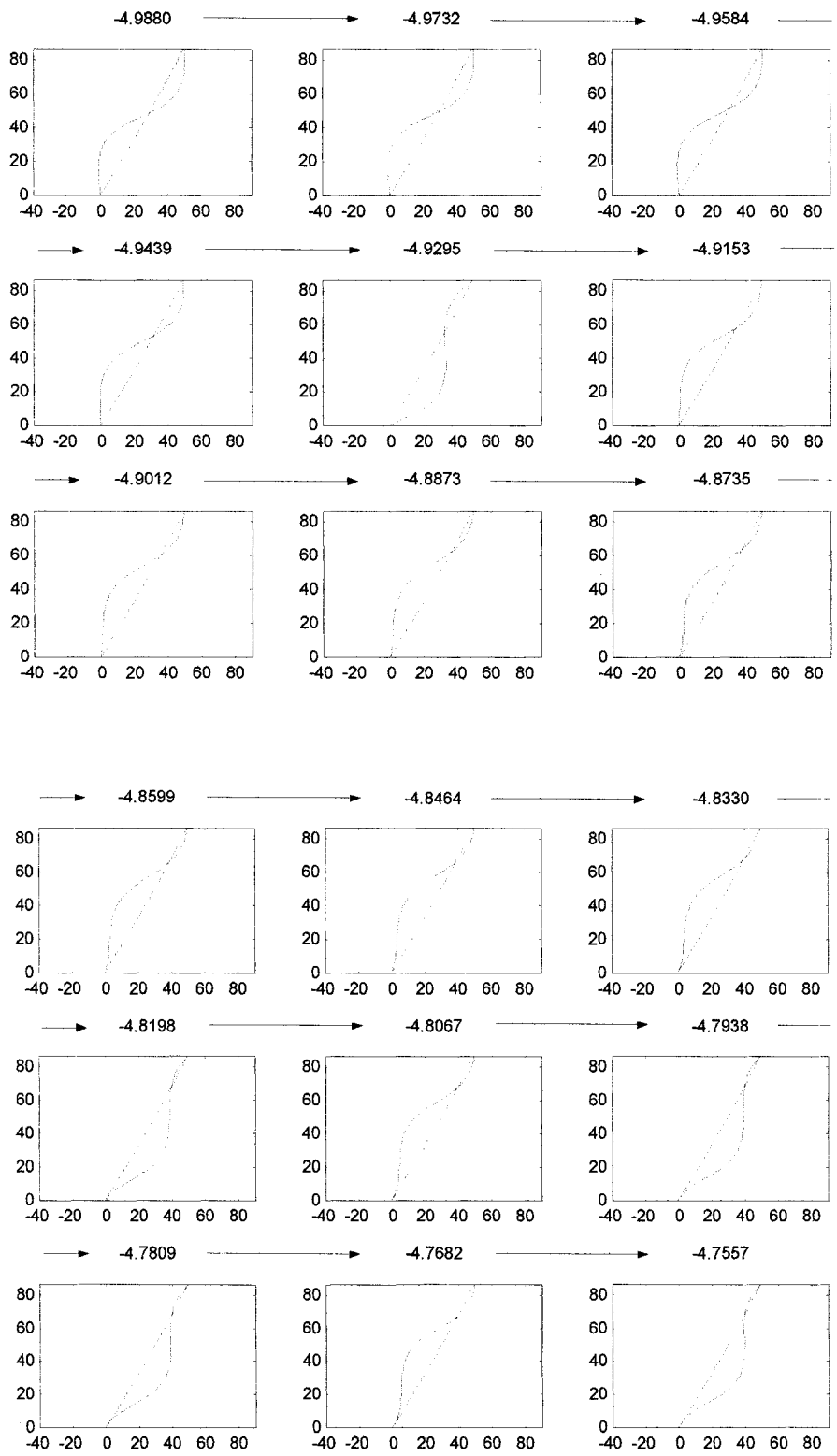

Fig. 4.41 Mode shapes between the transition range in the 2nd frequency line ($\theta = 60°$)

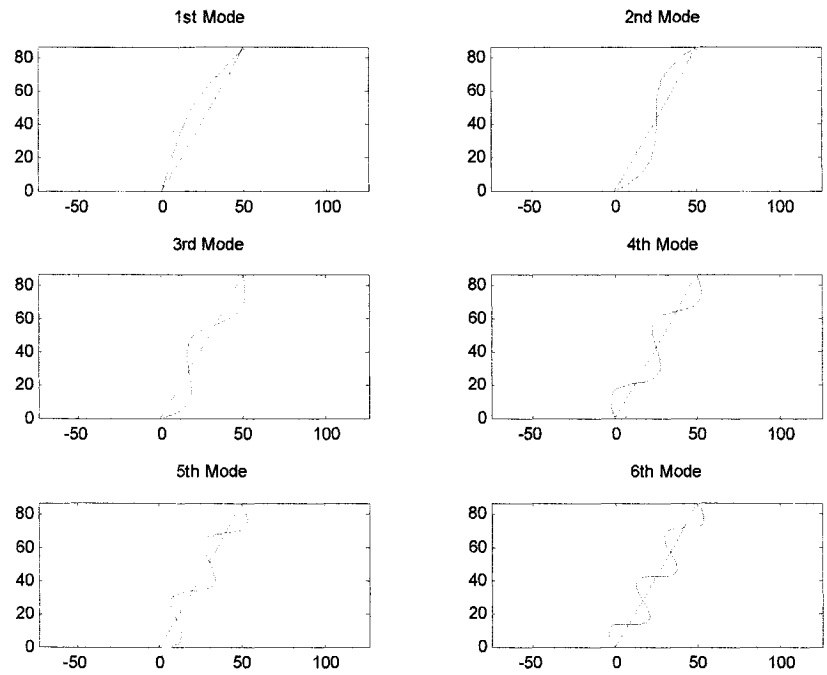

Fig. 4.42 Mode shapes at A ($\theta = 60°$)

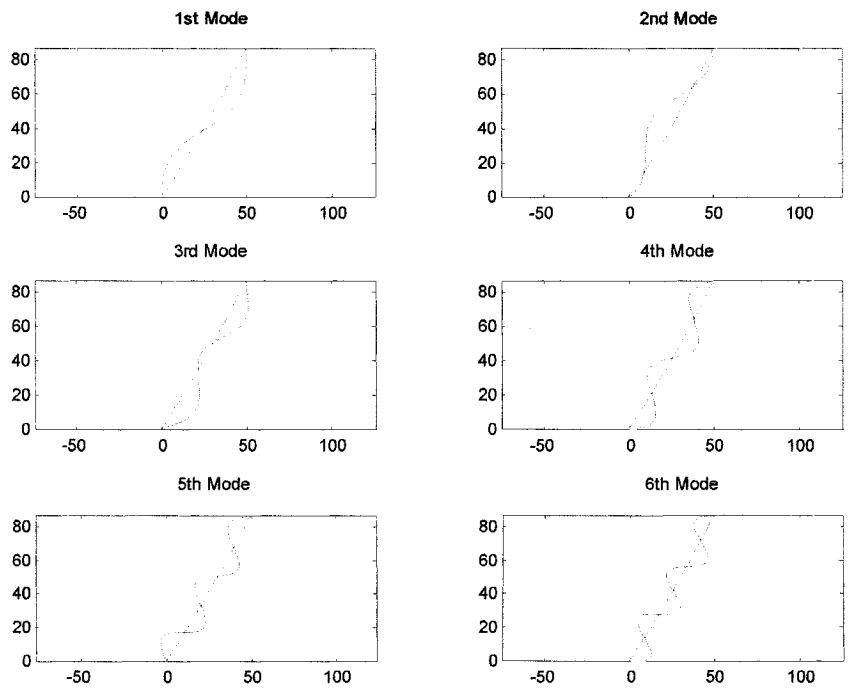

Fig. 4.43 Mode shapes at B ($\theta = 60°$)

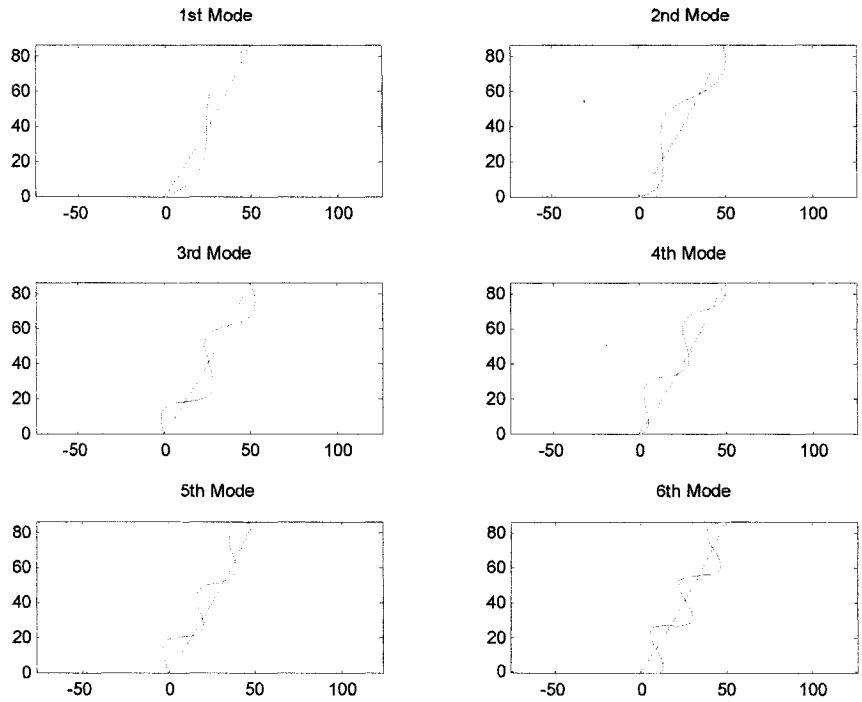

Fig. 4.44 Mode shapes at C ($\theta = 60°$)

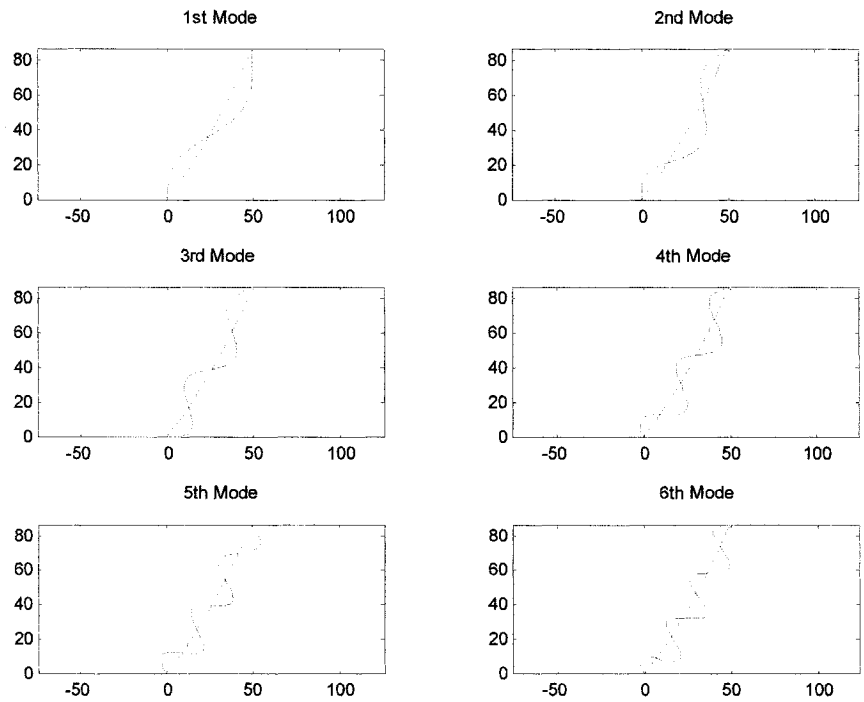

Fig. 4.45 Mode shapes at D ($\theta = 60°$)

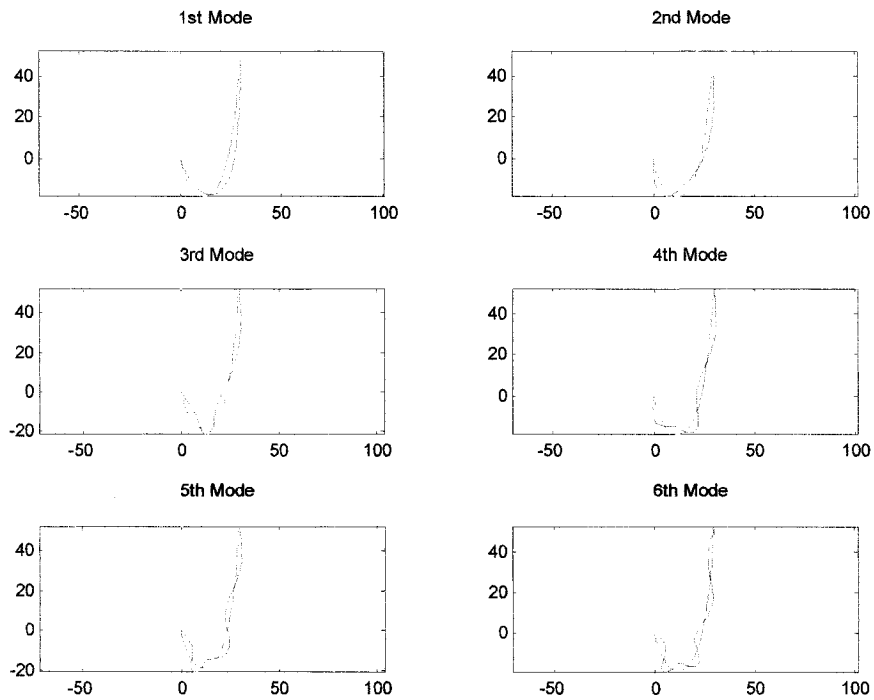

Fig. 4.46 Mode shapes at E ($\theta = 60°$)

4.2.7 Inclined Cable ($\theta = 80°$)

In Fig. 4.47, the first six frequencies are plotted against $\log(RR^3)$ when the inclination angle of a cable is $80°$. Once the inclination angle of a cable is very large, in this instance $\theta = 80°$, the mode shape transition happens quite differently. Figure 4.48 represents the mode shapes that correspond to each black dot on the first frequency line in Fig. 4.47. In the figure, the first symmetric mode shape begins to change as $\log(RR^3)$ increases and it approaches the shape of the asymmetric mode. However, before it makes form of the asymmetric mode shape, the node, which is a cross point of the mode shape line and static cable line (see Fig. 4.48), comes down after a certain level of $\log(RR^3)$. The reason for this phenomenon must be accredited to the significant effect of gravity force to the cable tension. Figure 4.49 represents the mode shapes corresponding to each red dot on the second frequency line in Fig. 4.47. It also shows that the first asymmetric mode shape does not really shape the form of symmetric.

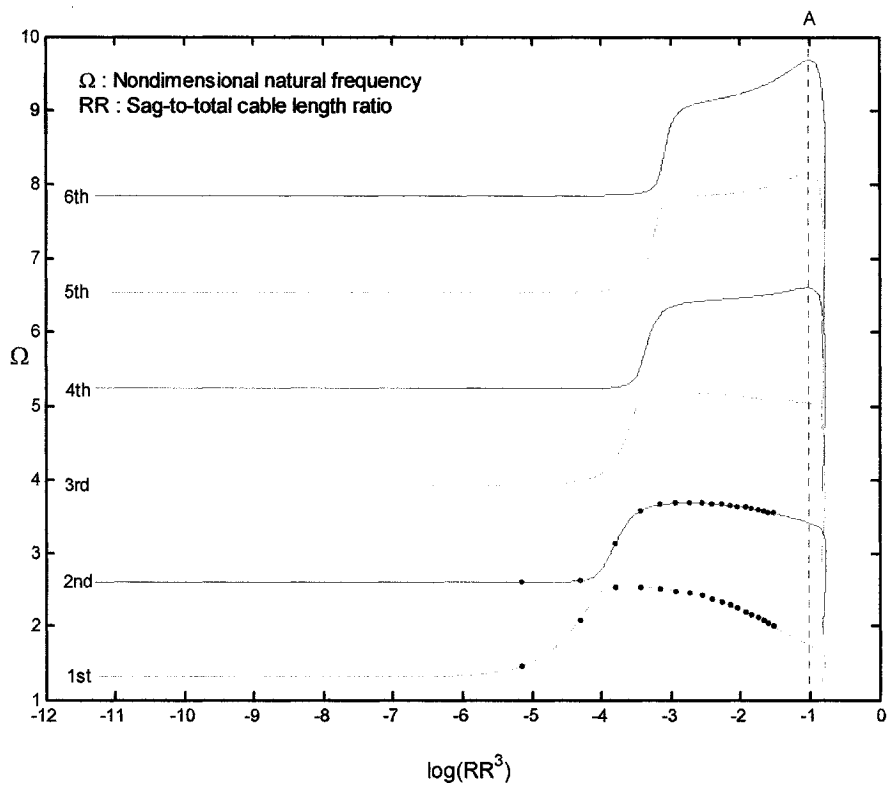

Fig. 4.47 Non-dimensional natural frequency vs. sag-to-total cable length ratio ($\theta = 80°$)

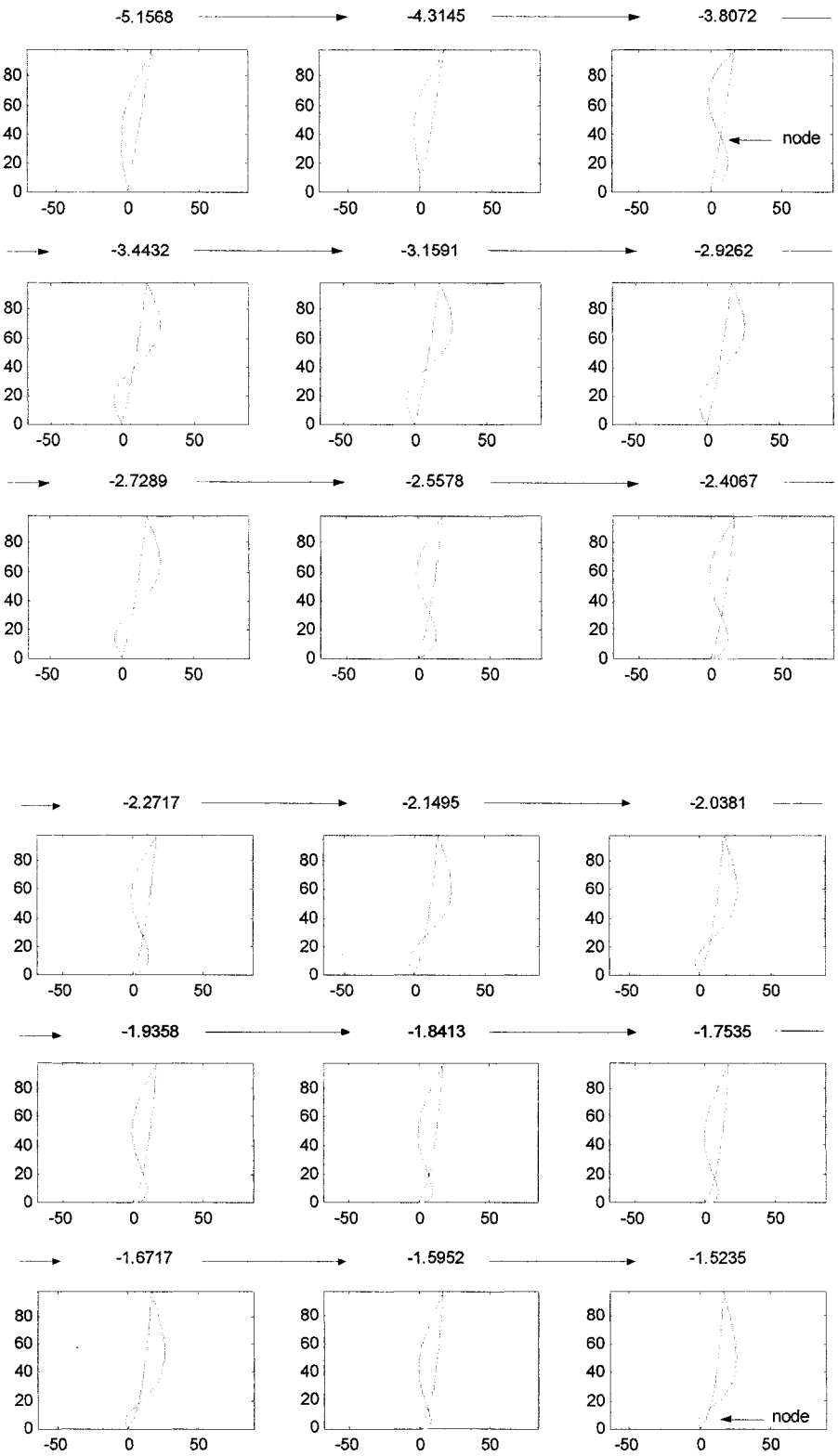

Fig. 4.48 Mode shapes along the black dots on the 1st frequency line ($\theta = 80°$)

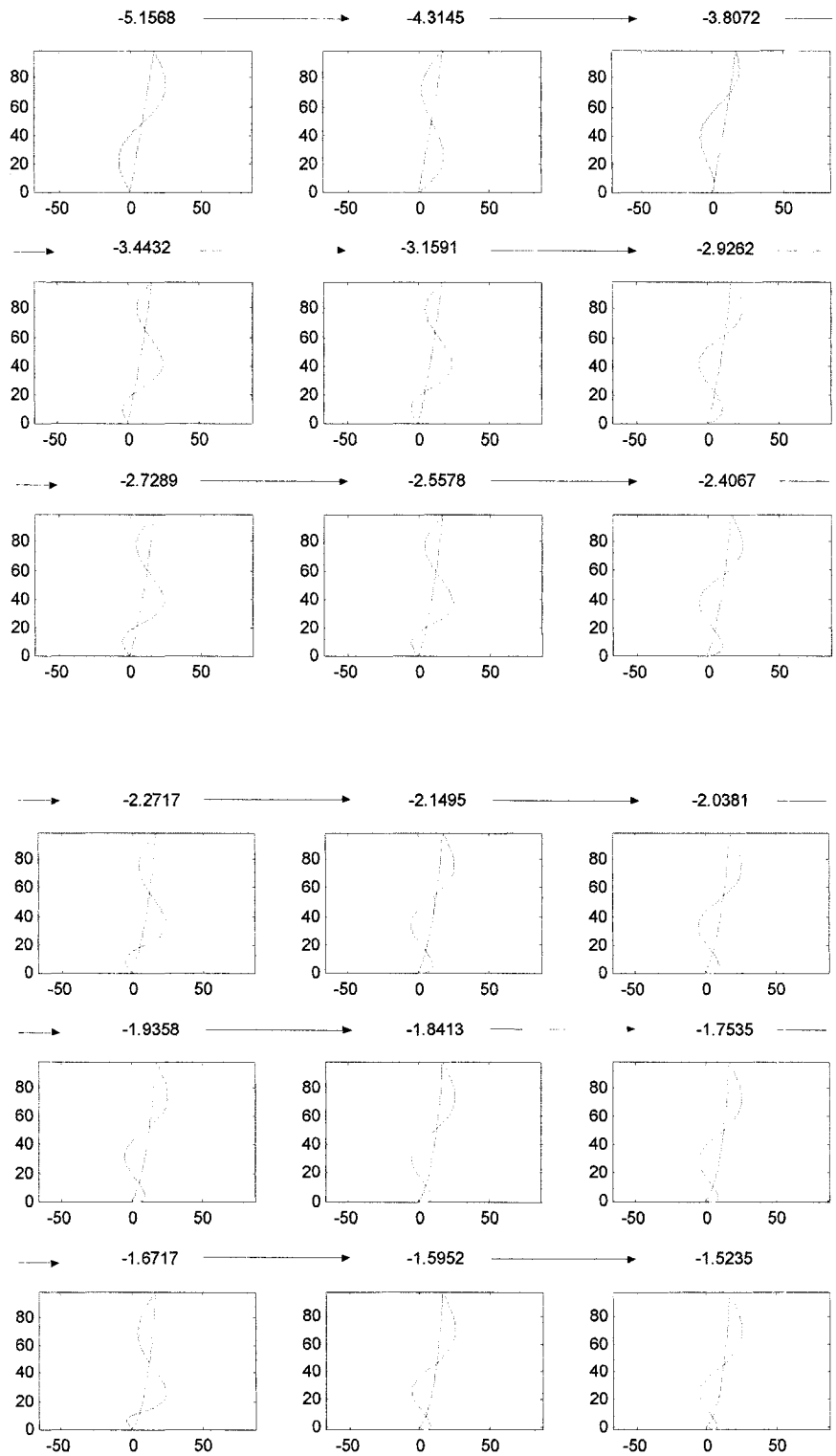

Fig. 4.49 Mode shapes along the red dots on the 2nd frequency line ($\theta = 80°$)

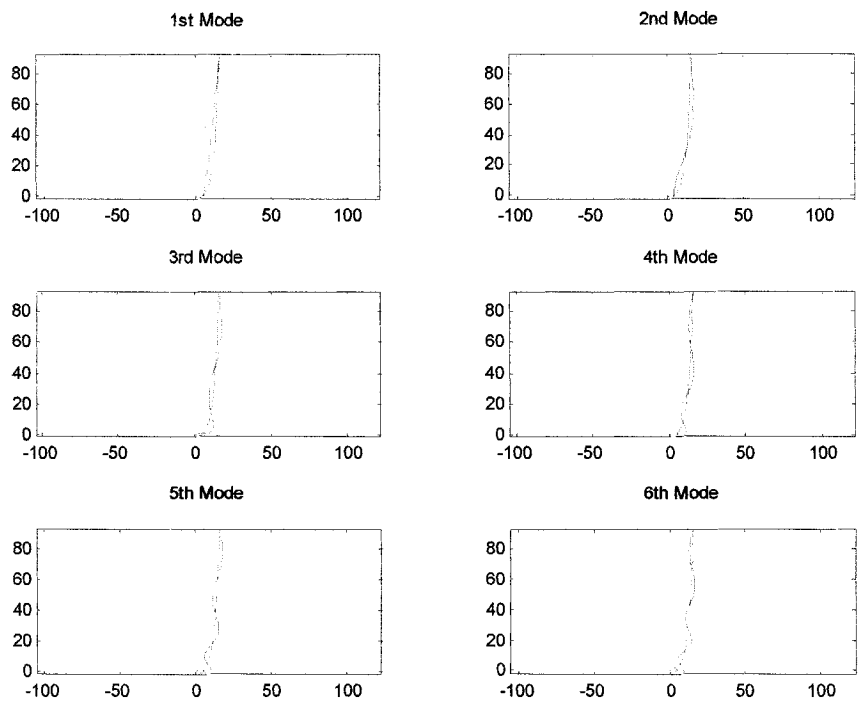

Fig. 4.50 Mode shapes at A ($\theta = 80°$)

4.3 Case #2

4.3.1 Input Parameters

The following properties are assumed for this case:

•Young's modulus (E): $2\times10^{10}\,N/m^2$	•Cable length (L): $100m$
•Mass per unit length of cable (M): $5.55kg/m$	•Cable diameter (Di): $0.03m$
•Inclination angle of cable (θ): 0, 30°, 60°	

This case is not representative of an actual material. To examine the effect of axial stiffness, a value of $0.1E$ as used in Case #1.

4.3.2 Horizontal Cable ($\theta = 0$)

In Case #2, a different Young's modulus reduced by a factor of 10, is used. Comparing with the previous results of the horizontal cable in Case #1, there are two noticeable differences in Case #2. One is the transition range near the modal crossover points, and the other is the shape of the fifth and sixth frequency lines when the cable tension is very high. Figure 4.51 shows the difference between Case #1 and Case #2 when the cable is horizontal.

In Fig. 4.51, the first, second, and third modal crossover points are shifted to the right side when Young's modulus is smaller. This indicates that the modal crossover occurs under the circumstance of smaller cable tension when the cable is softer or EA is smaller.

Figure 4.52 represents the amplified figure of the box in Fig. 4.51. P is the point that the inclination of the sixth frequency line changes to horizontal. The cable tension at the point P(σ_P) is $\sigma_P = 555.97MPa$. However, this cable tension is unrealistic since the ultimate stress of steel wire is usually from 550 to 1400 MPa. The Young's modulus of cable material here in Case #2 is 10 times less than the Young's modulus of steel. Therefore, the

ultimate stress of material used in Case #2 is expected much less than σ_P, since the material used in Case #2 would fail before the cable tension reaches σ_P. For this reason, the natural frequencies in this range will be ignored in the following discussion. Fig. 4.53 to Fig. 4.64 represent the first six frequencies and mode shapes when the cable is horizontal and E=$2\times10^{10} N/m^2$.

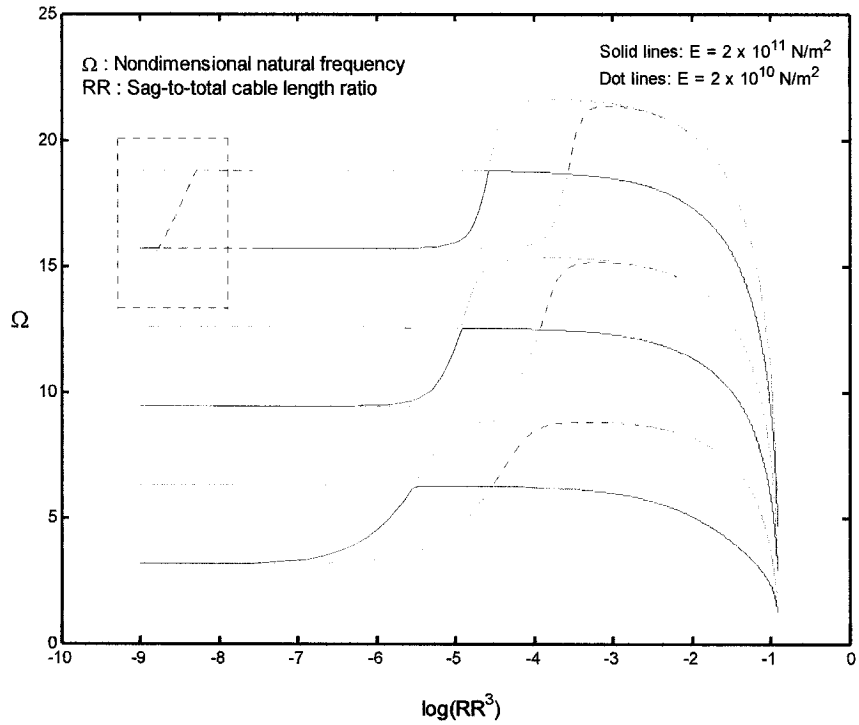

Fig. 4.51 Frequency lines of horizontal cable with different Young's modulus ($\theta = 0$)

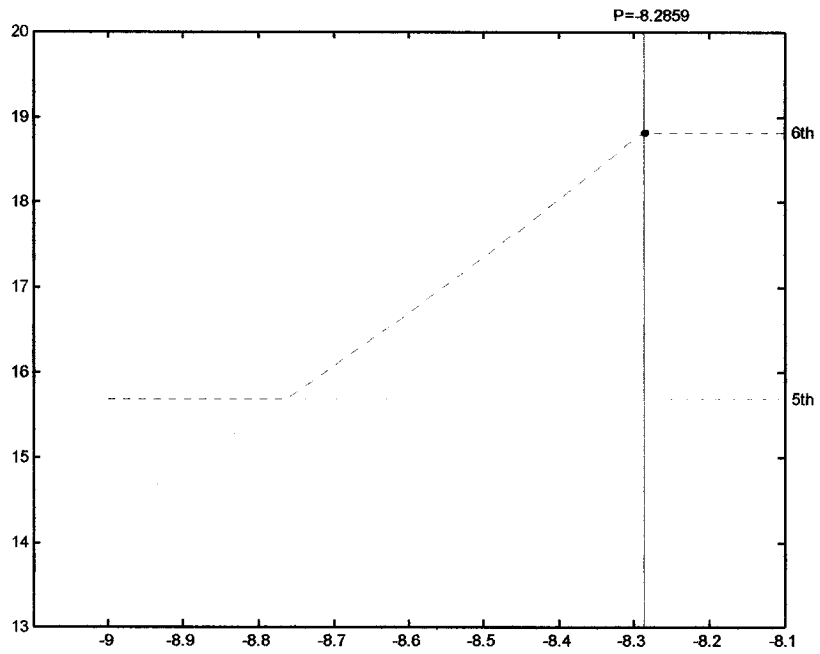

Fig. 4.52 5th and 6th frequency lines between $\log(RR^3) = -9$ and $\log(RR^3) = -8.1$ when $\theta = 0$ and E=$2\times10^{10} N/m^2$

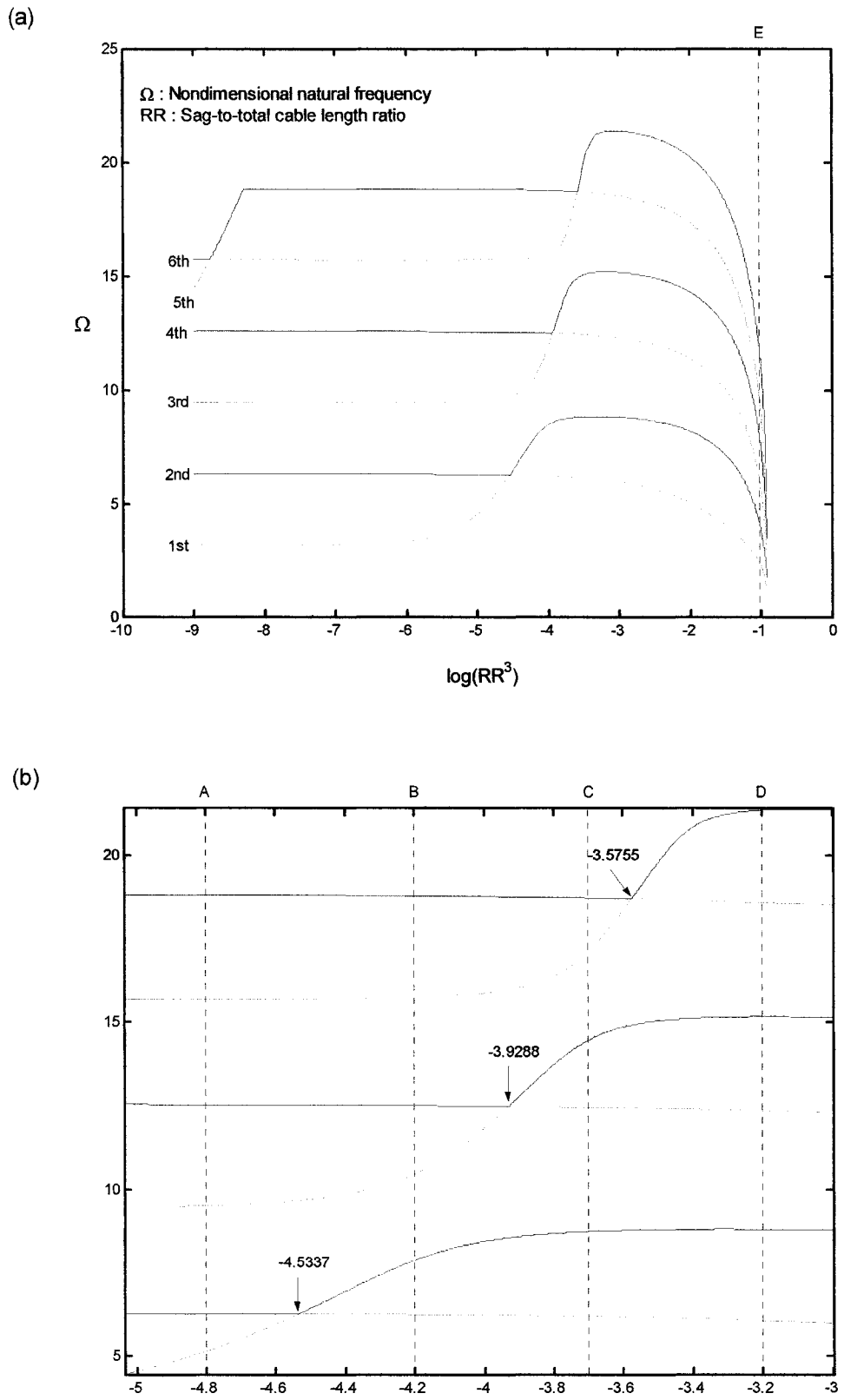

Fig. 4.53 Non-dimensional natural frequency vs. sag-to-total cable length ratio ($\theta = 0$)

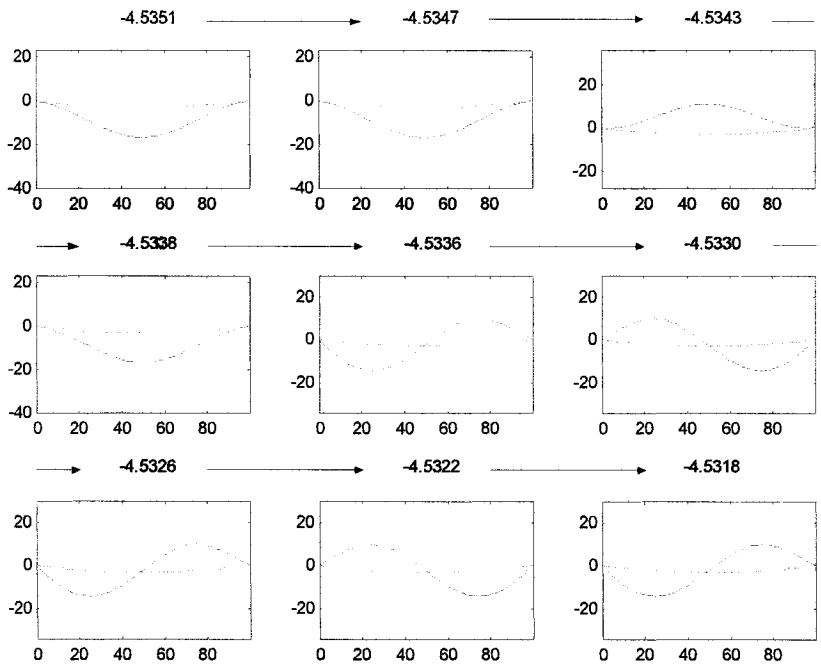

Fig. 4.54 Mode shapes right before and after at the point –4.5337 in the 1st frequency line ($\theta = 0$)

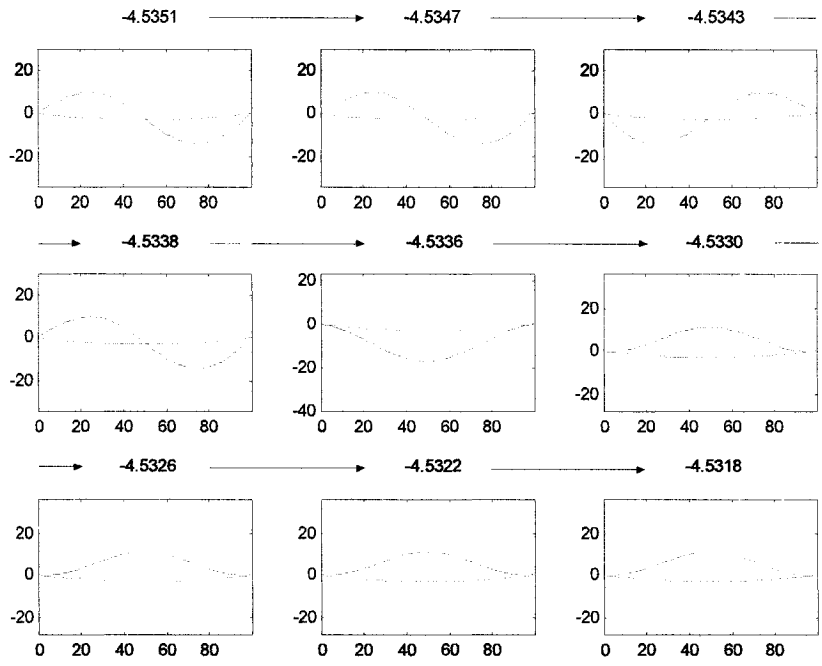

Fig. 4.55 Mode shapes right before and after at the point –4.5337 in the 2nd frequency line ($\theta = 0$)

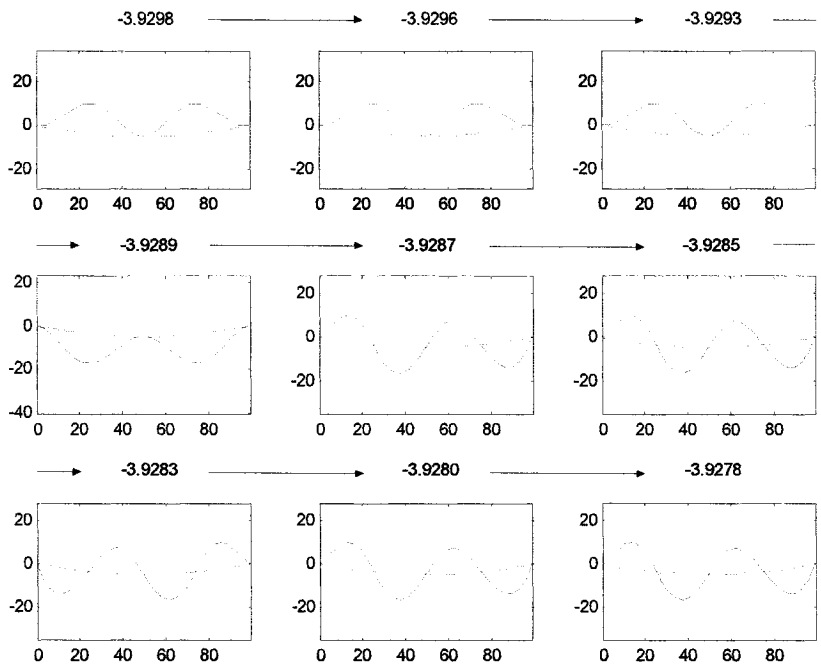

Fig. 4.56 Mode shapes right before and after at the point –3.9288 in the 3rd frequency line ($\theta = 0$)

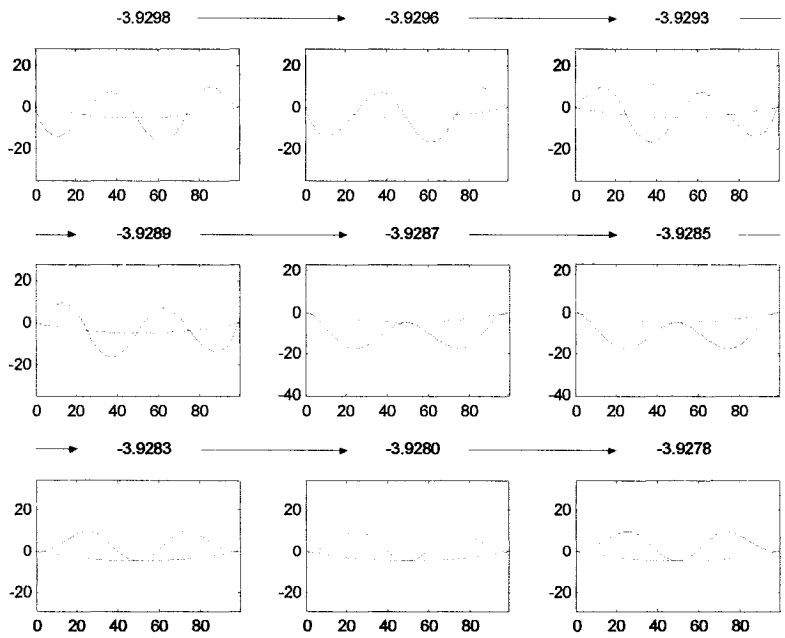

Fig. 4.57 Mode shapes right before and after at the point –3.9288 in the 4th frequency line ($\theta = 0$)

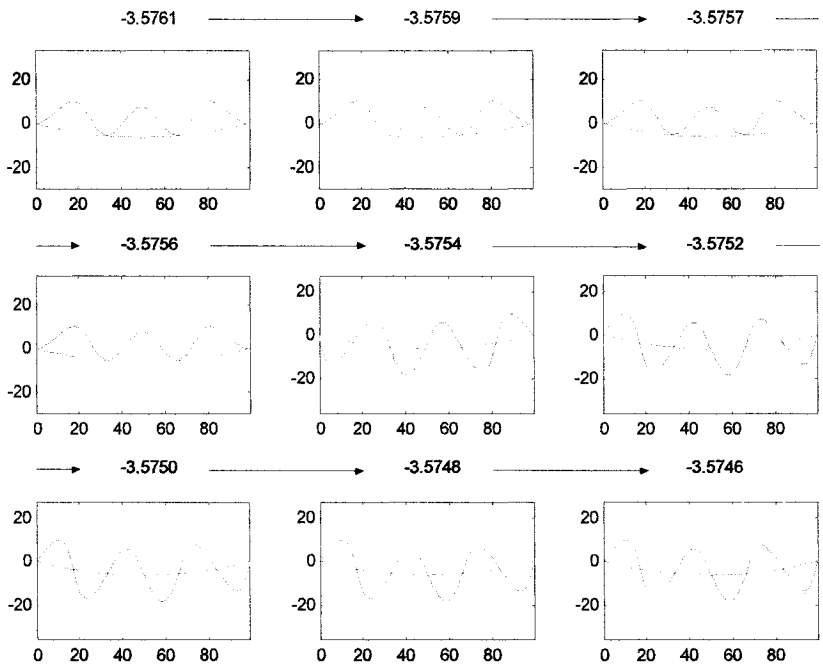

Fig. 4.58 Mode shapes right before and after at the point –3.5755 in the 5th frequency line ($\theta = 0$)

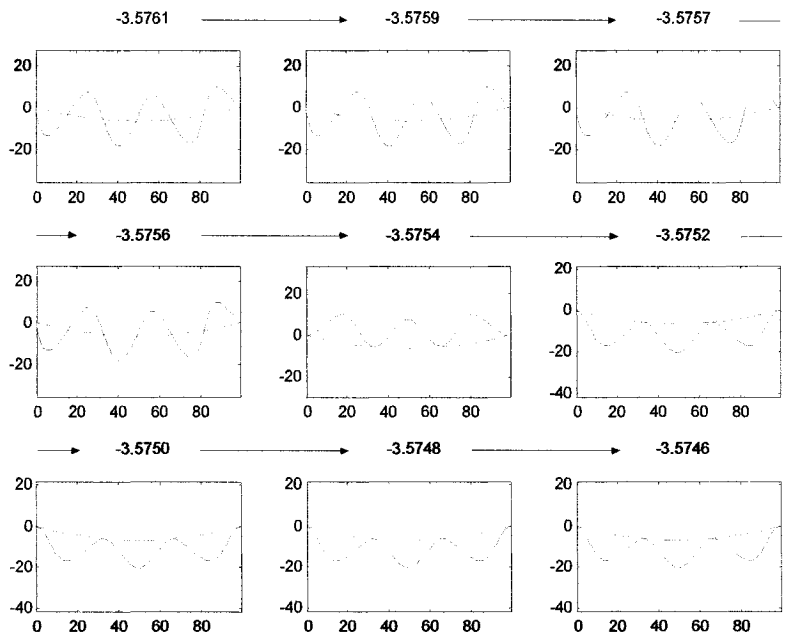

Fig. 4.59 Mode shapes right before and after at the point –3.5755 in the 6th frequency line ($\theta = 0$)

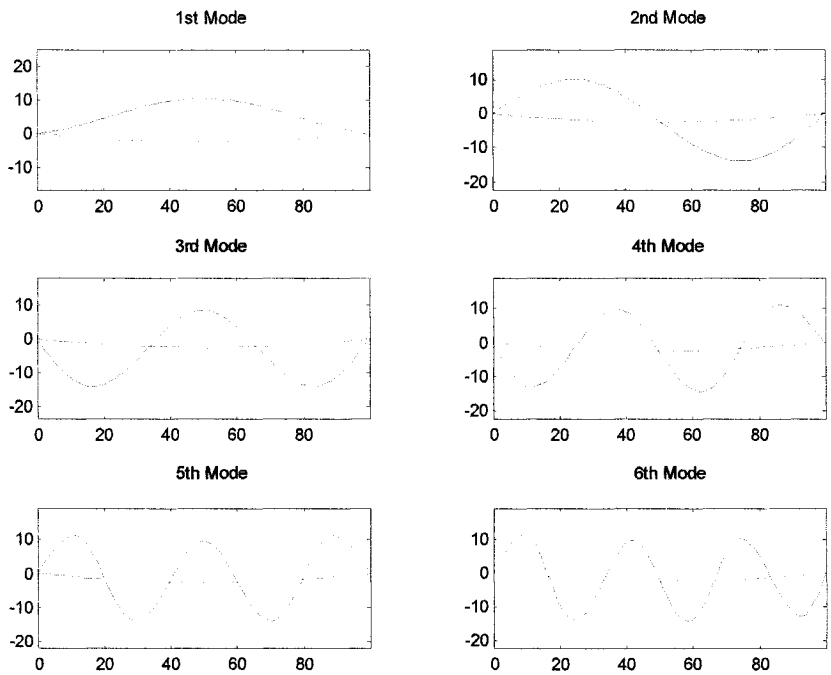

Fig. 4.60 Mode shapes at A ($\theta = 0$)

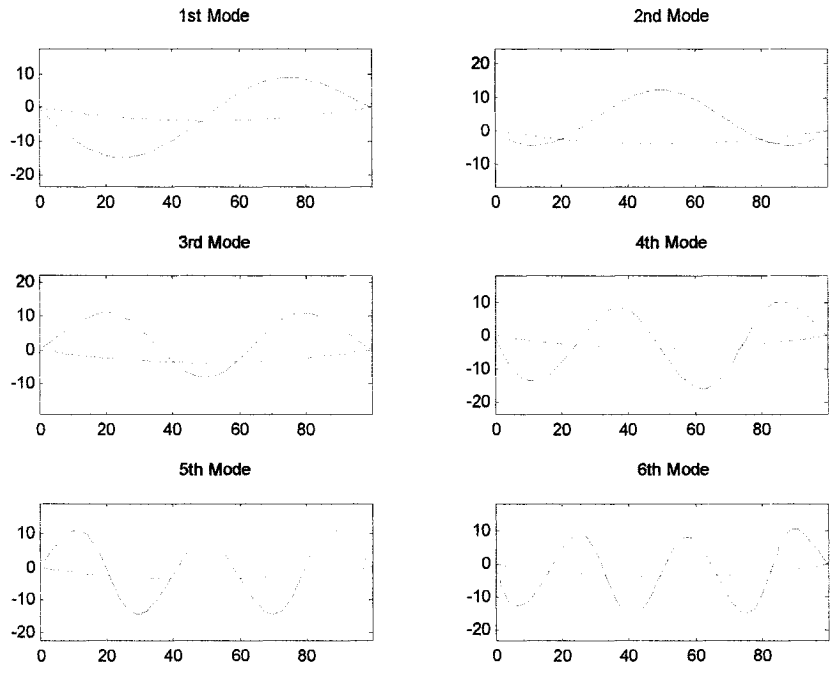

Fig. 4.61 Mode shapes at B ($\theta = 0$)

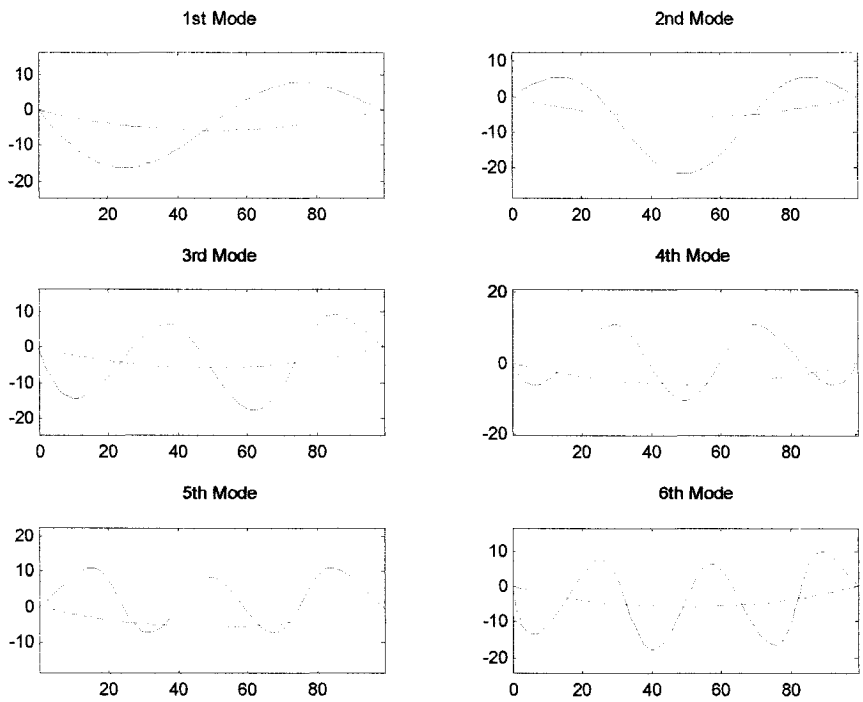

Fig. 4.62 Mode shapes at C ($\theta = 0$)

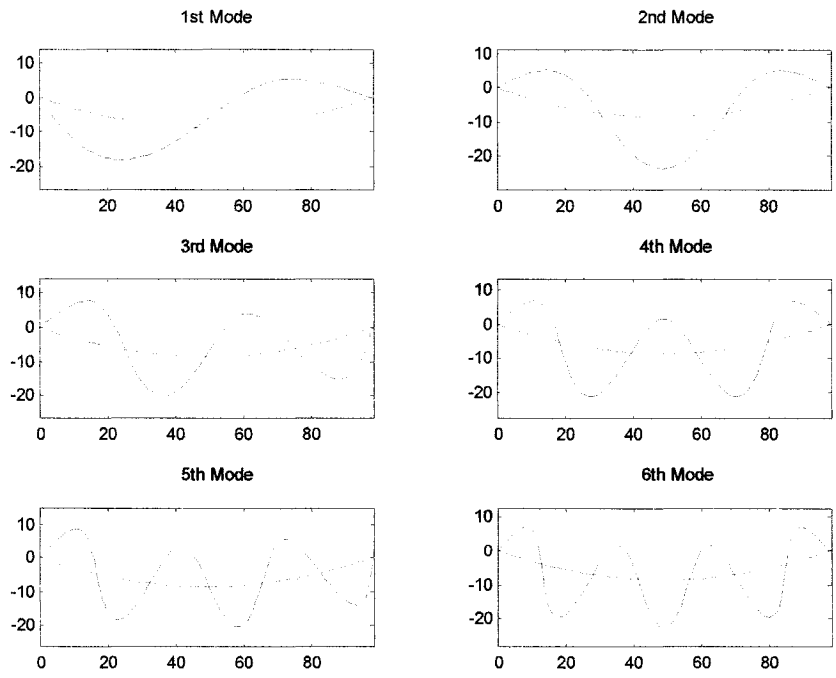

Fig. 4.63 Mode shapes at D ($\theta = 0$)

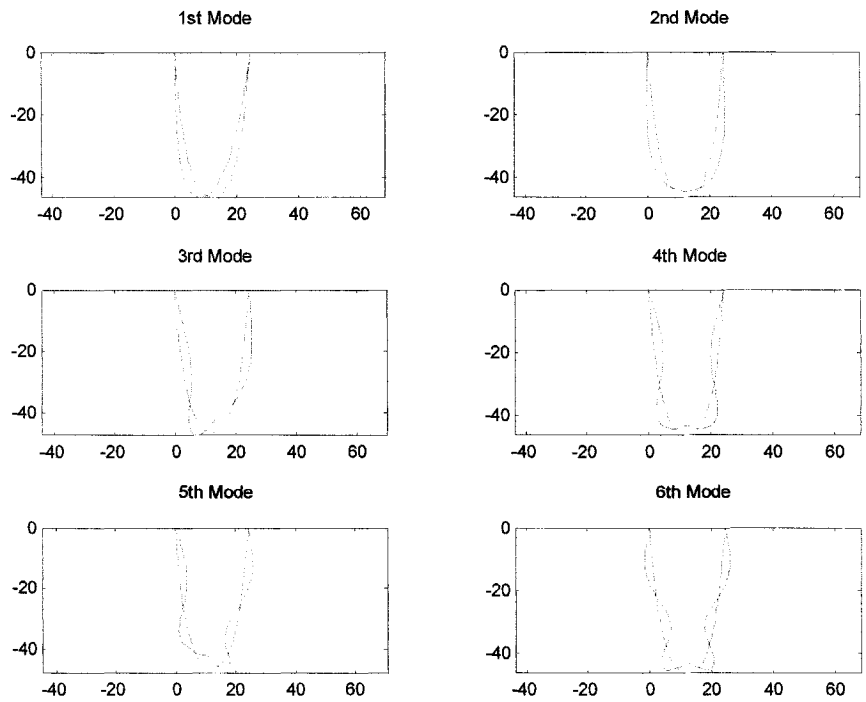

Fig. 4.64 Mode shapes at E ($\theta = 0$)

4.3.3 Inclined Cable ($\theta = 30^{\circ}$)

In Fig. 4.65, the first six frequencies of the inclined cable ($\theta = 30°$) are plotted when the Young's modulus is $2\times10^{10} N/m^2$. As expected, the modal crossover does not take place at one particular point once the cable span is inclined. Figure 4.66 shows that the transition ranges are shifted to the right when the value of Young's modulus is smaller.

Other than the shifting of transition ranges, there exists another difference between Case #1 and Case #2. Figure 4.67 represents the first and second frequency lines enlarged around the transition range when E $=2\times10^{11} N/m^2$ and E $=2\times10^{10} N/m^2$. The figure shows that the width of transition range in the axially softer cable is wider than that of the axially stiffer cable. This difference also appears when the inclination of the cable span is $60°$ (see Fig. 4.76). From Fig. 4.65 to Fig. 4.73 illustrate results of the calculations when the inclination angle of the cable span is 30° and Fig. 4.74 to Fig. 4.83 are the results when the inclination angle of the cable span is 60°.

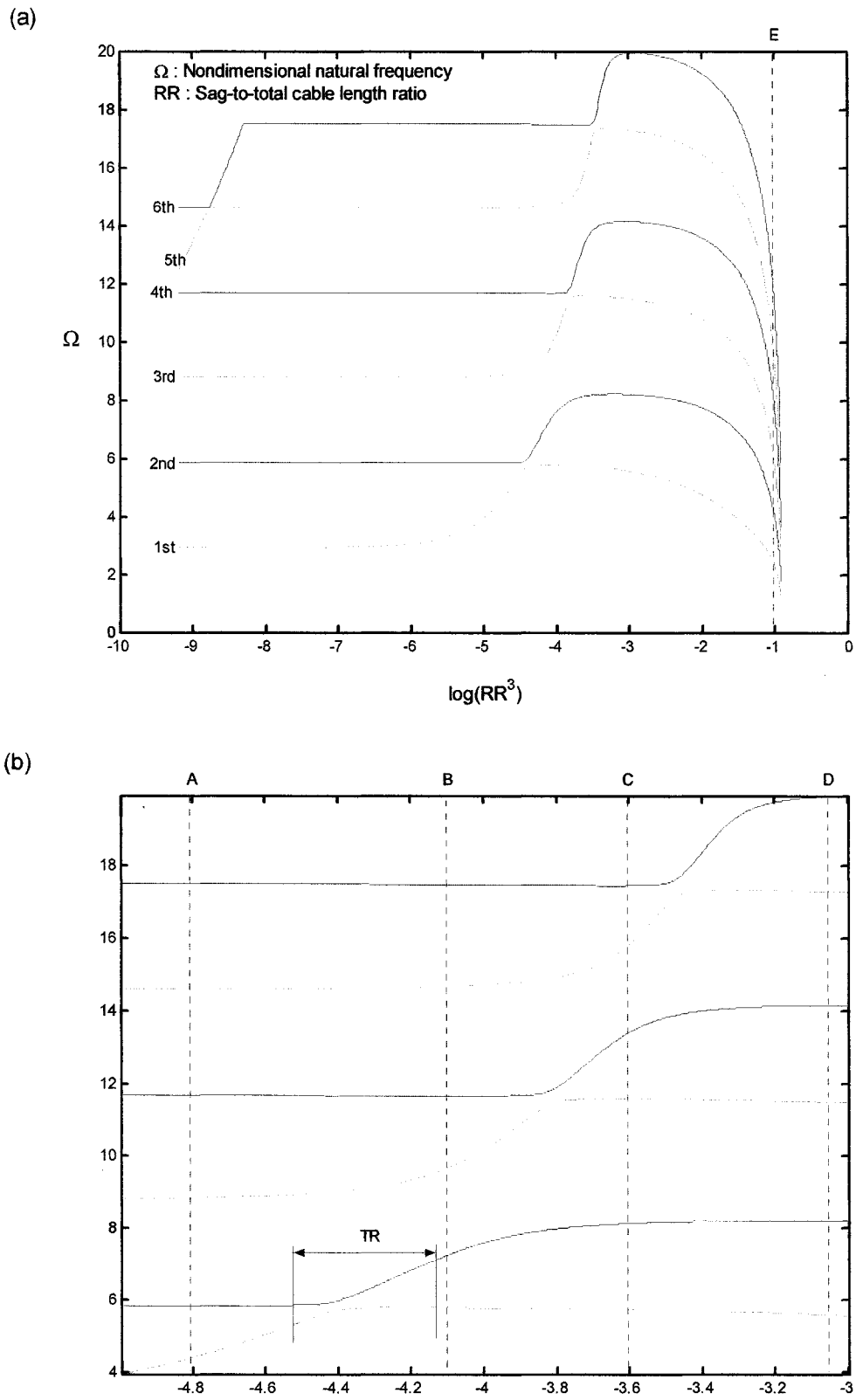

Fig. 4.65 Non-dimensional natural frequency vs. sag-to-total cable length ratio ($\theta = 30°$)

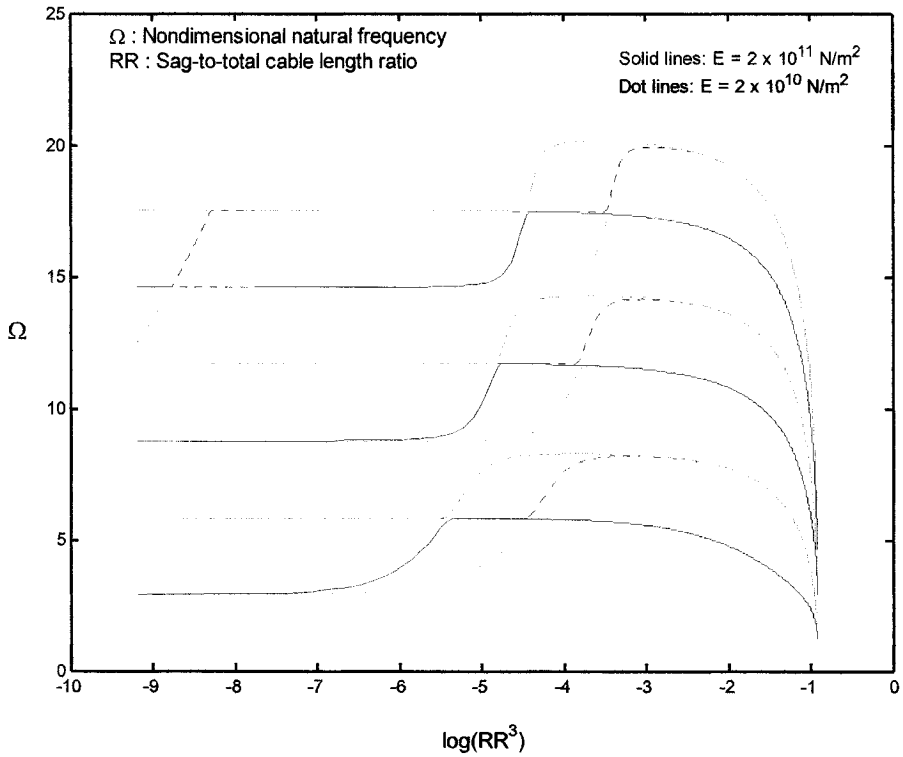

Fig. 4.66 Frequency lines of inclined cable with different Young's modulus ($\theta = 30°$)

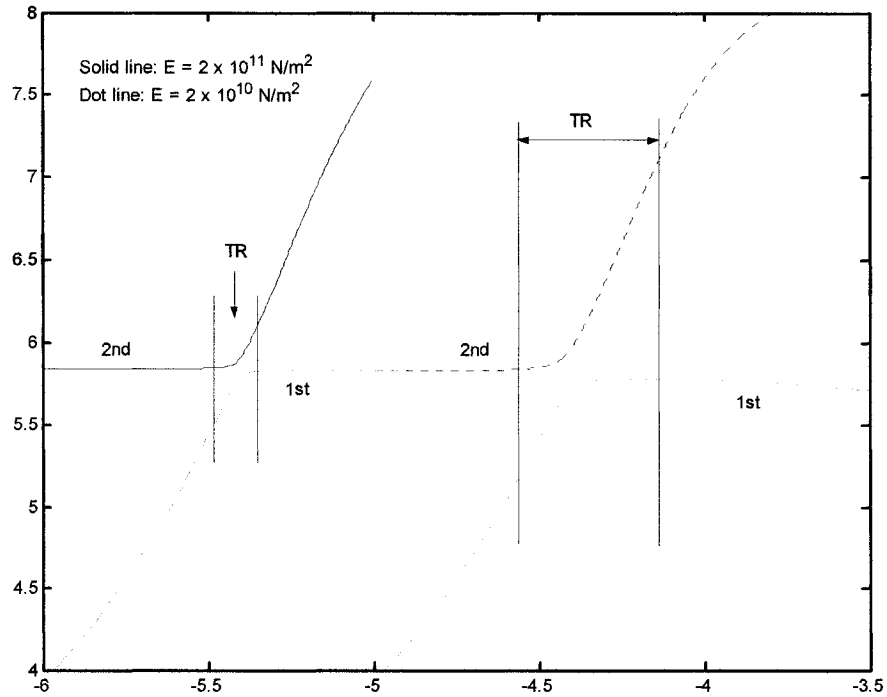

Fig. 4.67 1st and 2nd frequency lines at transition range with different E ($\theta = 30°$)

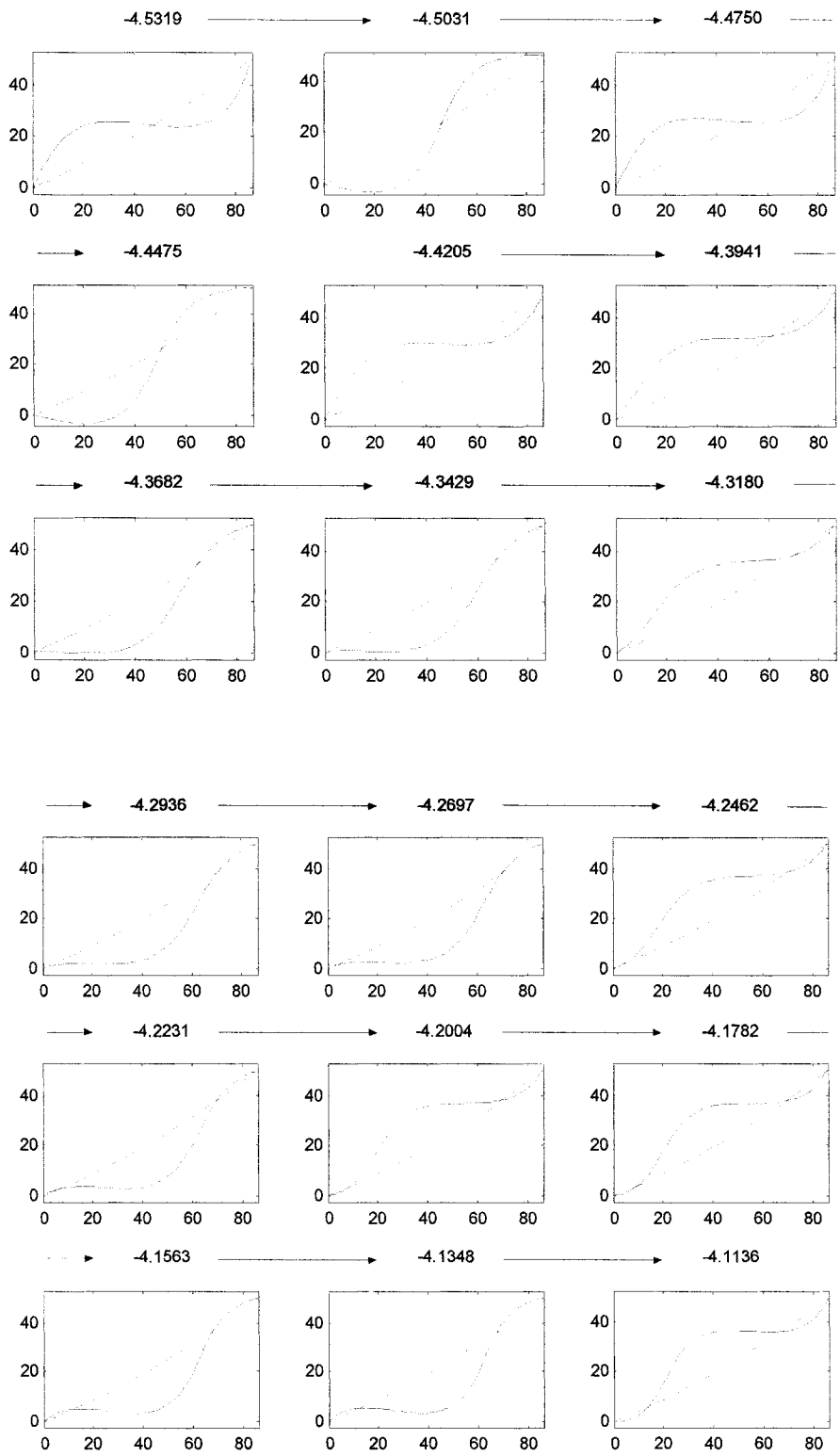

Fig. 4.68 Mode shapes between the transition range in the 2nd frequency line ($\theta = 30°$)

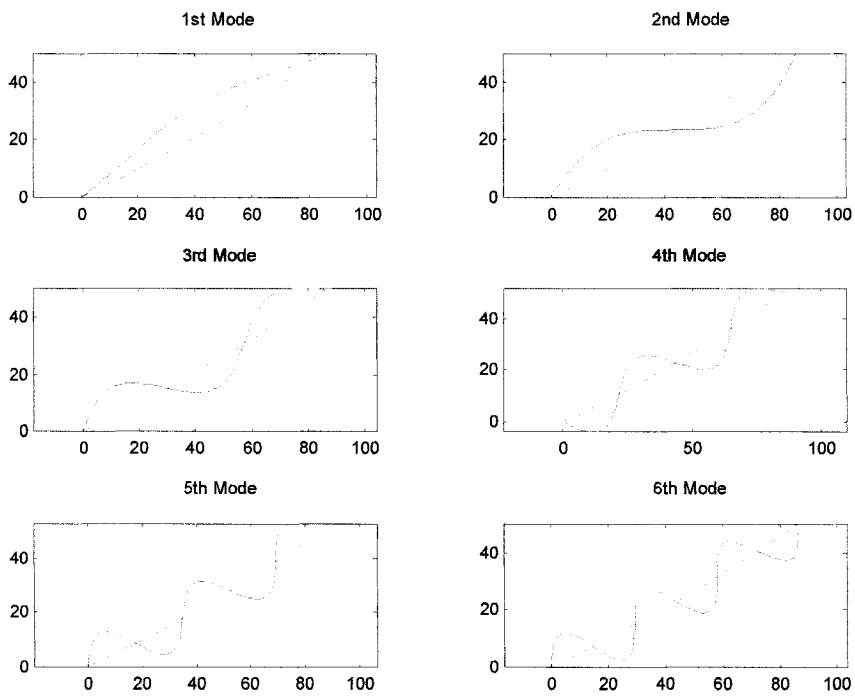

Fig. 4.69 Mode shapes at A ($\theta = 30°$)

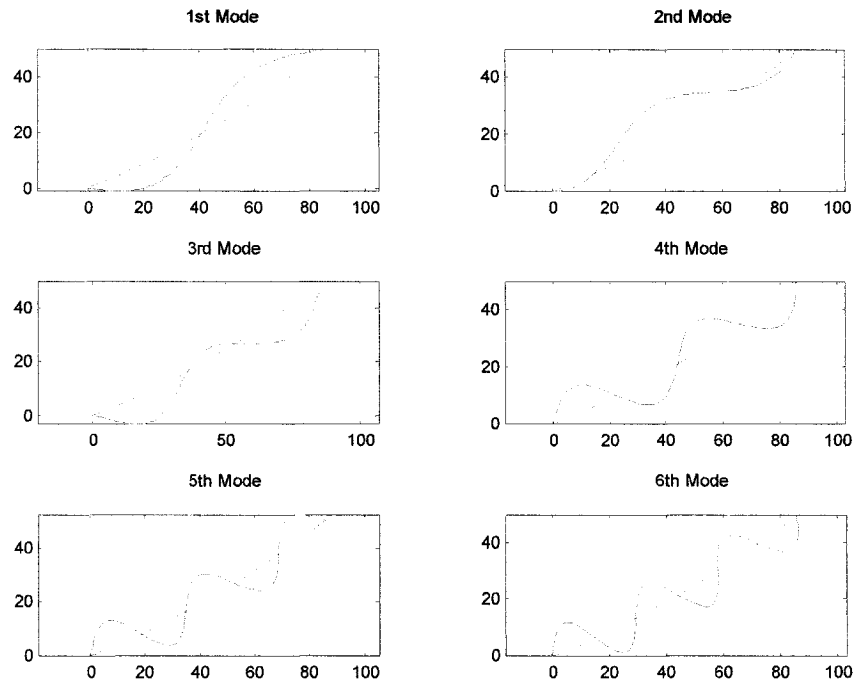

Fig. 4.70 Mode shapes at B ($\theta = 30°$)

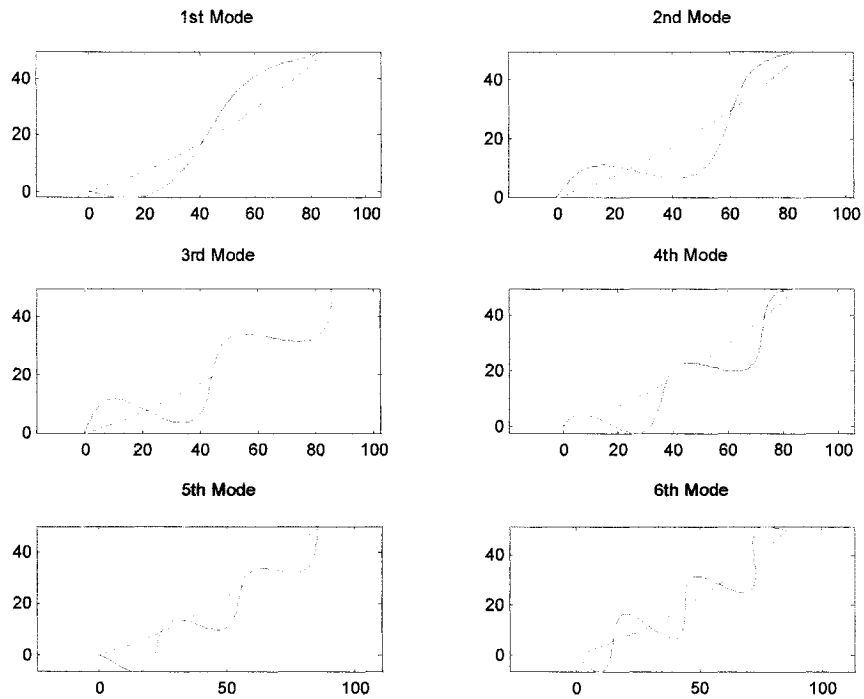

Fig. 4.71 Mode shapes at C ($\theta = 30°$)

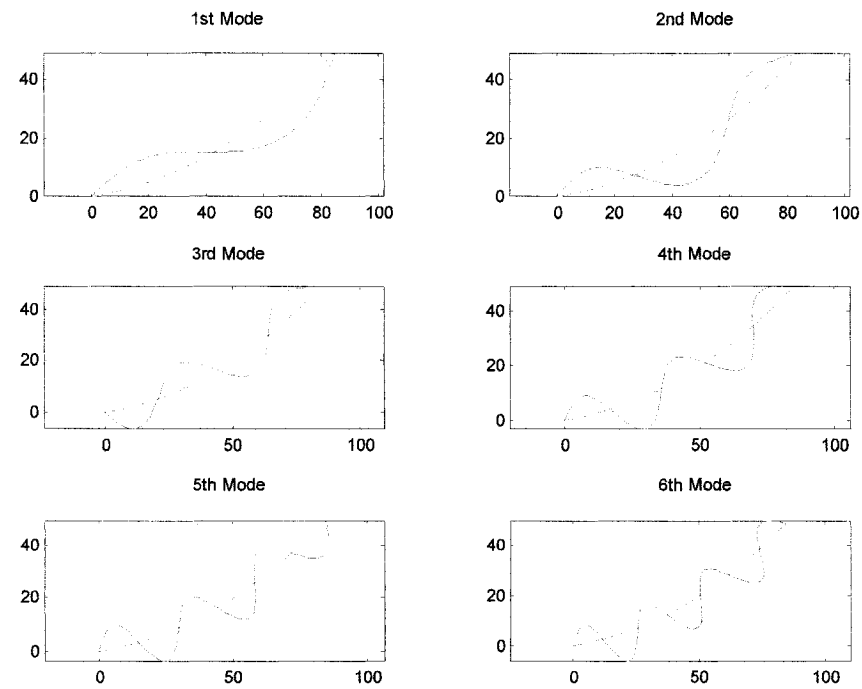

Fig. 4.72 Mode shapes at D ($\theta = 30°$)

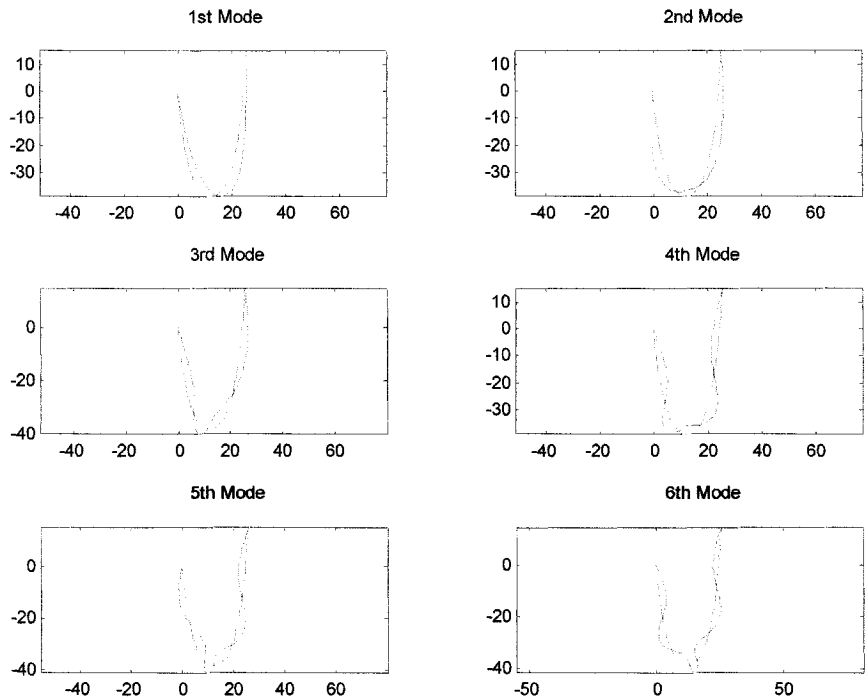

Fig. 4.73 Mode shapes at E ($\theta = 30°$)

4.3.4 Inclined Cable ($\theta = 60°$)

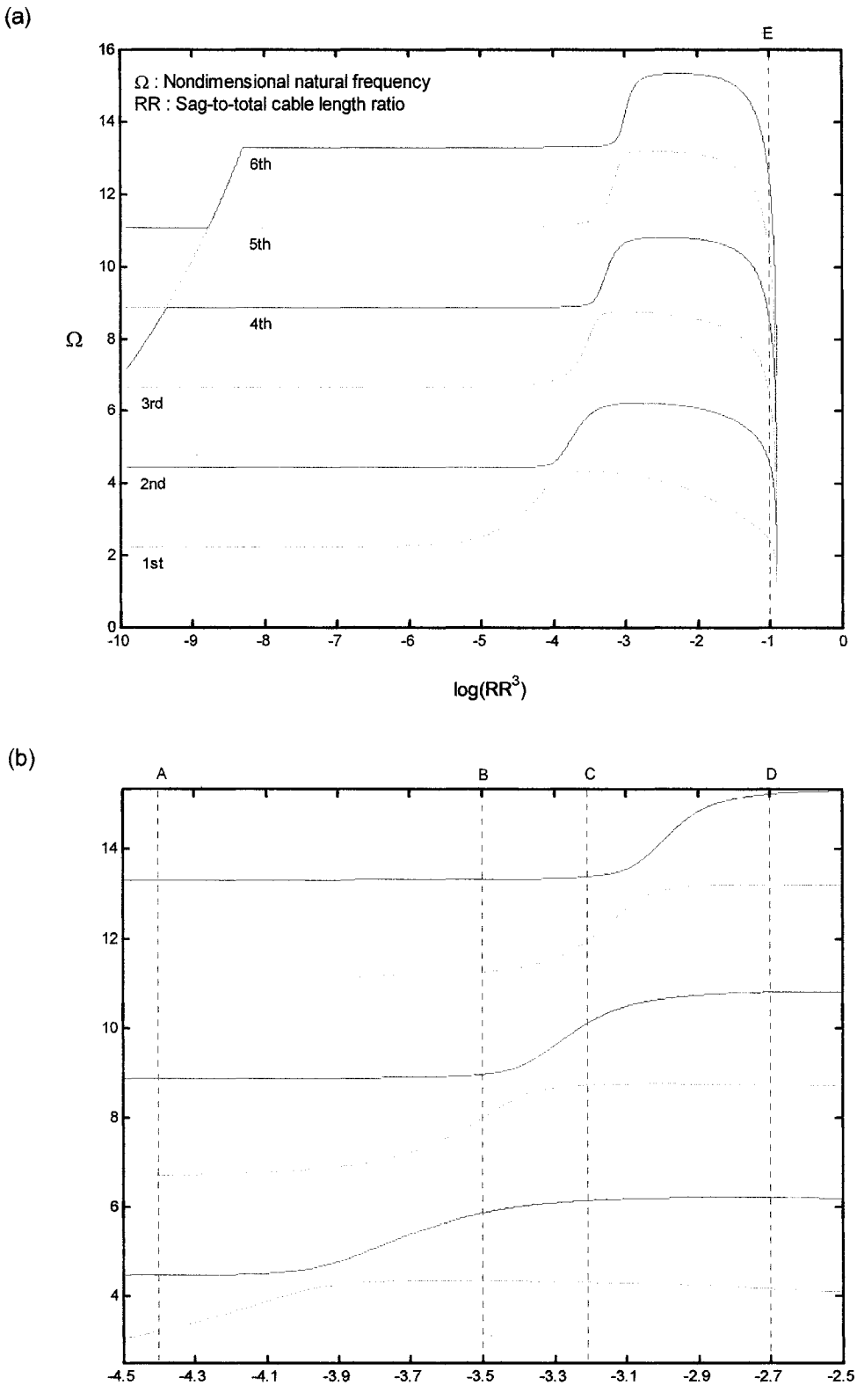

Fig. 4.74 Non-dimensional natural frequency vs. sag-to-total cable length ratio ($\theta = 60°$)

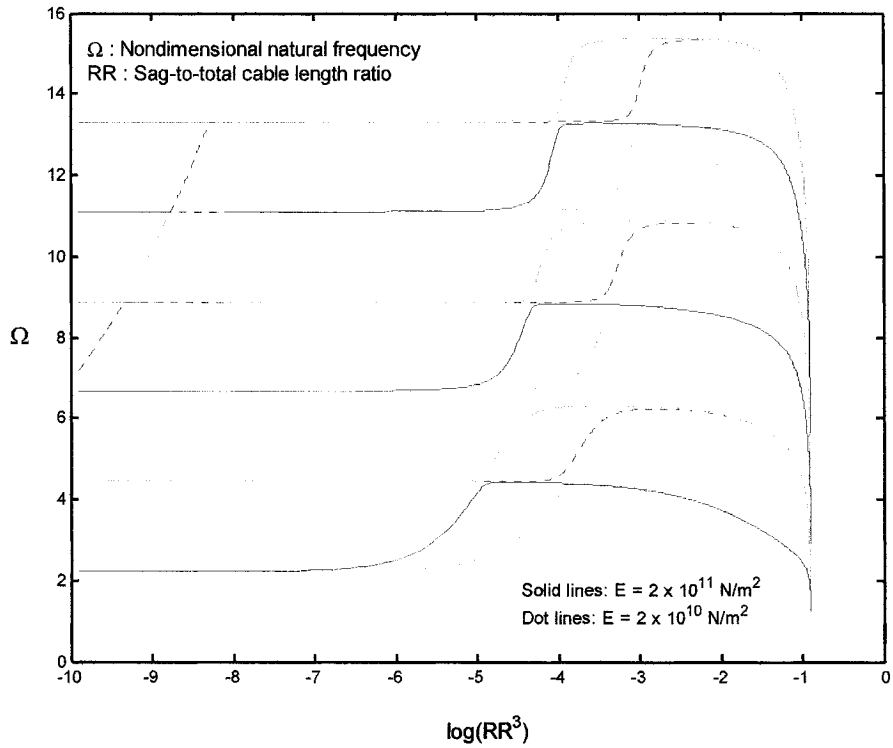

Fig. 4.75 Frequency lines of inclined cable with different Young's modulus ($\theta = 60°$)

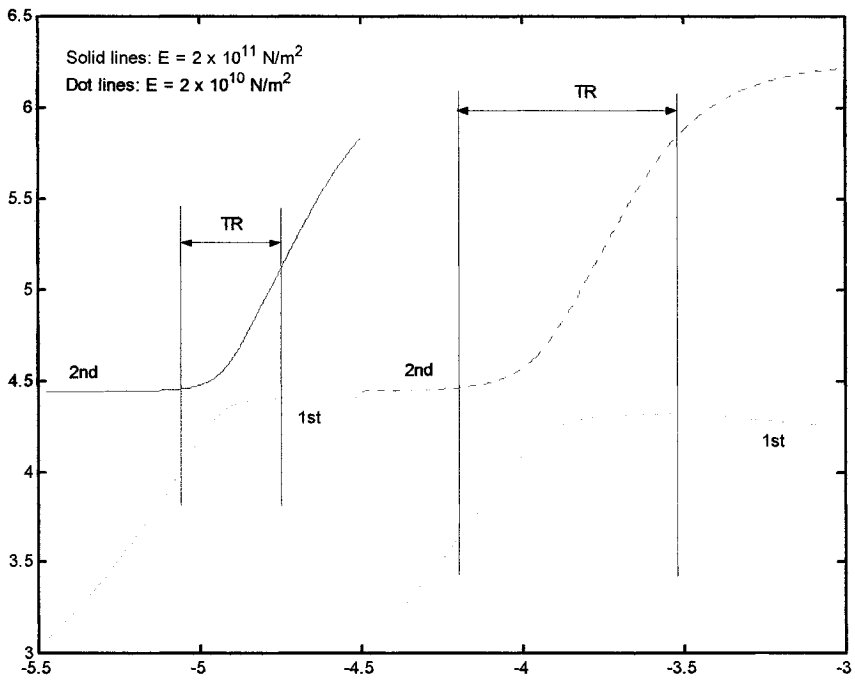

Fig. 4.76 1st and 2nd frequency lines at transition range with different E ($\theta = 60°$)

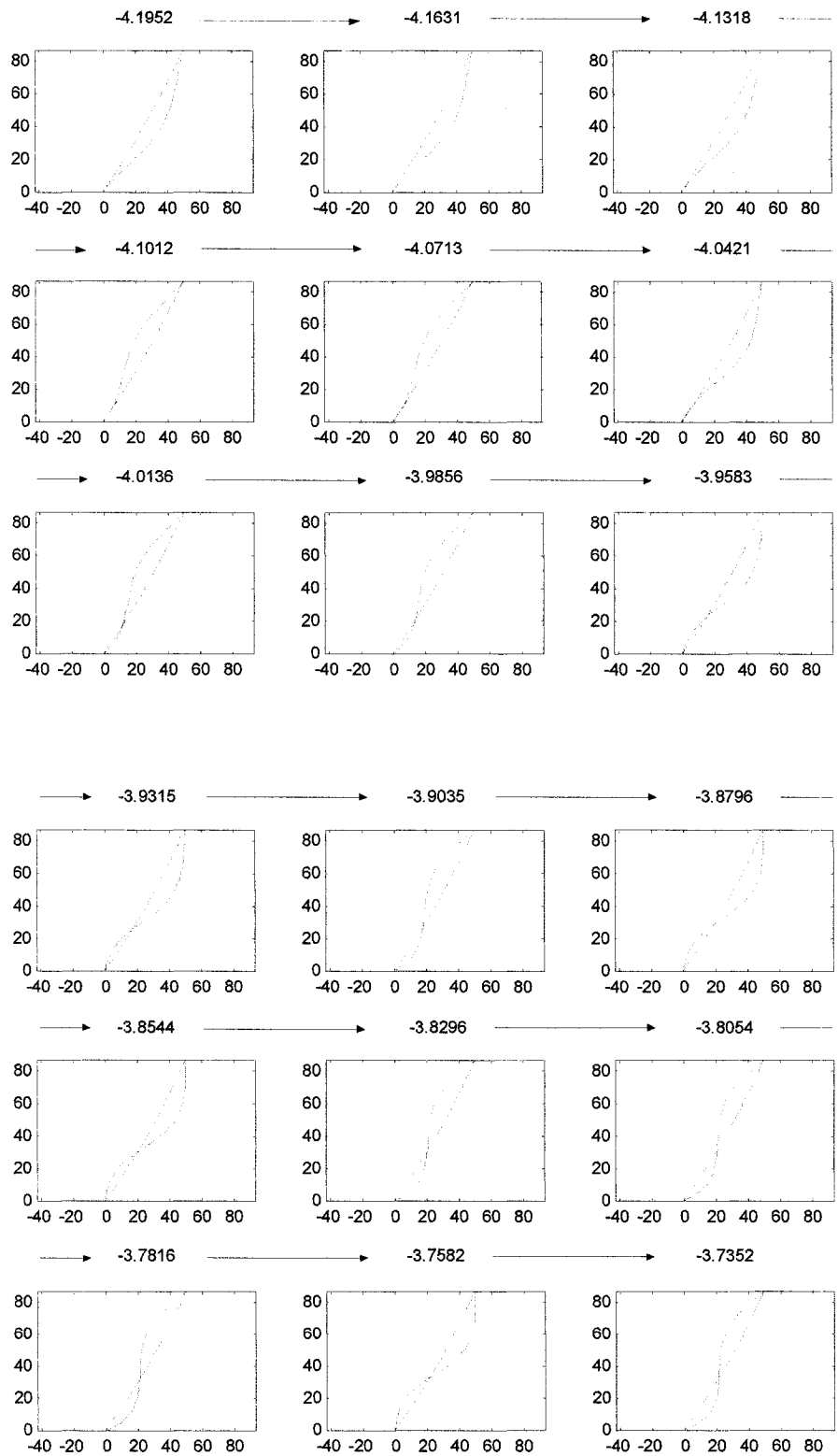

Fig. 4.77 Mode shapes between the transition range in the 1st frequency line ($\theta = 60°$)

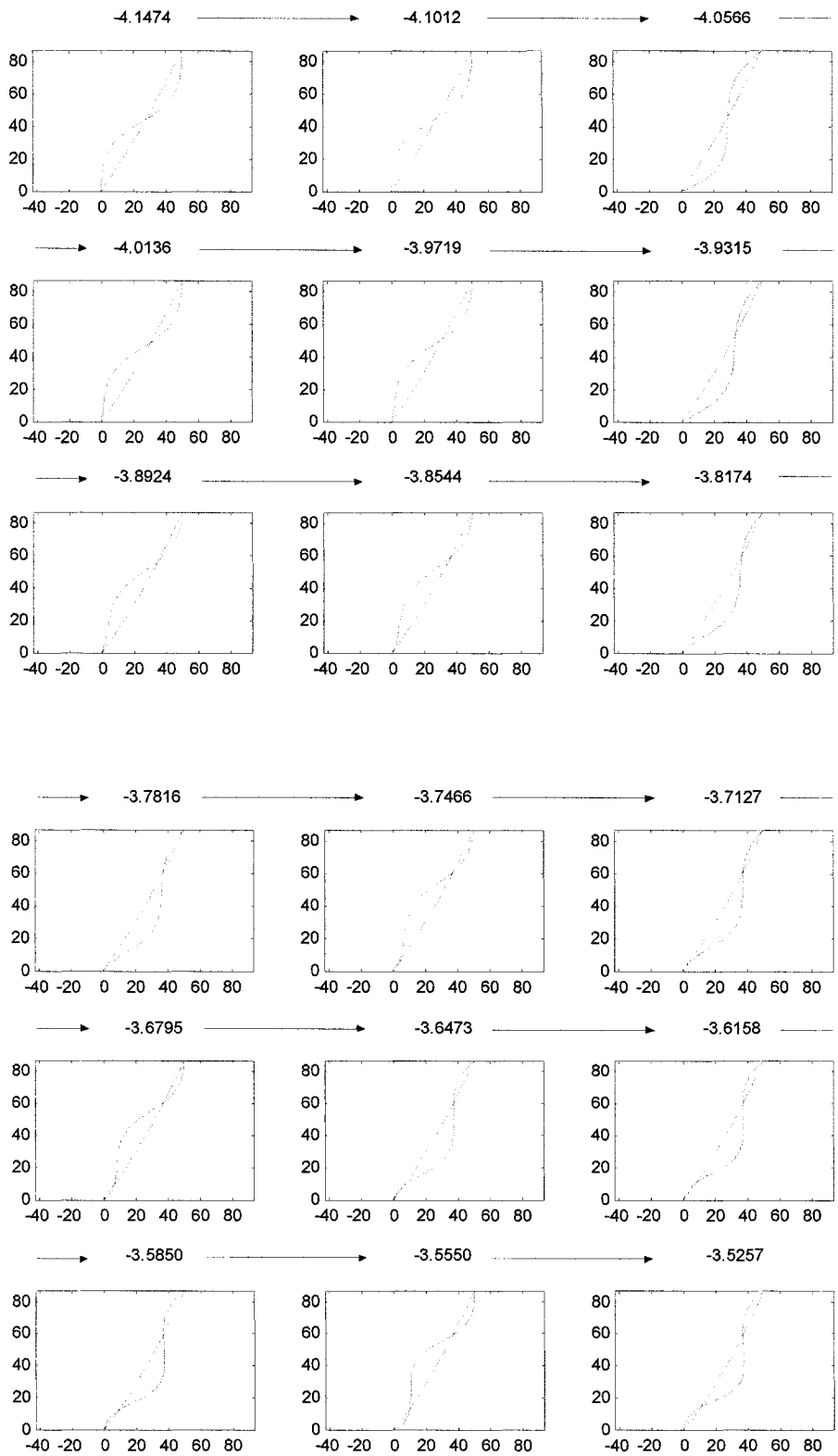

Fig. 4.78 Mode shapes between the transition range in the 2nd frequency line ($\theta = 60°$)

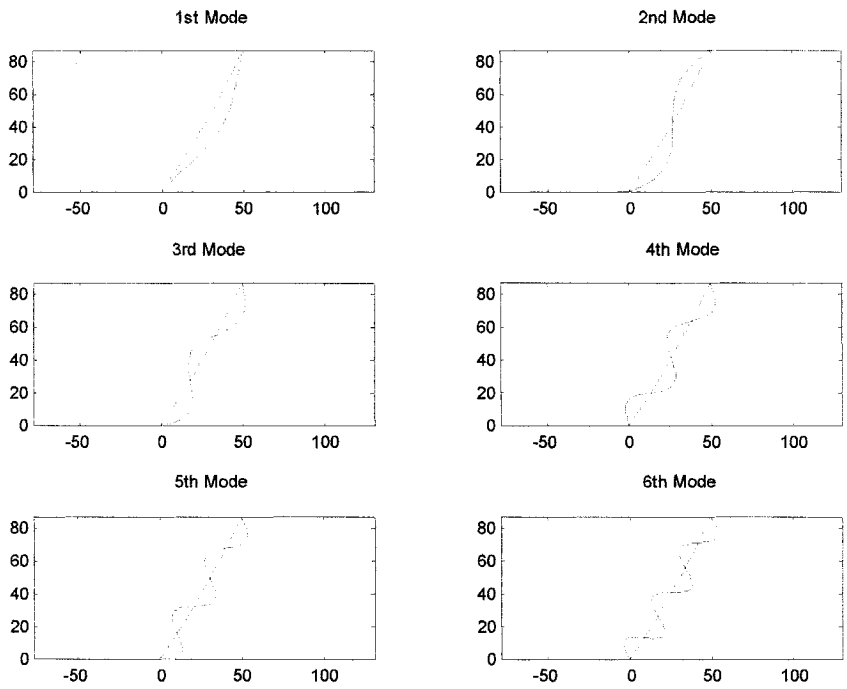

Fig. 4.79 Mode shapes at A ($\theta = 60°$)

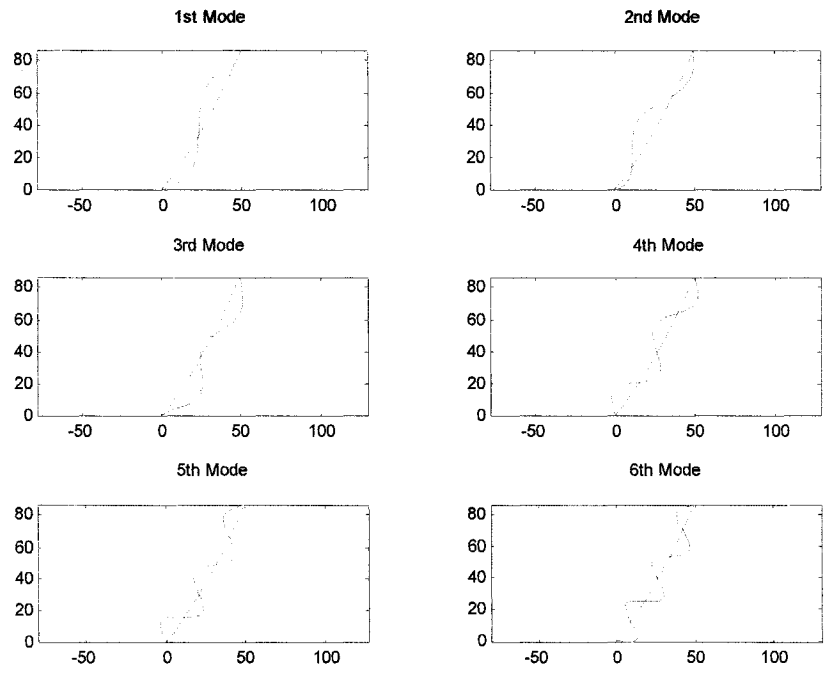

Fig. 4.80 Mode shapes at B ($\theta = 60°$)

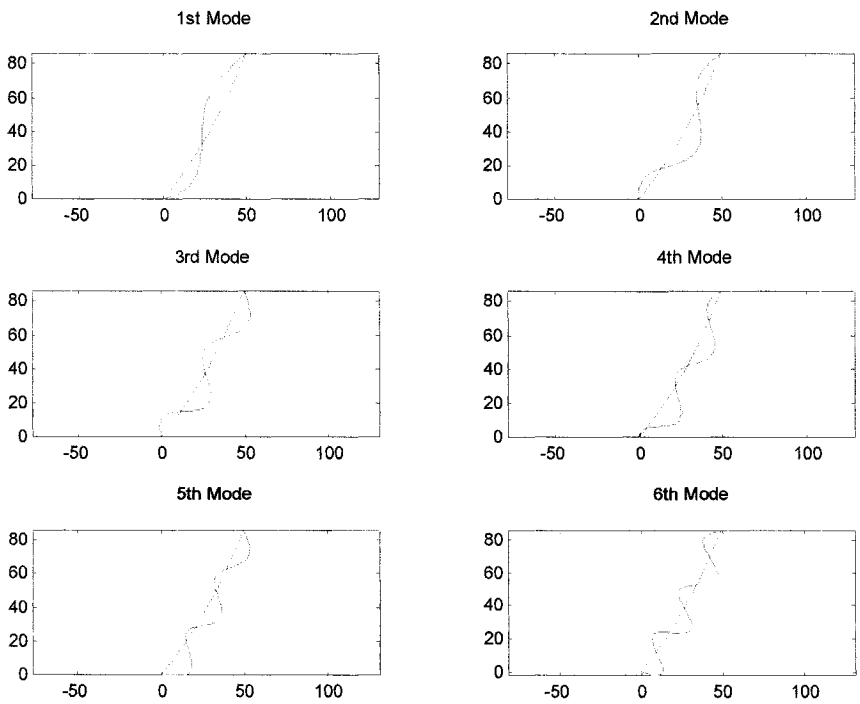

Fig. 4.81 Mode shapes at C ($\theta = 60°$)

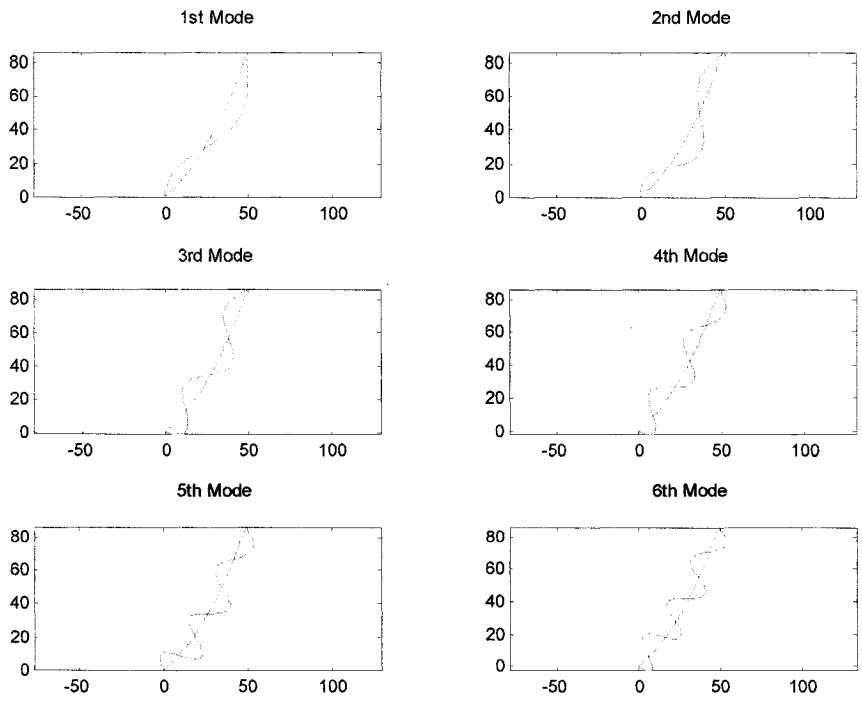

Fig. 4.82 Mode shapes at D ($\theta = 60°$)

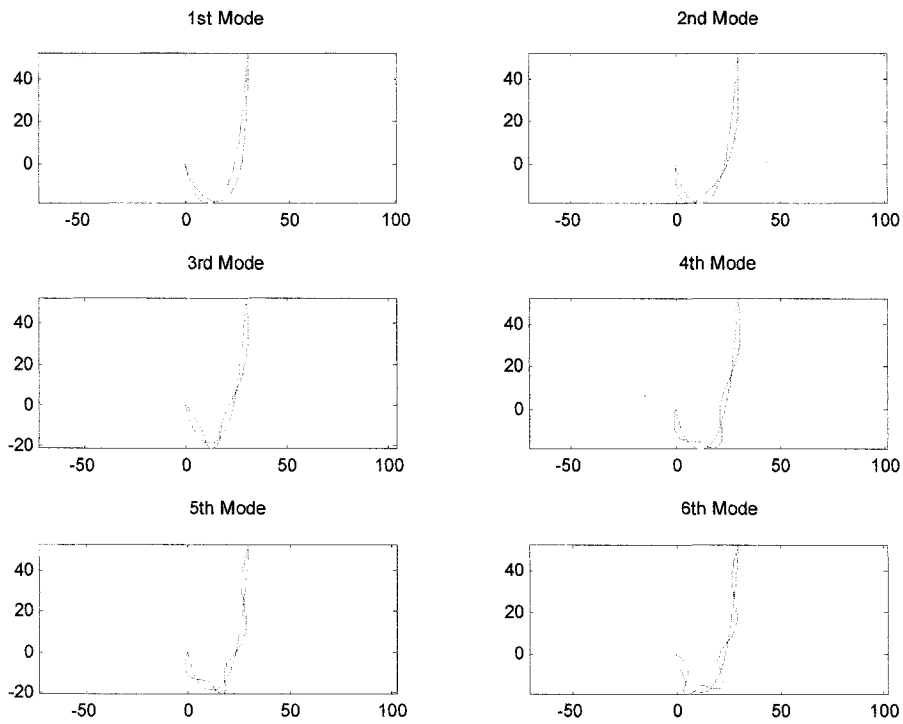

Fig. 4.83Mode shapes at E ($\theta = 60°$)

CHAPTER 5

CONCLUSION

The study of natural frequencies and mode shapes of vibration of suspended cables has been an interesting research topic for a long time. The present study treats the cable as an extensible linkage of linear rods connected by frictionless pins with concentrated masses at the connection pins. To determine the frequencies and corresponding mode shapes, the Finite Element Method formulation is applied and implemented under Matlab. Several parametic studies are conducted, and based on the results presented in the previous chapter, the following specific conclusions are made:

- In the case of horizontal cables, results exhibit that the first, third, and fifth frequency lines coincide with the second, fourth, and sixth frequency lines respectively, and mode shapes are clearly different immediately before and after each crossover point. The existence of modal crossover points for horizontal cables, which are defined by Irvin and Caughey [6] is demonstrated.

- In the case of inclined cables, the study illustrates that inclined cables have different behaviour from horizontal cables; the frequency crossover does not occur and the modal crossover takes place in a different way. The results in this study have been shown that the frequency crossings only occur for horizontal cables, and once the cable span has the angle of inclination, the crossings never happen (this study proved the phenomenon of frequency non-crossings starting from a cable with the

angle of inclination of 1-degree.). In the area of non-contact crossings of frequency (transition range), mode shapes are a mixture of symmetric and asymmetric modes. The width of this transition range depends on the inclination angle, θ; that is, the width becomes wider as the inclination increases.

- Once a cable is given a large inclination angle, the transition of mode shapes is different due to the effect of gravity force on the cable tension.

- By using a different Young's modulus as cable material in the calculation, the effects of axial stiffness of the cable on the cable dynamics are as follows: (1) modal crossover points for horizontal cables and transition ranges for inclined cables give an equivalent effect as having the lower tension when Young's modulus is smaller; that is, the modal crossover occurs under the circumstance of smaller cable tension when EA is smaller; and (2) the width of the transition ranges for inclined cables is wider when EA is smaller.

- As the sag-to-total cable length ratio increases, the frequencies and mode shapes converge to those of the vertically suspended cable; that is, all non-dimensional frequencies becomes zero and mode shapes take on the form of virtually suspended cable hanging from the top when the sag-to-total cable length ratio is fairly large.

APPENDIX

PROGRAM IMPLEMENTED IN MATLAB 6.5

==========Ainput.m==========

```
% Diameter of cable
Di=0.03;

% Young's modulus of elasticity
E=2e11;

% Total cable length
L=100;

% Mass per unit length of cable
M=5.55;

% Inclination of cable
theta=(pi/180)*0;

% Sag to span ratio of cable
R=0.1;

% Number of element
k=100;
```

==========

==========Bprofile.m==========

```
%Define parameters

function f=alpha(a)
global R C theta

C=-a+asinh(a*tan(theta)/sinh(a));
f=(1/(2*a))*(tan(theta)*(asinh(tan(theta))-C)-sec(theta)+cosh(C))-R;
```

==========

==========Csubroutine.m==========

```
run Ainput

%Value H & l
al=fzero(@Bprofile,1);

global C R theta
W=9.8*M;
l=(L*al)/sqrt((sinh(al))^2+(al*tan(theta))^2);
H=(W*l)/(2*al);

sag=(H/W)*(tan(theta)*(asinh(tan(theta))-C)-sec(theta)+cosh(C));
RR=(sag/L);

% Geometric node pointX(1)=0;
Y(1)=0;

for i=2:k+1;
   X(i)=((H/W)*asinh((W*L)/(H*k)+sinh((W/H)*X(i-1)+C))-(H/W)*C);
end

for j=2:k+1;
   Y(j)=(H/W)*(cosh((W/H)*X(j)+C)-cosh(C));
end

clear i j

% Mass matrix generation
Mm=zeros(2*(k+1),2*(k+1));
for i=3:2*k;
   Mm(i,i)=(M*L)/k;
end
clear i

% Stiffness matrix generation
el=L/k;
for i=1:k
   cosine(i)=(X(i+1)-X(i))/el;
end

for j=1:k
   sine(j)=(Y(j+1)-Y(j))/el;
end
clear i j

A=pi*Di^2/4;
```

```
EA=E*A;

for i=1:k
  F(i)=H/cosine(i);
end

clear i

Ke=zeros(2*k+2,2*k+2,k);

%(1,1,i)----------


for i=1:k
  Ke(2*i-1,2*i-1,i)=(EA/el)*(cosine(i))^2+(F(i)/el)*(sine(i))^2;
end

%(1,2,i)----------

for i=1:k
  Ke(2*i-1,2*i,i)=(EA/el)*(sine(i)*cosine(i))-(F(i)/el)*(sine(i)*cosine(i));
end

%(1,3,i)----------

for i=1:k
  Ke(2*i-1,2*i+1,i)=-(EA/el)*(cosine(i))^2-(F(i)/el)*(sine(i))^2;
end

%(1,4,i)----------

for i=1:k
  Ke(2*i-1,2*i+2,i)=-(EA/el)*(sine(i)*cosine(i))+(F(i)/el)*(sine(i)*cosine(i));
end

%(2,1,i)----------

for i=1:k
  Ke(2*i,2*i-1,i)=(EA/el)*(sine(i)*cosine(i))-(F(i)/el)*(sine(i)*cosine(i));
end

%(2,2,i)----------

for i=1:k
  Ke(2*i,2*i,i)=(EA/el)*(sine(i))^2+(F(i)/el)*(cosine(i))^2;
end
```

```
%(2,3,i)----------

for i=1:k
   Ke(2*i,(2*i)+1,i)=-(EA/el)*(sine(i)*cosine(i))+(F(i)/el)*(sine(i)*cosine(i));
end

%(2,4,i)----------

 for i=1:k
    Ke(2*i,2*i+2,i)=-(EA/el)*(sine(i))^2-(F(i)/el)*(cosine(i))^2;
 end

 %(3,1,i)----------

 for i=1:k
    Ke(2*i+1,2*i-1,i)=-(EA/el)*(cosine(i))^2-(F(i)/el)*(sine(i))^2;
 end

 %(3,2,i)----------

 for i=1:k
    Ke(2*i+1,2*i,i)=-(EA/el)*(sine(i)*cosine(i))+(F(i)/el)*(sine(i)*cosine(i));
 end

 %(3,3,i)----------

 for i=1:k
    Ke(2*i+1,2*i+1,i)=(EA/el)*(cosine(i))^2+(F(i)/el)*(sine(i))^2;
 end

%(3,4,i)----------

for i=1:k
   Ke(2*i+1,2*i+2,i)=(EA/el)*(sine(i)*cosine(i))-(F(i)/el)*(sine(i)*cosine(i));
end

%(4,1,i)----------

for i=1:k
   Ke(2*i+2,2*i-1,i)=-(EA/el)*(sine(i)*cosine(i))+(F(i)/el)*(sine(i)*cosine(i));
end

%(4,2,i)----------

for i=1:k
   Ke(2*i+2,2*i,i)=-(EA/el)*(sine(i))^2-(F(i)/el)*(cosine(i))^2;
end
```

```
%(4,3,i)-----------------------------------------------------------------------

for i=1:k
   Ke(2*i+2,2*i+1,i)=(EA/el)*(sine(i)*cosine(i))-(F(i)/el)*(sine(i)*cosine(i));
end

%(4,4,i)-----------------------------------------------------------------------

for i=1:k
   Ke(2*i+2,2*i+2,i)=(EA/el)*(sine(i))^2+(F(i)/el)*(cosine(i))^2;
end

clear i
Kk=zeros((2*k)+2,(2*k)+2);
i=1;
while (i<=k)
   Kk=Kk+Ke(:,:,i);
   i=i+1;
end
clear i

MM=Mm(3:(k)*2,3:(k)*2);
KK=Kk(3:(k)*2,3:(k)*2);

% Natural frequency(Wn) & Mode shape(U)
D2=eig(KK,MM);
D=sort(D2);
[U,D1]=eig(KK,MM);
clear D1
Wn=sqrt(D);

for i=1:k-1
   Ux(i,:)=U(2*i-1,:);
   Uy(i,:)=U(2*i,:);
end
clear i

Uxx=zeros(k+1,2*k-2);
Uyy=zeros(k+1,2*k-2);
Uxx(2:k,:)=Ux;
Uyy(2:k,:)=Uy;

clear Ux
clear Uy
```

==========Dpostprocess.m==========

```
LRR=log10(RR^3);
%Post process
run Csubroutine

stc=fopen('result','w');
fprintf(stc,'Diameter of cable(m) = %5.2f\n',Di);
fprintf(stc,'Modulus of Elasticity(N/m) = %-5.2d\n',E);
fprintf(stc,'Total cable length(m) = %-5.d\n',L);
fprintf(stc,'Mass per unit length of cable(Kg/m) = %-5.2f\n',M);
fprintf(stc,'Inclination of cable(degree) = %-5.1f\n',theta*(180/pi));
fprintf(stc,'Cable sag(m) = %-5.5f\n',sag);
fprintf(stc,'Sag to span ratio = %-5.7f\n',R);
fprintf(stc,'Sag to total cable length = %-5.7f\n',sag/L);
fprintf(stc,'Span(m) = %-10.5f\n',l);
fprintf(stc,'Horzontal force(N) = %-10.5f\n\n\n',H);
fprintf(stc,'Natural frequency (rad/sec)\n\n');
for i=1:10
   fprintf(stc,'%5.0f %11.3f\n' ,i,Wn(i));
end
satus=fclose(stc);

for i=1:6
   figure(1)
   subplot(3,2,i)
   plot(X,Y,'r')
   hold on
   plot(transpose(X)-Uxx(:,i)*150,transpose(Y)-Uyy(:,i)*150)
   title('Mode shape')
end
```

==========

REFERENCES

[1] Broughton, P. & Ndumbaro, P. (1994), *The Analysis of Cable and Catenary Structures*, Thomas Telford, London

[2] Forghani-Arani, S. (2003), "Dynamical Behaviour of Inclined Cables", *A report submitted to the University of Ottawa*

[3] Henghold, W. M. & Russell, J. J. & Morgan, J. D. (1977), "Free Vibration of Cable in Three Dimensions", *Journal of Structural Engineering*, ASCE, 103, 5, pp. 1127-1136

[4] Humar, J. L. (1990), *Dynamics of Structure*, Prentice Hall, Inc.

[5] Irvine, H. M. (1981), *Cable Structures*, The MIT Press

[6] Irvine, H. M. (1978), "Free Vibration of Inclined Cables", *Journal of Structural Engineering*, ASCE, 104, ST2, Technical Notes, pp. 343-347

[7] Irvine, H. M. & Caughey, T. K. (1974), "The Linear Theory of Free Vibrations of a Suspended Cable", *Proceedings of the Royal Society of London*, Series A, Vol. 341, pp. 299-315

[8] Pugsley, A. G. (1949), "On The Natural Frequencies of Suspension Chains", *Quarterly Journal of Mechanics and Applied Mathematics*, Vol. 2, Pt. 4, pp. 412-418

[9] Ramberg, S. E. & Griffin, O. M. (1977), "Free Vibration of Taut and Slack Marine Cables", *Journal of Structural Engineering*, ASCE, 103, ST11, pp.2079-2092

[10] Ross, C. T. F. (1985), *FINITE ELEMENT METHODS IN STRUCTURAL MECHANICS*, Ellis Horwood series in mechanical engineering

[11] Tanaka, H. (2000), "Cable Vibration", *IMAC Project Workplan WP1*

[12] Triantafyllou, M. S. (1984), "The Dynamics of Taut Inclined Cables", *Quarterly Journal of Mechanics and Applied Mathematic*, Vol. 37, Pt. 3, pp. 421-440

[13] Triantafyllou, M. S. and Grinfogel, L. (1986), "Natural Frequencies and Modes of Inclined Cables", *Journal of Structural Engineering*, ASCE, 112, 1, pp. 139-148

[14] West, H. H. & Geschwindner, L. F. & Suhoski, J. E. (1975), "Natural Vibration of Suspension Cables", *Journal of Structural Engineering*, ASCE, 101, 11, pp. 2277-2291

[15] Yamaguchi, H. (1997), "Fundamentals of Cable Dynamics", *Proceedings of International Seminar on Cable Dynamics*, Tokyo, pp. 81-94